8-2019

Organic-Inorganic Hybrid Materials for Piezoelectric/Triboelectric Nanogenerator

Aminur Rashid Chowdhury
The University of Texas Rio Grande Valley

ORGANIC-INORGANIC HYBRID MATERIALS FOR PIEZOELECTRIC/TRIBOELECTRIC NANOGENERATOR

A Thesis

by

AMINUR RASHID CHOWDHURY

Submitted to the Graduate College of
The University of Texas Rio Grande Valley
In partial fulfillment of the requirements for the degree of

MASTER OF SCIENCE

August 2019

Major Subject: Chemistry

ORGANIC-INORGANIC HYBRID MATERIALS FOR PIEZOELECTRIC/TRIBOELECTRIC NANOGENERATOR

A Thesis
by
AMINUR RASHID CHOWDHURY

COMMITTEE MEMBERS

Dr. Mohammed Jasim Uddin
Chair of Committee

Dr. Elamin E. Ibrahim
Committee Member

Dr. Javier Macossay-Torres
Committee Member

Dr. Hassan Ahmad
Committee Member

August 2019

ABSTRACT

Chowdhury, Aminur Rashid, Organic-Inorganic Hybrid Materials For Piezoelectric/Triboelectric Nanogenerator. Master of Science (MS), August, 2019, 135 pp., 1 table, 67 figures, references, 170 titles.

Nanogenerator has been a major focus among researchers of recent time due to its versatile use in everyday life. Though the discovery of the piezoelectricity and the triboelectricity dates back to 19th century, the use of these phenomena has not been in practical use till 2006. In this study we demonstrate the practical application of piezoelectric and triboelectric nanogenerator comprised of different copolymer and piezoelectric ceramic. The largely known piezoelectric polymer Polyvinylidene fluoride (PVDF) has also been utilized. The enhancement of piezoelectric properties of PVDF has been achieved by utilizing surface activation of accommodating ceramic. The Li doped ZnO has been used because of its high d33 values. However, no electromagnetic poling has been utilized. Not only the piezoelectric and triboelectricity and nanogenerator has been studied, its application in real-life has also been utilized. We have been able to use the triboelectric nanogenerator as body motion sensor and effectively measure the body motion as well as plot for energize small smart devices. Overall the research has been able to generate new hybrid and mon nanogenerators and utilize for everyday use in daily life.

DEDICATION

The completion of my master's studies would not have been possible without the love and support of my family and friends. My mother KULSUMA AKTER CHOWDHURY, my father Late HELAL AHMAD CHOWDHURY, my brother HUMAYUN RASHID CHOWDHURY, my second player TANIA ALVAREZ and my best friend FORHAD AHMED, wholeheartedly inspired, motivated and supported me by all means to accomplish this degree. Thank you for your love and patience.

ACKNOWLEDGEMENTS

I will be always grateful to my advisor Dr. Mohammed Jasim Uddin for his invaluable supervision in scientific research and encouraging me with infinite patience and relentless support instead of his limitations to complete my research work. He has been a great mentor for me. I am grateful to every single member of Photonics and Energy Research Laboratory. I would be wrong doing if I do not mention Istiak Hussain and Abu Musa Abdullah. Since the beginning of my journey in UTRGV Istiak Hussain played a role of my brother and supported whole heartedly. Even after leaving from the Valley for his greater career goal, his support remained subservient. I am unreservedly indebted to his effort to my academic and personal goal. Without his brotherly support this journey could have been next to impossible. Abu Musa Abdullah's dedication towards nanogenerator, personal motivation and mental support helped me to achieve this goal. I cannot defy the help from all Bangladeshi Students and Community living in the Rio Grande Valley during my research period. I should mention especially Md Ruhul Amin, Israt Tarannum, Sakib Hussain for their support. I cannot defy assistance in my research from my roommates Md. Noman Hossain and Abdullah Al Masum. I must mention about Abdullah Al Masum, who has been an elder brother and a big support for me during my stay and research in UTRGV. He showed affection and care towards me and advised me on several personal issues throughout whole research journey which made me more focused in my research. I would like to thank my best supporting friends Dr. Leela Joshi, Grecia Torreblanca and Tania Alvarez (future Dr. Alvarez) for

understanding me and suffer through all the pains that I gave them. When I came to this country, I never had to think about the cultural gap because of these highly intelligent people. I would like to particularly thank my second player Tania Alvarez for her unprecedented effort towards my ignorance. Her appearance remains a blessing for me. I wish her same old mental support recurs and illume in me. I would like to also show my gratitude to the Department of Chemistry, UTRGV as well as Dean's Office, College of Science, UTRGV for her support during my Journey of achieving the goal. I am grateful to Dr. Yuanbing Mao, Dr. Evangelia Kotsikorou, Dr. Tülay Ateşin, Dr. Elamin E. Ibrahim, Dr. Hassan Ahmad, Dr. Javier Macossay-Torres. I should particularly express my gratitude to Dr. Parwinder Grewal (Executive Vice President, Office of the Executive Vice President for Research, Graduate Studies & New Program Development) for his support for my MS expedition in UTRGV. Financial support initiated by Dr. Grewal was a great backing for tension free research. At last I would like to thank the biggest support for me in this research work Dr. Mohammed Jasim Uddin, who has been mentoring me even before I arrived in UTRGV. His given flexibility made me think out of the box and utilize most of my potential. Without his support this could have been next to impossible.

TABLE OF CONTENTS

LIST OF TABLES

Page

LIST OF FIGURES

Page

CHAPTER I

INTRODUCTION

Technology has brought us into a smarter world where harvesting normally wasted energy from the environment is not only feasible but a potentially massive untapped source of power. The use of nanotechnologies in this research field encompasses a continuous study and development in order to obtain materials with improved properties. Modern consumer electronics have also advanced to the point where we cannot imagine life without the sensors around us serving our every need; diesel fuel injectors, fast response solenoids, stack actuators, stripe actuators, dot matrix printer, course changing bullets, microphones, accelerometer, speakers, and stress sensors are all vitally important for the functioning of modern society. Many of these sensors are based on piezoelectric materials, and significant advancements in our understanding of piezoelectric materials have been necessary to advance sensor technology to the current level. It may seem that piezoelectric technology has reached the pinnacle of its development. But a great deal of scientific research is still taking place with the goal of advancing piezoelectric technology for efficient energy harvesting and sensor applications.

Although the large-scale utilization of piezoelectric materials only began shortly after the First World War [1], the piezoelectric effect was discovered quite some time previous to the war by the Curie Brothers in 1880 [2]. Previously it was only seen as having marine and military applications. However, it was soon found that piezoelectric materials have myriad potential a

pplications in everyday life as well [3]. This discovery prompted scientists to further develop piezoelectric materials, and eventually led to the piezoelectric technology that we have in the modern era: from tiny sensors to efficient piezoelectric-based energy harvesting devices. Figure 1 clearly shows how piezoelectric nano-generator research has become increasingly popular in recent years; it is obvious that interest in piezoelectric nano-generators is growing day by day [4].

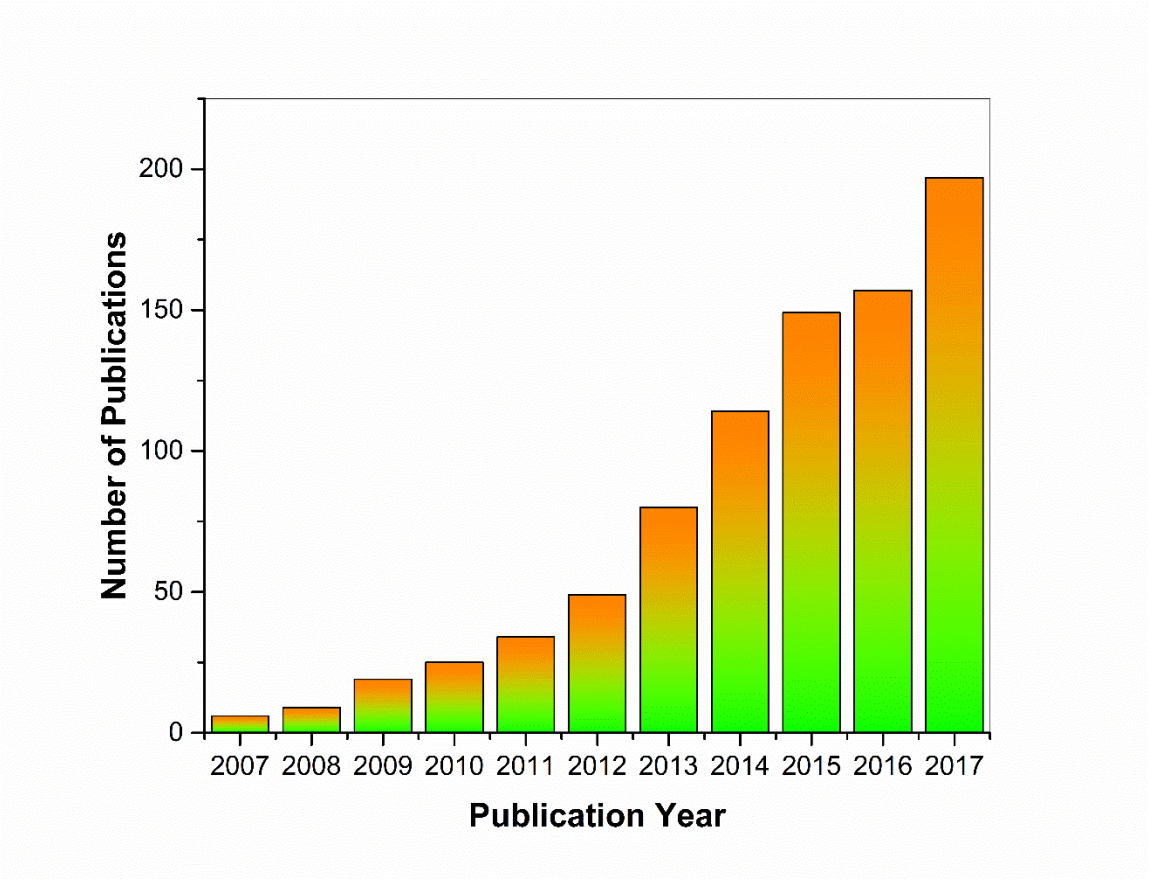

Figure 1: Number of scientific papers published in the last ten years on piezoelectric nanogenerator research [4].

Though piezoelectricity is an age-old phenomenon, nanostructured piezoelectric devices have only recently been developed. Indeed the development of nanostructured piezoelectric

material is a popular topic for scientific research [5–10]. The tremendous potential applications of nano-scale piezoelectric devices have attracted much interest in recent years, and indeed a large variety of energy harvesting devices has been developed. However, regardless of the extraordinary advances made concerning synthetic methodologies, quantitative mechanical and electromechanical characterization of the produced nanostructures is still limited because of the challenges of characterizing and developing a mechanistic understanding of mechanical and electromechanical properties in nanostructures below a dimension of 100nm. Measurement of properties through a particular experimentation technique is not sufficient to understand the behaviour of nanostructures completely. Thorough structural characterization is required to fully understand the quantification of defects and impurities. It also clearly evident that different approach to nanostructure may cause the same nanostructure in different characteristics [11].

Self-powered nanogenerator is a system that can work and function without an external power supply. In the last few years tremendous progress in the development of new piezoelectric self-powered systems have been studied. Also, it is receiving a high research interest due to its ease and versatility of use [7,12]. This is well reflected in Figure 1. Scientists have found effective the use of piezoelectric nanogenerator in a plethora of applications, such as power wearable, embedded, implanted and/or portable electronics and sensors [13,14]. Not only ferroelectrics inorganic materials have been studied for piezoelectric behaviour, but ferroelectric polymers have also been considered thoroughly with a number of approaches [12,15,16]. This review summarises recent developments relevant to piezoelectric nanogenerators, from the nanostructured materials to multicomponent/functional nano-generators. The theoretical basis of the piezoelectric effect is also discussed, with an emphasis on understanding the mechanism of

the piezoelectric effect in different materials, synthesis techniques of piezoelectric nanostructures along with future developments of piezoelectric nanogenerator.

CHAPTER II

LITERATURE REVIEW

Types of Piezoelectric materials

Up to now, many piezoelectric materials have been discovered/developed, including many natural and synthetic materials; a brief overview of these materials is given in Table 1. In the early period of discovery of piezoelectric materials in the late 19th century, Pierre brothers communicated their finding in zinc blende, sodium chlorate, boracite, tourmaline, quartz, calamine, topaz, tartaric acid, cane sugar, and Rochelle salt in the French scientific journal *Comptes Rendus* [17]. Typically, piezoelectric ceramics are polycrystalline materials that consist of irregular domains that are forced to align in the same direction by "poling", a process in which a high electric field gradient is applied across the material at an elevated temperature. This domain alignment remains even after removal of the poling field. As a result of this process, the new piezoelectric material exhibits "macro-piezoelectric" properties, thus macroscopic perturbation of the material will produce a current. Piezoelectric crystals, which refer to single-crystalline materials, are typically asymmetrical in the lattice structure and therefore exhibit piezoelectric properties without the prior need for poling [18,19].

Category	Typical materials
Natural crystals	Berlinite ($AlPO_4$), sucrose, quartz, Rochelle salt, topaz, and tourmaline-group minerals
Natural materials	Bone, tendon, silk, wood, enamel, dentin, DNA, and viral proteins
Synthetic crystals	Gallium orthophosphate ($GaPO_4$), langasite ($La_3Ga_5SiO_{14}$), and diisopropylammonium bromide (DIPAB)
Synthetic ceramics	$BaTiO_3$, $PbTiO_3$, $Pb(Zr,Ti)O_3$, $KNbO_3$, $LiNbO_3$, $LiTaO_3$, Na_2WO_3, ZnO, $Ba_2NaNb_5O_5$, $Pb_2KNb_5O_{15}$, and so forth
Lead-free piezoceramics	$(K,Na)NbO_3$, $BiFeO_3$, $Bi_4Ti_3O_{12}$, $Na_{0.5}Bi_{0.5}TiO_3$, and so forth
Polymers	Polyvinylidene fluoride (PVDF)
Organic nanostructures	Self-assembled diphenylalanine peptide nanotubes (PNTs)
Organic-inorganic materials	Trimethylchloromethyl Ammonium Trichloromanganese(II), halogenoantimonates(III), halogenobismuthate(III)

Table 1: Different types of typical piezoelectric materials [18,20,21].

Precisely, piezoelectric ceramic materials typically show high piezoelectric constants and dielectric permittivity. Thus, these ceramics are suitable for use in high power energy transducers and harvesters. But their typically low mechanical quality (e.g. ductility) makes them unsuitable for high-frequency applications. Natural piezoelectric materials have the superior mechanical quality to piezoelectric ceramics, but they also suffer from lower piezoelectric constants and lower dielectric permittivity. Hence natural piezoelectric materials have been commonly used in high-frequency piezoelectric applications. Other than quartz, crystalline high-quality perovskite-structured piezoelectric single crystals such as the $Pb(A_{1/3}B_{2/3})O_3$-$PbTiO_3$ (where A = Zn^{2+}, Mg^{2+}; B = Nb^{5+}) with much higher piezoelectric constants (d_{33} = 2600 pC/N), electromechanical coupling coefficients (k_{33}=0.95), and strain (>1.7%) have been prepared [22]. However, the preparation of these single crystals requires a costly precision controlled process, which limits their application in many fields [18].

Organic piezoelectric materials such as PVDF have shown promising characteristics, including lower density [23], higher flexibility [24], lower resistance [25], and higher piezoelectric voltage [25] values which has attracted recent research efforts. However low d_{33} values remain a disadvantage of organic piezoelectric and limit their potential applications [18].

Materials for Piezoelectric Nanogenerator:

Piezoelectric materials can be found in nature, or they can be synthetically produced. Some of the common natural inorganic piezoelectric materials are quartz (SiO_2), Rochelle salt, topaz, tourmaline-group minerals and some organic substances as silk, wood, enamel, dentin, bone, hair, rubber [26]. Man-made piezoelectric materials are with crystals with a similar structure of quartz, ceramics, and composites [27]. Out of 32 crystal classes, only 20 exhibits piezoelectric properties. Furthermore, only 10 crystal classes out of these 20 piezoelectric classes

are polar, while others show behavior as nonpolar piezoelectric materials [27]. Many piezoelectric polymer materials have been found with considerable dielectric constants (e.g., PVDF, PVDF-TrFE, Parylene-C, Polyimide (β-CN) APB/ODPA). But PVDF and poly(vinylidene fluoride-co-trifluoroethylene) (PVDF-TrFE) have caught the eyes of the scientific community due to their extensive dielectric constants and variable polarity depending on processing techniques [3]. Polymer composites have been found to have several advantages compared to bulk materials, hence a large amount of researches has been conducted in this area. Approval of PVDF and PEG by FDA has opened a big horizon for piezoelectric nanogenerator in the field of biomedicine [28,29].

The Mechanism of Piezoelectricity

To maintain the overall charge balance within crystals, they must possess exactly equal numbers of positive and negative atoms/ions, so that the overall charge is zero and the material is stable. In crystalline materials, these positive and negative charges are arranged in rigid lattice structures. Taking into consideration this aspect, when an external stress is applied, this lattice structure is disrupted, and thus the local charge balance within the crystal is perturbed; hence a current in the crystal is generated. On the contrary, in the reverse piezoelectric effect, an external electrical field is applied which generates a perturbation of the lattice structure (and thus the overall dimensions) of the crystal. C. Falconi *et al.* demonstrated that piezoelectricity is effectively a linear relation between the mechanical and electrical properties of dielectric materials [30]. Here we will follow Zhao Wang *et al.* in their demonstration of the theoretical study of the piezoelectric effect on the crystal [18].

The electrical displacement (D_i) and the electrical field (E_j) have a linear relationship that can be expressed as:

$$D_i = \sum_{j=1}^{3} \varepsilon_{ij} E_j \quad (1)$$

Where ε_{ij} is the permittivity of dielectric materials which is considered as a second-rank tensor represented by 3 x 3 matrix. As the matrix is symmetric ($\varepsilon_{ij} = \varepsilon_{ji}$) there are most 6 independent coefficients. Relation between stress and strain can be showed for mechanical properties as:

$$T_{ij} = \sum_{k,l=1}^{3} c_{ij} S_{kl} \quad (2)$$

Here C_{ij} is elastic stiffness of the material. This above equation can also be interpreted as:

$$S_{ij} = \sum_{k,l=1}^{3} S_{ijkl} T_{kl} \quad (3)$$

Where S_{ijkl} is elastic compliance of the materials. As the stiffness related to second rank tensor stress and strain, they are a fourth-rank tensor. Due to symmetric stress and strain ($T_{ij}=T_{ji}$ and $S_{ij} = S_{ji}$), the number of C_{ijkl} can be reduced to 36.

Also, the piezoelectric constitutive equation can be reduced to:

$$D_i = \varepsilon_{ij}^{T} E_j + d_{ij} T_j \quad (4)$$

$$S_I = d_{ij} E_j + S_{IJ}^{E} T_j \quad (5)$$

Here Superscripts T and E denotes the coefficients are at constant stress and electric field, respectively. While the piezoelectric strain/charge constant denoted as d_{ij} .

The piezoelectric constitutive equation for a one-dimensional (1D) simplified hypothesis can be interpreted as:

$$S = s^E T + dE \tag{6}$$

$$D = dT + \varepsilon^T E \tag{7}$$

$$S = s^D T + gD \tag{8}$$

$$E = -g^T + \frac{D}{\varepsilon} \tag{9}$$

$$T = c^E S - eE \tag{10}$$

$D = eS + \varepsilon^S E$ (11)$T = c^D S + hD$

(12)$E = -hs + \frac{D}{\varepsilon S}$ (13)

Here d, e, g, and h are the piezoelectric constants and can be linked as:

$$d = \varepsilon^T g = S^E e \tag{14}$$

$$e = \varepsilon^S h = c^E d \tag{15}$$

$G = \frac{d}{\varepsilon T} = s^D h$ (16)$h = \frac{e}{\varepsilon S} = c^D g$

(17)

$$\varepsilon^T = \varepsilon^S + de \tag{18}$$

Applications of Piezoelectric Materials

The number of applications for piezoelectric materials is now larger than it has ever been since their first use as sonar transducers or megacycle quartz resonators [31]. This unique class of materials is now included in a huge diversity of products, ranging from tiny pacemakers to

state of the art spacecraft [32,33]. This vast array of applications can be broadly classified according to the operational mode of the piezoelectric material as follows:

Sensors: Piezoelectric materials used for detection of pressure variations in longitudinal, transversal, and shear modes. The most common use of piezoelectric materials as a sensor is in accelerometers [34]. Second to this sensor application is the use of piezoelectric sensors to detect sounds as in microphones, acoustic/electric guitar pickups, and for the detection of waves of lower frequencies. Piezoelectric materials have also found uses in ultrasonic medical imaging and non-destructive testing [18,35].

Actuators: The reverse piezoelectric effect has enabled piezoelectric materials to be used as precision actuators. Since a carefully controlled electric signal can create precisely (albeit typically very minuscule) deformations in piezoelectric materials, they have been used in applications that require extremely precise positioning [18]. Piezoelectric actuators are already being used in high tech position-based atomic microscopy instrumentation, including scanning tunneling microscopy (STM) and atomic force microscopy (AFM) equipment. Piezoelectric actuators are also used in many every-day consumer devices including digital cameras and cellular phone terminals [36,37].

Frequency Controlling Devices: Crystal oscillator is that uses the mechanical resonance of a vibrating piezoelectric crystal as an electronic oscillator circuit to create an electrical signal with a very precise frequency [38]. This is used to create very stable clock signals in electronic circuits. An excellent example of this kind of device is the timekeeping oscillator based on a vibrating quartz crystal found in many everyday electronic devices [18,39].

Energy Scavenging Nano/Micro-Generators: Since applying an external mechanical force creates a potential difference in piezoelectric crystals, they can be used as nano/micro-generators [18]. They have been used for this purpose in many applications, including for the ignition of lighters, roadside lamp posts, etc. Utilization of this characteristic for the scavenging of frictional and other typically wasted energy sources has also been explored; some products that harvest waste energy in this way are already commercially available, such as chargers that harness waste energy to power low-energy devices [40].

Biomedical Application: As piezoelectric nanogenerators have been found with very high efficiency and sensitivity, their use has been initiated in biomedical fields. Animal tests show that use of piezoelectric nanogenerator inside the human body is not far away. Nanogenerator has found its way in the use in an unconventional way too. Li *et al.* have demonstrated that muscle-driven nanogenerator from a living rat's heart and diaphragm can generate a considerable amount of energy [41]. Besides rat, it was also tested with other animals (e.g. swine) that nanocomposite nanogenerator can generate energy from the animal's heart beat as well as body movement [42]. Feng *et al.* have discussed the use of piezoelectric nanogenerator as pacemakers, cardiac sensor, blood pressure sensor, pulse sensor, deep brain stimulation, neuronal cell differentiation, osteoblast cells' differentiation, microbe inactivation by electroporation, anti-biofouling activity, post-charge disinfection, etc [12].

Synthesis Techniques for Piezoelectric Nanostructures:

The substantial interest in piezoelectric nano-generators has produced many novel synthetic techniques; these techniques can be broadly classified as follows.

Sol-Gel Template Method: This is the template method for preparing nanostructures entailing synthesis of the desired materials within the pores of the nanoporous membrane or other solid. This method gathers nanofibril or tubule of the desired materials inside the pores [43]. Hydrolysis followed by condensation of molecular precursors are the main steps in any sol-gel based method. Templating is used to grant the finished material a nanostructured morphology. Sol-gel methods begin with the hydrolysis of molecular precursors to obtain a suspension of colloidal particles (the sol) which is used to generate the "gel" composed of aggregated sol component on the substrate that is to be coated. Thermal treatment of the substrate follows the deposition of this gel to generate the desired nanostructured layer and drive off any residual solvent. Two advantages of the sol-gel template-based method are the ability to produce high purity materials at comparably low temperatures, and the facile preparation of homogenous, multi-component component systems by simple mixing of the precursors which allows for easy and variable chemical doping of prepared materials [44].

Hydrothermal Method: This method includes techniques of crystallizing substances from high-temperature aqueous solutions. This technique is very useful for the production of 1D nanostructures as well as multidimensional nanostructures. It offers some significant advantages in control of the length of structure and ease of integration along with cost-effective utilization [45].

Solvent Casting Method: This method is primarily used for the preparation of nano-films. Flexible films are obtained by spreading a precursor solution over a clean substrate followed by crystallization of the precursor upon evaporation of the solvent. It has been proven

as a reliable method to develop two-dimensional piezoelectric materials. PVDF or similar materials are typically used with this solvent casting method [45,46].

Electrospinning Method: Electrospinning is a fiber production method using an applied electric field to create a charged jet of polymer solutions or solid polymers. Electrospinning shares characteristics of both electrospraying and conventional dry spinning of fibers. Though this method has mostly been used for the preparation of the micro-piezoelectric generators, sub-micrometer diameter fibers have also been produced [45,47].

Solid State Techniques: Solid state techniques have been widely used to prepare materials with excellent piezoelectric properties. It is one of the oldest processing technologies and is by far the most commonly used technique for fabricating ceramic materials [48]. It can be defined as an irreversible thermodynamic process in which powder compacts are fused into a single material using thermal energy to obtain dense, polycrystalline ceramics. The main driving force of the fusion of the individual powder granules is the decrease of the surface free energy of an assembly of particles relative to a collection of individual particles; this driving force can be enhanced by decreasing the starting particle size. Other than driving particle agglomeration by decreasing the size of the individual particles / the amount of exposed surface area, agglomeration can be encouraged via the application of external pressure or with a chemical reaction [49,50].

Types of Piezoelectric Nano-generators:

In this review, piezoelectric nanogenerators are discussed and classified as basis of the different dimensionality of piezoelectric nanomaterials. Taking into consideration this aspect, piezoelectric nanogenerator can be classified as:

(i) Zero-Dimensional Piezoelectric Nanogenerator

(ii) One-Dimensional Piezoelectric Nanogenerator

(iii) Two-Dimensional Piezoelectric Nanogenerator

(iv) Three-Dimensional Piezoelectric Nanogenerator

These dimensional analyses are described as per below.

Zero-Dimensional Piezoelectric Nanogenerators: Zero-dimensional (0D) piezoelectric nano-generators have attracted much scientific interest in recent years. Because of the higher surface area, feasibility of incorporation and easy preparation techniques of nanoparticles compared to other dimensional nanomaterials, 0D piezoelectric materials are more aspiring in use of flexible nanogenerators [51]. This has led to that creation of many new types of piezoelectric nano-generators based on 0D nanomaterials. In 0D piezoelectric nano-generators, nano-clustered materials and nano-dispersions are isolated from each other as shown in Figure 2 [44].

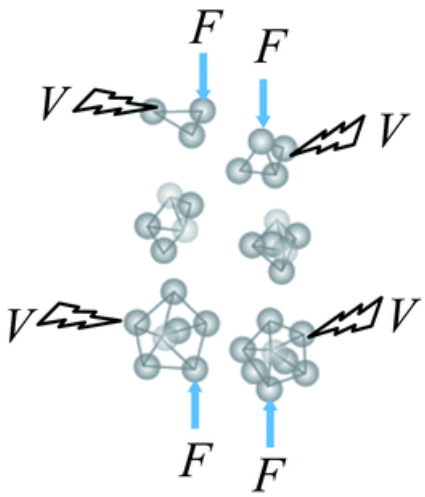

Figure 2: Zero-Dimensional Piezoelectric Nano-generators (Force and Voltage) **[44]**

It was found that the piezoelectric, as well as the ferroelectric properties of the material, can be improved by the addition of ferrite nanoparticles in polymer-based piezoelectric nano-generators [52]. It was also shown that the dielectric permittivity of the composite increases proportionately with the volume fraction of the nanoparticles [53]. Dodds *et al.* found that ZnO nanoparticles incorporated into poly(vinylidenefluoride-co-trifluoroethylene) (P(VDF–TrFE)) thin films enhanced the piezoelectric response of the films while still allowing them to maintain satisfactory mechanical properties [54]. Prasanthi *et al.* also demonstrated that ZnO nanoparticles embedded into an SU-8 polymer (i.e., epoxy-based negative photoresist) matrix granted the polymer a high degree of piezoelectric properties while still sustaining photo-patternability and optical transparency inherent to the SU-8 polymer [55]. Hadiji *et al.* demonstrated that alumina nanoparticles dispersed in PVDF–TrFE displayed a high piezoelectric coefficient [56]. Ahmed *et al.* showed that $Dy_{2.8}Sr_{0.2}Fe_5O_{12}$ (DySrIG) nanoparticles possess electric memory by which they remember their original shapes with thermalization (shape memory materials): their dielectric parameters change as a function of temperature over a range of 25-400°C yet return to the original state at room temperature) [57]. It was also found that processed $(Bi_{0.5}Na_{0.5})TiO_3$ subsequently doped with 8 mole % $BaTiO_3$ particles can produce a material with a large d_{33} value [58].

Mupeng Zheng *et al.* have described how the uniform distribution and dispersion degree of nanoparticles can enhance both the piezoelectric and ferroelectric properties of composite materials. It was experimentally determined that the intrusion of silver nanoparticles in a lead Zirconate Titanate matrix led to enhanced mechanical stability [59]. Hence there is much interest in determining whether good ferroelectric and piezoelectric properties can be obtained from ferroelectric-metal composites that have improved mechanical stability [60]. Some compositions

were tested in the study done by M. Zheng *et al.*, as follows: $Pb(Zn_{1/3}Nb_{2/3})_{0.20}(Zr_{0.50}Ti_{0.50})_{0.80}O_3$ + *x* Ag (PZN-PZT/*x*Ag), where *x* is varied from 0 vol. % to 10 vol.%. Ag_2O was mixed with Pb_3O_4, ZrO_2, TiO_2, ZnO and Nb_2O_5 according to the above stoichiometry in ball mills, followed by calcination in a covered alumina crucible at 850 °C. This calcined product was later pressed into discs with a diameter of 11.5 mm at a pressure of around 100 MPa followed by sintering at 1050°C for 2 hours [60]. $Pb(Zn_{1/3}Nb_{2/3})_{0.20}(Zr_{0.50}Ti_{0.50})_{0.80}O_3$ / 6 vol. % Ag (PZN–PZT/Ag) nanocomposites were prepared and characterized to evaluate their piezoelectric and ferroelectric properties. It was found that PZN-PZT / Ag has superior ferroelectric and piezoelectric properties, likely due to nanodomain formation during sintering with few unit cell long (Figure 3).

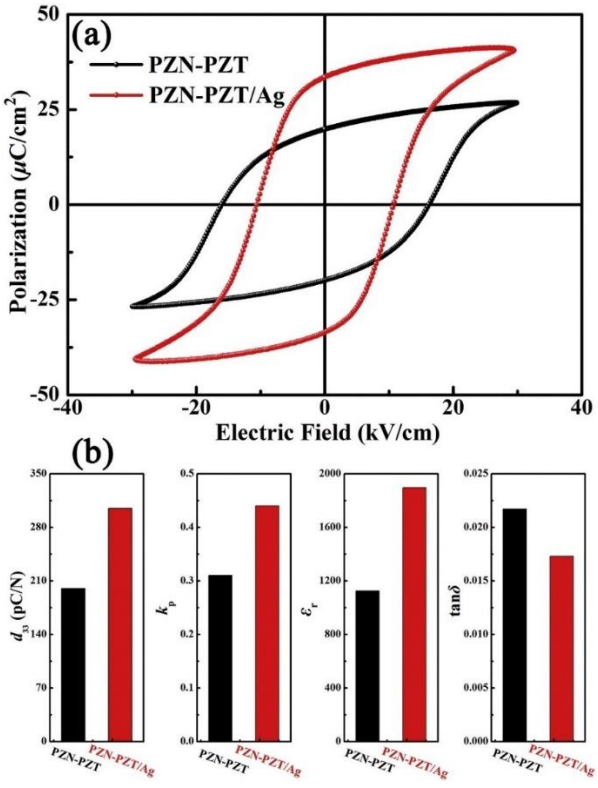

Figure 3: (a) The polarization–electric field (***P***–***E***) hysteresis loops and (b) ***d***33, ***k***p, ***ε***r, and tan***δ*** values for PZN–PZT and PZN–PZT/Ag specimens **[60]**.

PZN-PZT/Ag nanodomains are illustrated in the below TEM images (Figure 4) as little stripes. The 6 vol % Ag samples are nanoscale (5-10 nm) in width. Domain size is directly proportional to the square root of domain wall energy [61,62]. The multidomain state with the smallest crystal size exhibits the largest value of the longitudinal piezoelectric constant, and hence, it is more favorable .

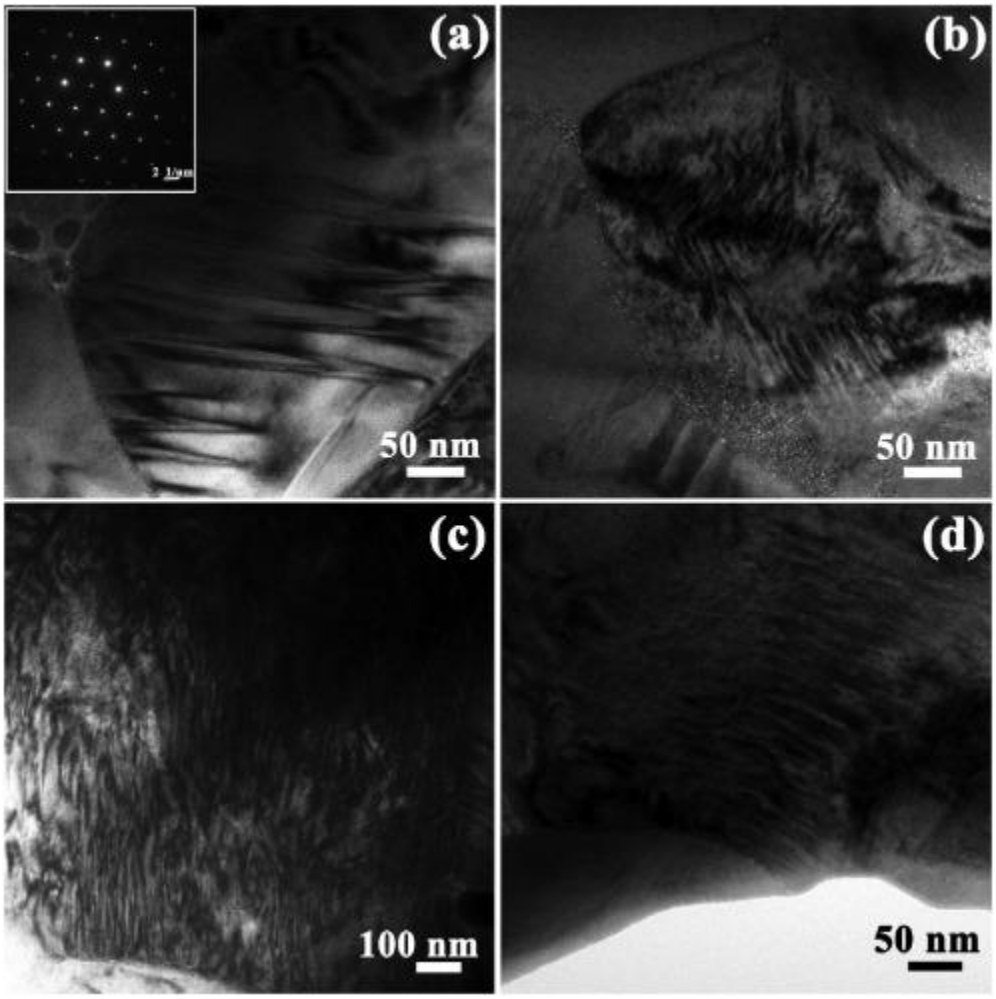

Figure 4: (a) Typical TEM bright-field image of the domain structure in single crystal PZN–PZT ceramic; (b)–(d) TEM bright-field images of nanodomains in 6 vol % Ag composite **[60]**.

Though recent research has been mostly focused on the development of piezoelectric materials with unique dimensionality, little research has been carried out with the goal of using

different dimensional combinations to enhance piezoelectric performances. Chngyeon Baek *et al.* have demonstrated how the combination of nanoparticles and nanowires can create a material with improved piezoelectric response [63]. They constructed a nanocomposite-based energy harvester with 4:1 wt ratio, and were able to generate a maximum open-circuit voltage and short-circuit current of 60 V and 1.1 μA respectively [63], which is a dramatic enhancement compared to nanogenerators based on either straight rods or particles [64].

While experimenting with the piezoelectric response of polyglycolide zinc ferrite incorporated PVDF composites, Ispita Chinya *et al.* demonstrated that the piezoelectric response of the composite was enhanced due to surface modification of the zinc ferrite (ZF) (Figure 5). Sol-gel prepared ZF nanoparticles with an average diameter of 50 nm were layered with polyethylene glycol (PEG-400, PEG-6000) and yielded outstanding results. This surface modification enhanced the proportion of the polar phase of 10 wt % ZF-PEG/PVDF up to 92% in the absence of poling treatment [65].

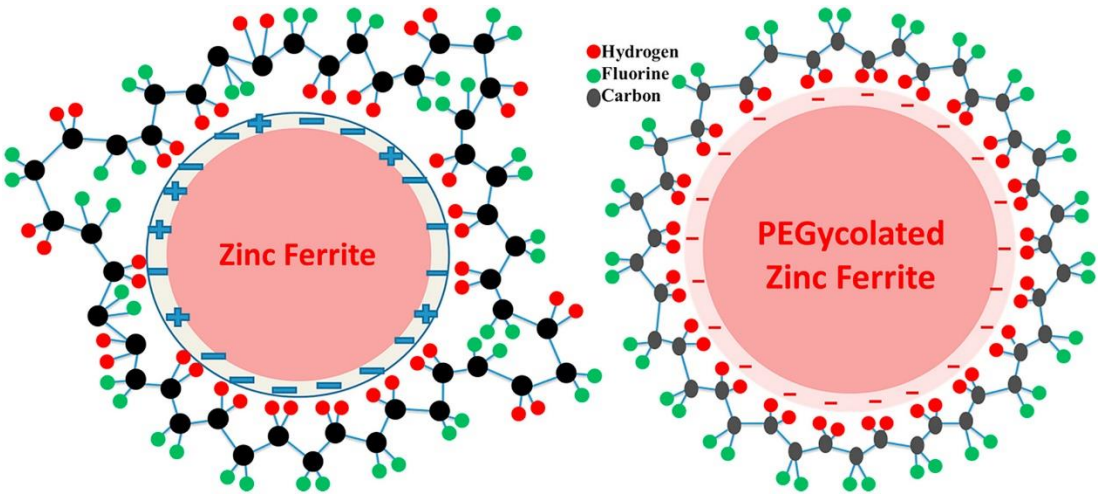

Figure 5: Proposed interaction between untreated and surface treated ZF with PVDF **[65]**.

The dried powder of ZF/PEG with ZF was characterized via FTIR spectroscopy. The FTIR spectra of PEG-modified ZF and untreated ZF are shown in Figure 6. The peak at about 432 cm^{-1} corresponds to the tetrahedral Zn-O bond stretching, and the peak at 555 cm^{-1} corresponds to the octahedral Fe-O stretching vibration in the body-centered cubic (BCC) zinc ferrite structure [66]. After the treatment with PEG, the peaks at 1625 cm^{-1} and 3405 cm^{-1}, correspond to water dehydration, were eroded. This also occurred due to the presence of extra -OH groups after glycolisation. The results of the FTIR spectrum indicate that the PEG completely covered the surface of the ZF and was robustly bound (Figure 6) [65].

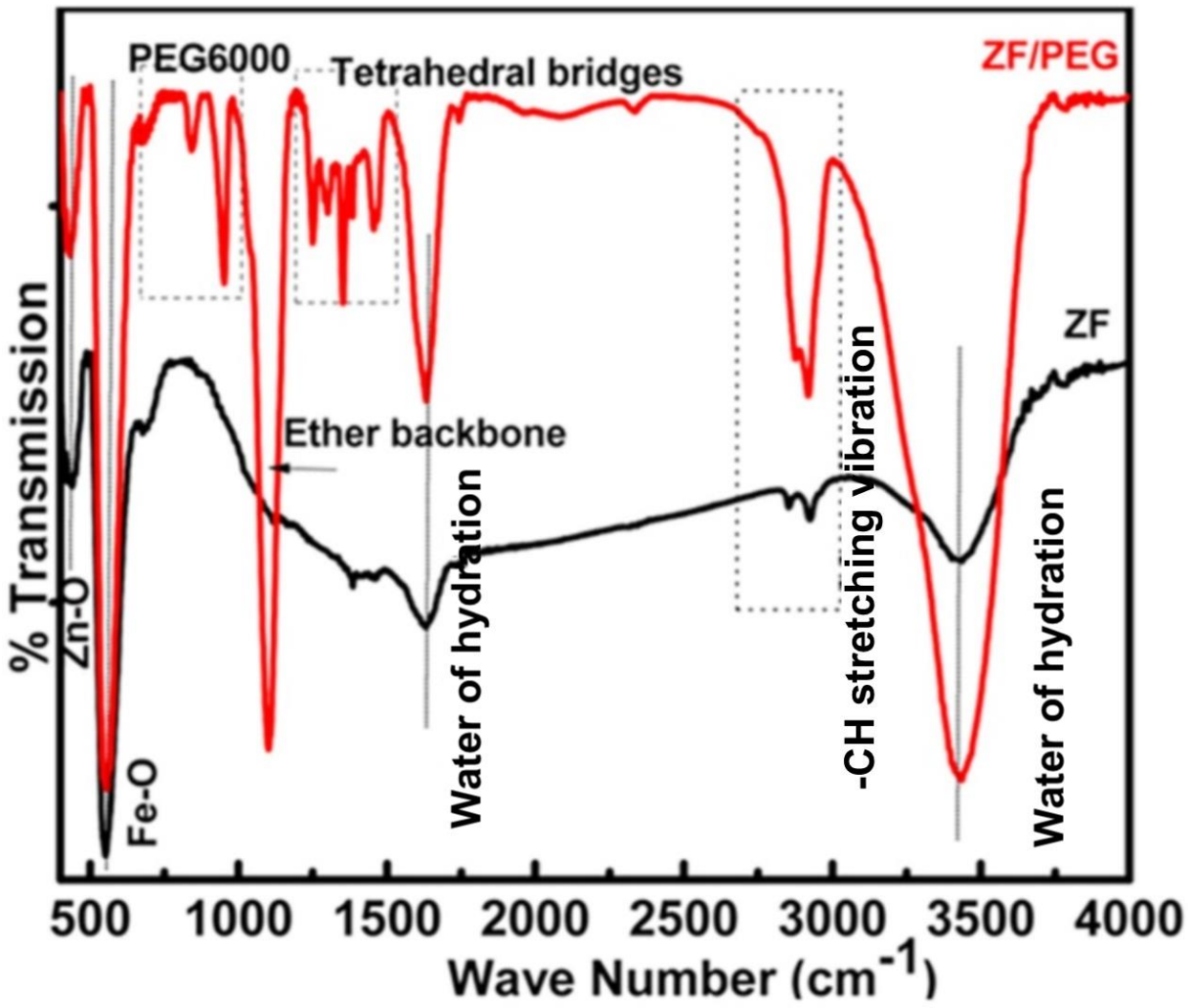

Figure 6: FTIR spectra of ZF and ZF/PEG powders **[65]**.

Nanogenerators were prepared with ZF/PEG-PVDF and ZF-PVDF films and characterized in terms of their dielectric constants (Figure 7). It is immediately evident that the surface modification of the nanoparticles enhanced the piezoelectric response of the nanogenerators [65].

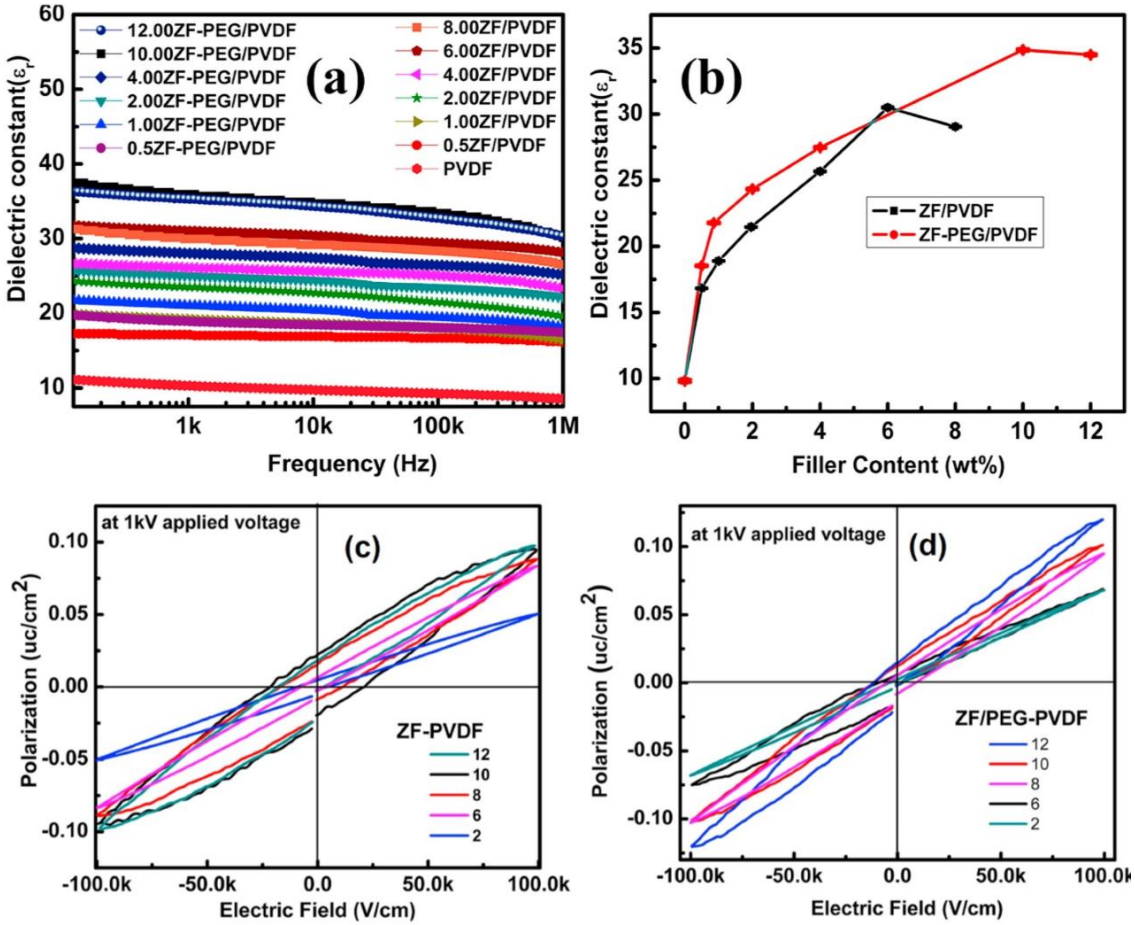

Figure 7. (a) Comparative dielectric constants, (b) increment in dielectric constant in the composite film with nanoparticle loading of ZF-PVDF and ZF/PEG-PVDF. (c) P-E hysteresis loop of ZF/PVDF (d) and ZF-PEG/PVDF composite (d) **[65]**.

Different percentage of the component can bring change in piezoelectric responses. Denis *et al.* have shown that a small percentage change in the multicomponent zero-dimensional system could bring a lot of changes in piezoelectric behavior. They have demonstrated the effectiveness of the difference of proportion with $(Na_{0.5}Bi_{0.5})TiO_3$–$xBaTiO_3$ (NBT–xBT)

prepared by ball-milling assisted solid-state reaction synthesis in the range of 4% ≤ x ≤ 13% [67].

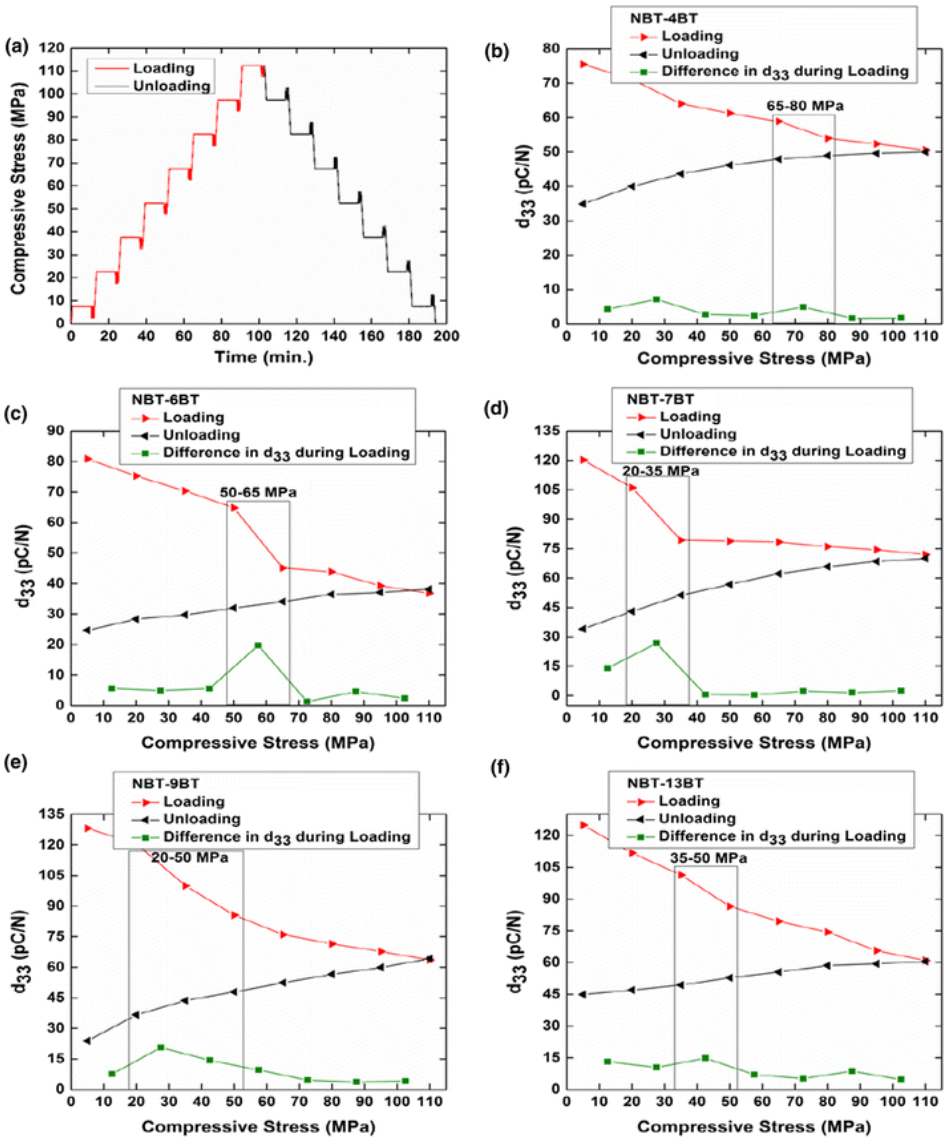

Figure 8: (a) The mechanical depoling sequence and corresponding graphs of decreasing piezoelectric coefficient (d33) as a function of applied mechanical pressure for different x value (b) 4% (c) 6% (d) 7% (e) 9% (f) 13% **[67]**.

NBT-xBT mechanical depoling sequence (in loading, unloading) is shown in Figure 8(a). The piezoelectric coefficient (d_{33}) value of NBT-xBT as a function of applied compressive stress is exhibited in Figure 8(b-f) in different compositions. The lowest depoling stress range (σ_d) was found in NBT-7%BT. This 7% is determined as the Morphotropic phase boundary (MPB). But it was also found that composition near MPB, materials undergo depoling at lower stresses. This implies that enhanced ferroelastic domain switching occurs in compositions near the MPB, which means that there is a strong correlation between compositions within the vicinity of MPB, piezoelectric properties and increased domain wall motion [67,68].

One-Dimensional Piezoelectric Nanogenerators:

Most nano-generator systems consist of One- Dimensional (1D) piezoelectric materials [44]. These 1D piezoelectric nanogenerators have nanostructural component's dimensions of less than 100 nm and lengths of more than 1 nm. One of the advantages of 1D piezoelectric nanogenerators is that they can be made in different configurations for different applications, including nanowires (NWs), nanobelts (NBs), nanosprings, nanorings, nanobows, and nanohelices [69]. Other advantages of 1D nanomaterials are: high surface area, low energy consumption and easier integration [70]. These 1D piezoelectric materials have been found to possess improved charge transfer characteristics as well as higher piezopotential compared to two-dimensional piezoelectric materials. Nanowires specifically have been found to possess three distinct advantages: high piezoelectric coefficient values, superior mechanical properties, and increased sensitivity due to better flexibility leading to better piezoelectric responses [44,71]. It was found that wurtzite structure and perovskite materials both acting as promising 1D Nanogenerator. However piezoelectric coefficient in wurtzite was found much lower than that of perovskite materials or polymer. But the unique properties of wurtzite lies in the advantages of

it's in use as a semiconducting device [70]. Defected 1D nanomaterials was investigated and found with a sharp peak in bandgap depending on localized bandgap. Which has great uses in practical field considering its specific electronic characteristics [72]. The different configuration has also been discussed by Yu *et al.* including simple, core-shell/coated, hierarchical/heterostructured, porous/mesoporous, hollow structured nanowires and discussed that different properties can be achieved through the use of different kinds of 1D nanomaterials [73].

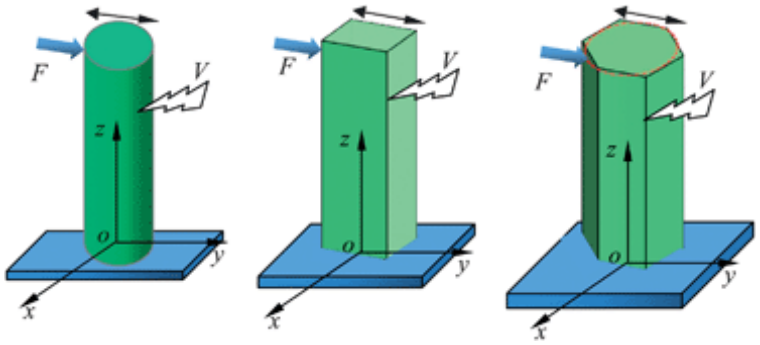

Figure 9. A schematic representation of one-dimensional piezoelectric nanogenerators **[44]**.

Because ZnO nanowire has significant mechanical strength compared to other materials, it is considered a promising piezoelectric material [74]. Other 1D materials like aluminum nitride (AlN) nanowires, PZT nanobars, and $BaTiO_3$ nanowires have also been investigated. But ZnO nanowires/nanotubes are still retaining an outstanding position among 1D nanomaterials for their high degree of ductility [44].

As only a few polymers have notable piezoelectric constants, PVDF has been the primary focus of polymer-based piezoelectric research. PVDF nanobars and nanowires have been shown to be viable sources of piezoelectric activity [3]. Cauda *et al*. have demonstrated that nano-confinement of PVDF as well as poly(vinylidene fluoride-trifluoroethylene) (PVDF-TrFE) in an

anodic porous alumina (APA) matrix yields a piezoelectric material that can act as an efficient harvester of electromechanical energy. Nanoconfinement was also demonstrated to encourage the preferential crystallization of both polymers into their ferroelectric β phase [75].Bao Liu *et al.* have experimented with lead-free $(Na_{0.5}Bi_{0.5})TiO_3$–$BaTiO_3$ (NBT–0.07BT) based energy harvester. (NBT–0.07BT) based nanogenerator was formed with perovskite structured nanofibers using electro-spinning technique combined with sol-gel method [76]. Characterization of these nanofibers with SEM, TEM, and XRD analyses revealed that the fiber diameter had been significantly reduced (500nm to 100-200nm) after annealing due to volatilization of the polymer (Figure 10 (a-d)). Surface roughness was also found to be increased due to the crystallization process (Figure 10 (c-d)). Figure 10(e-f) confirms the perovskite structure and the high crystallinity of the nanoparticles forming the fibers. A nanogenerator based on these NBT–0.07BT nanofibers was assembled as shown below in Figure 11(a). The NBT-0.07BT (BNT-BT) fiber was placed inside the PDMS matrix with an interdigital electrode. It was tested under an applied finger bending force (Figure 11(b, c)) with excitation frequencies of ~0.6 Hz and ~1.8 Hz, the results of which are presented in Figure 11 (d, e). Under a pressing frequency of 0.6 Hz an output voltage of 15 V was obtained. The output frequency increased with increasing pressing frequency. The maximum output potential of the nanogenerators was 30V with an output current of 80nA [76].

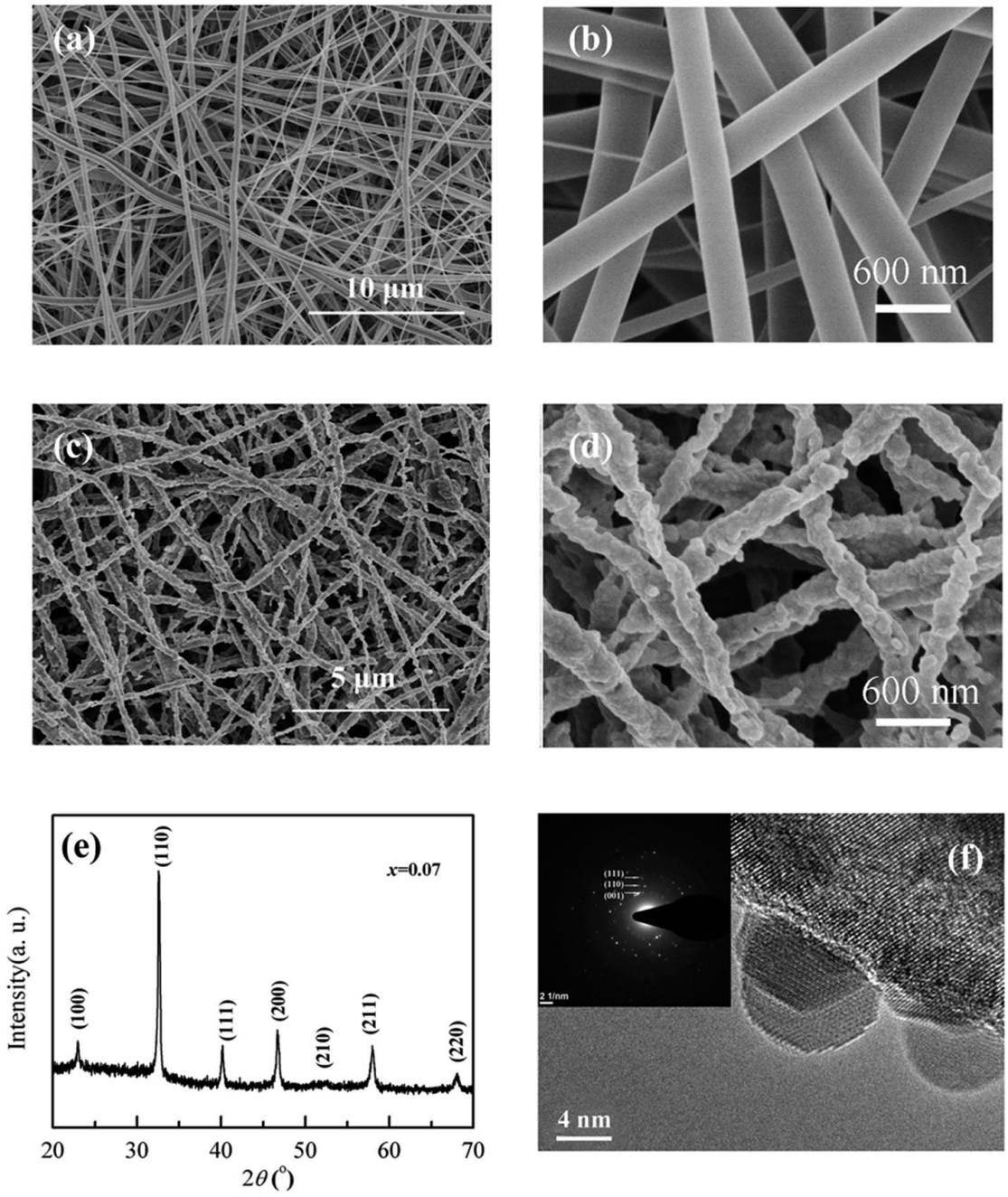

Figure 10. (a–d) The morphologies of the as-spun (a and b) and annealed (c and d) NBT–0.07BT nanofibers, (e) the corresponding XRD pattern of the NBT–0.07BT nanofibers in the 2θ range of 20–70°, and (f) the high-resolution TEM image of a portion of a nanofiber and the associated electron diffraction pattern (shown in the inset) **[76]**.

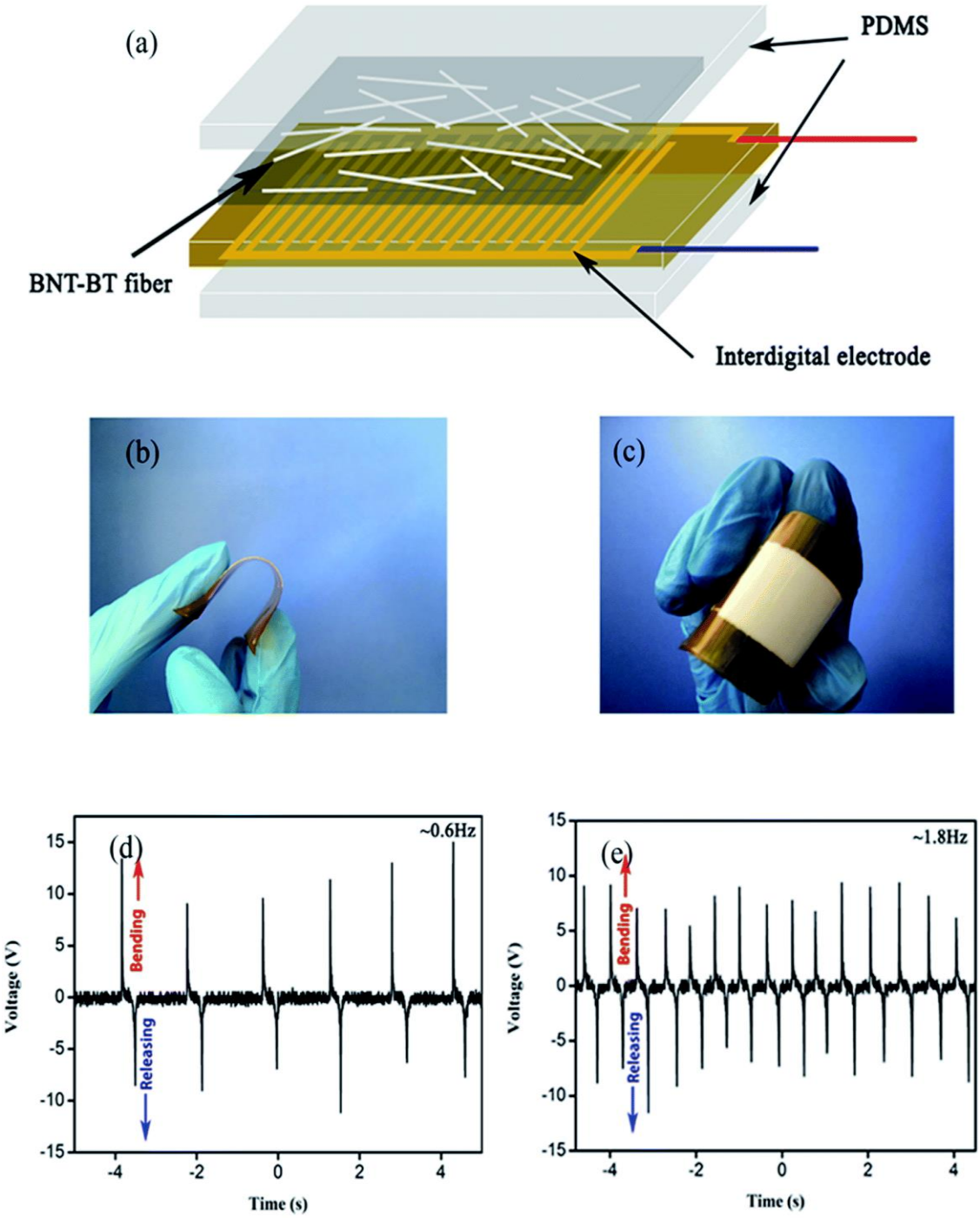

Figure 11. (a) The proposed structure of the flexible piezoelectric energy harvester, (b and c) photographs of the prototype device under bending conditions, and (d and e) the voltage output when the device was subjected to a periodic finger excitation **[76]**.

YongAn Huang *et al.* prepared piezoelectric nano/microfibers for a hyper-stretchable self-powered sensor with high stretchability, low detection limits, and excellent durability. It was experimentally shown that helical electrohydrodynamic piezoelectrical materials show improved piezo response as well as extra mechanical stimuli. Though this work is focused on the produced material's application as a sensor, it also demonstrates novel uses for piezoelectric materials in different geometric shapes [77]. The sensor was prepared (Figure 12) with self-similar PVDF fibers on a 100μm thick PDMS film in a helical geometry with a syringe pump. This was subsequently embedded with a metal electrode on an Ecoflex substrate. This helix structured PVDF polymer-based sensor showed extraordinary stretchability (up to 320%), low detection limits (0.2mg), and excellent stability under reciprocating deformation tests (1400 times at a stretching degree of 150%) [77].

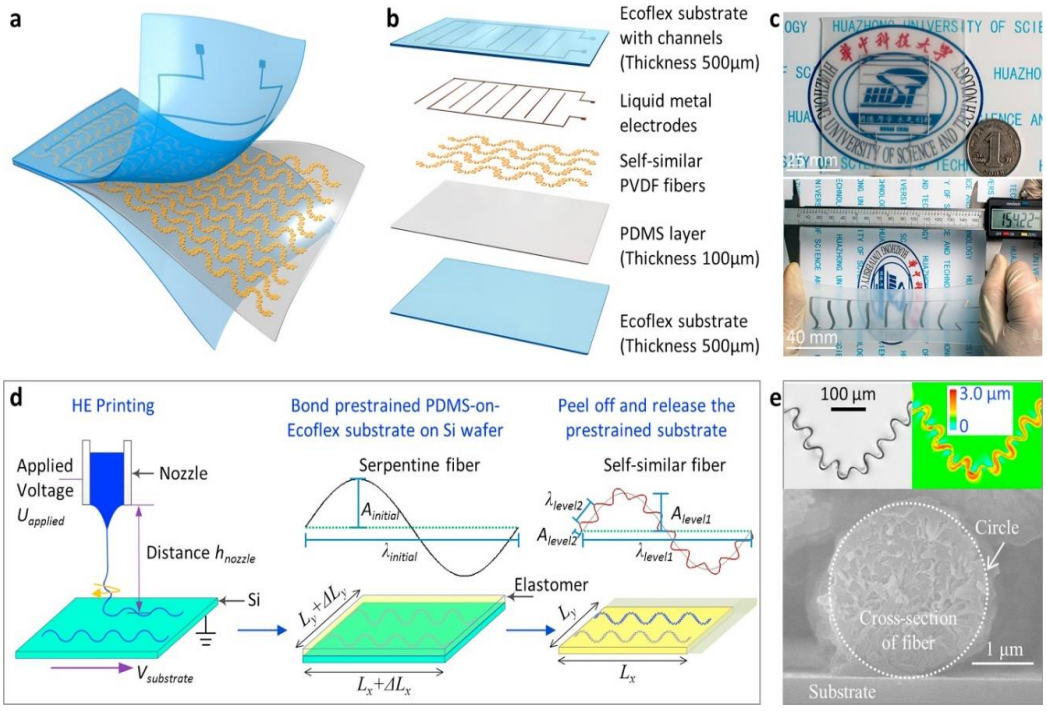

Figure 12. (a) Schematic diagram of the hyper-stretchable self-powered sensor Huang et al, (b) Schematic depiction of the hyper-stretchable self-powered sensor in a layer by layer format with description of each layer, (c) Images of the hyper-stretchable self-powered sensor and comparison between initial and stretched status, (d) Schematic diagram of self-similar nano/microfibers fabrication processes , (e) Laser Scanning Confocal Microscopy (LSCM) images of a self-similar nano/microfiber and SEM image of cross-section of the nano/microfiber **[77]**.

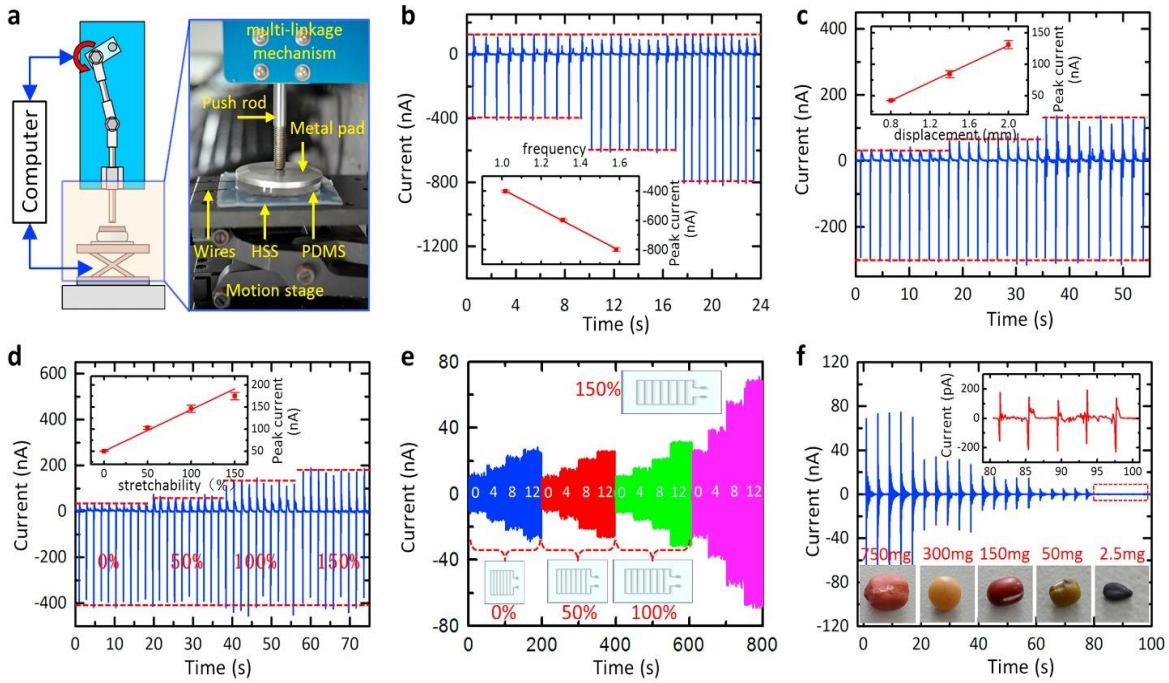

Figure 13. (a) Picture and schematic diagram of loading platform to test sensor by Huang et al., (b) Current output sensor subjected to lateral loading with the same amplitude (2 mm) and various frequencies (1.0 Hz, 1.3 Hz and 1.6 Hz) (c) Current output of sensor subjected to lateral loading with the various amplitudes (0.8 mm, 1.4 mm and 2 mm) and same frequency (1.6 Hz) (d) Current output sensor subjected to the same loading (0.8 mm) under different stretched status e) Current output of freestanding hyper-stretchable self-powered sensor subjected to various lateral loadings under different applied strains. For each tensile state of device, the displacement loadings are 0 mm (touchness), 4 mm, 8 mm and 12 mm, respectively from left to right, (f) Sensing of various grains, including peanut (~ 0.75 g), soybean (~ 0.3 g), azuki bean (~ 0.15 g), mung bean (~ 50 mg), and sesame (~ 2.5 mg). **[77]**.

Wang *et al.* demonstrated how different 1D materials could undergo different responses to stress. The group experimented with GaN nanorods, AlN nanocones, AlGaN nanocone, and InN nanocones with an AFM tip to induce stress on the piezoelectric materials and to measure

their response. It was found that all of these nanomaterials were producing a measurable response except for AlN, likely due to its high resistance [78].

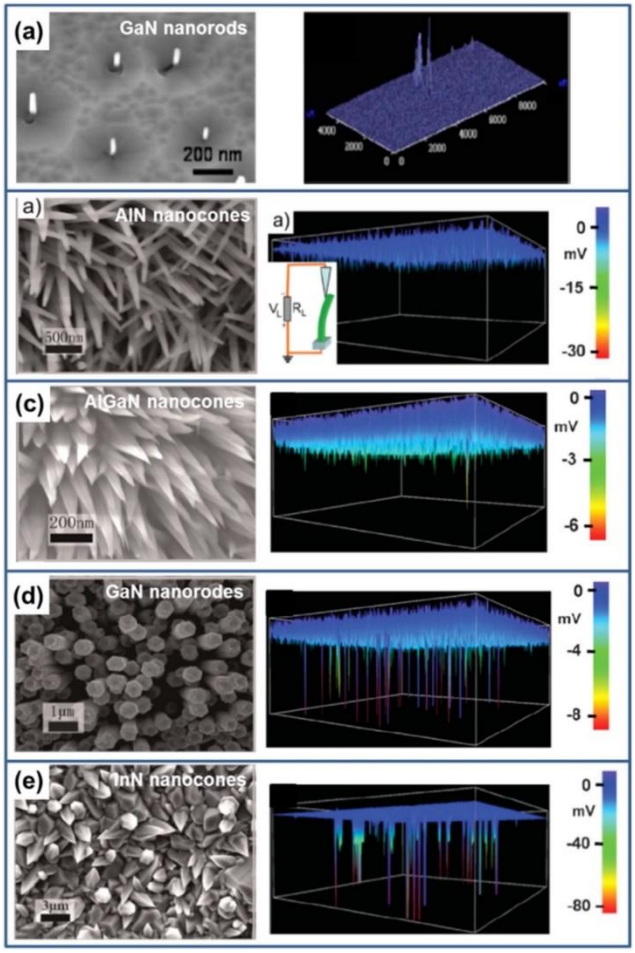

Figure 14. SEM images describing the morphology and output signal mapping of (a) GaN nanorods (b) AlN nanocones, (c) AlGaN nanocones, (d) GaN nanorods and (e) InN nanocones **[78]**.

Though there has not been much research conducted into how organic and inorganic piezoelectric materials interact with one another, Singh *et al*. demonstrated how ZnO nanorods can enhance the piezoelectric behavior of PVDF by increasing its β-phase up to a value of 76.1% without subjecting the material to polling. It was also demonstrated that a PVDF-ZnO (15 wt %) film exhibited a d_{33} value of approximately -1.17 pC N^{-1} [79]. This nanocomposite was formed by mixing hydrothermally grown ZnO nanorods with varying percentages of PVDF in DMF followed by drop casting the mixture on clean glass substrates. The produced film was characterized via X-ray diffraction (XRD) and Fourier transform infrared (FTIR) spectroscopy, and it was found that the proportion of the β-phase increased with increasing amounts of ZnO. The produced material was tested as a nanogenerator by e-beam evaporation and deposition of a conductive layer on two sides of the film followed by impact of this substrate with a cylinder of a diameter of 1cm with a constant force of ~15 kPa; the material's response to stress is presented in Figure 15 [43]. The 15 wt % ZnO-loaded PVDF nanocomposite film produced nearly 1.81 V and a short circuit current of 0.57 μA. It also produced an instantaneous output power density up to 0.21 $\mu W/cm^2$, with a load resistance of 7 MΩ. This clearly shows the enhancement of the piezoelectric response of the nanocomposite material compared with bulk PVDF [79].

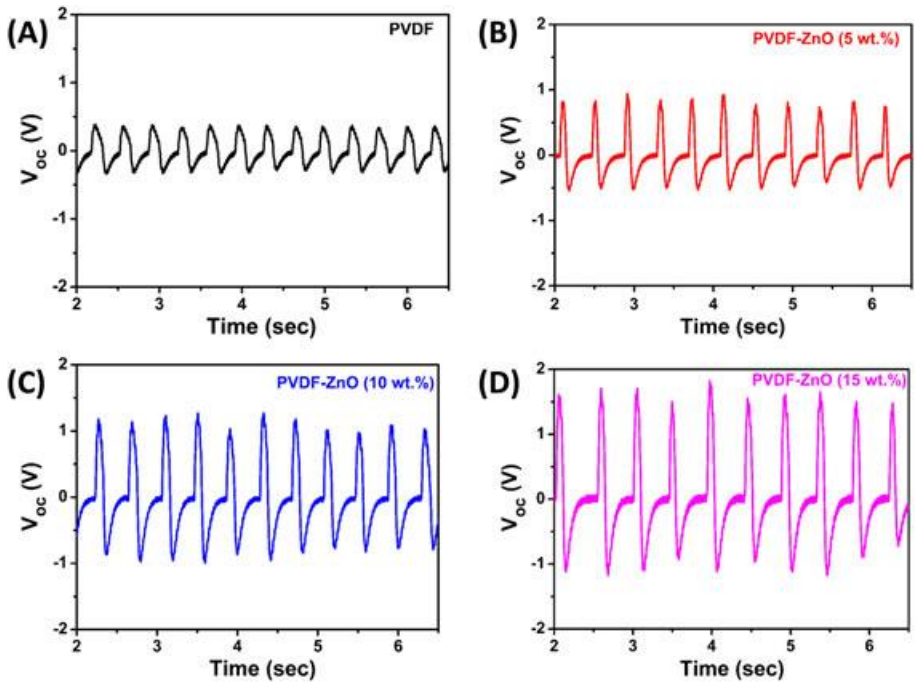

Figure 15. VOC generation from (a) polyvinylidene fluoride (PVDF), (b) PVDF-ZnO (5 wt%), (c) PVDF-ZnO (10 wt%), and (d) PVDF-ZnO (15 wt%) thin films by repeated hitting **[79]**.

Nanocomposite composed of micropillar and polymer has also experimented. Chen *et al.* have shown that P(VDF-TrFE)/$BaTiO_3$ nanocomposite micropillars have an outstanding electrical and mechanical performance compared to P(VDF-TrFE) bulk film. PVDF-TrFE/$BaTiO_3$ micropillar nanocomposite was formed by molding and pressing action to form micropillars followed by layering with PDMS thin layer. Morphology and structure of nanopillar arrays are shown in the SEM images reported in Figure 16 [80].

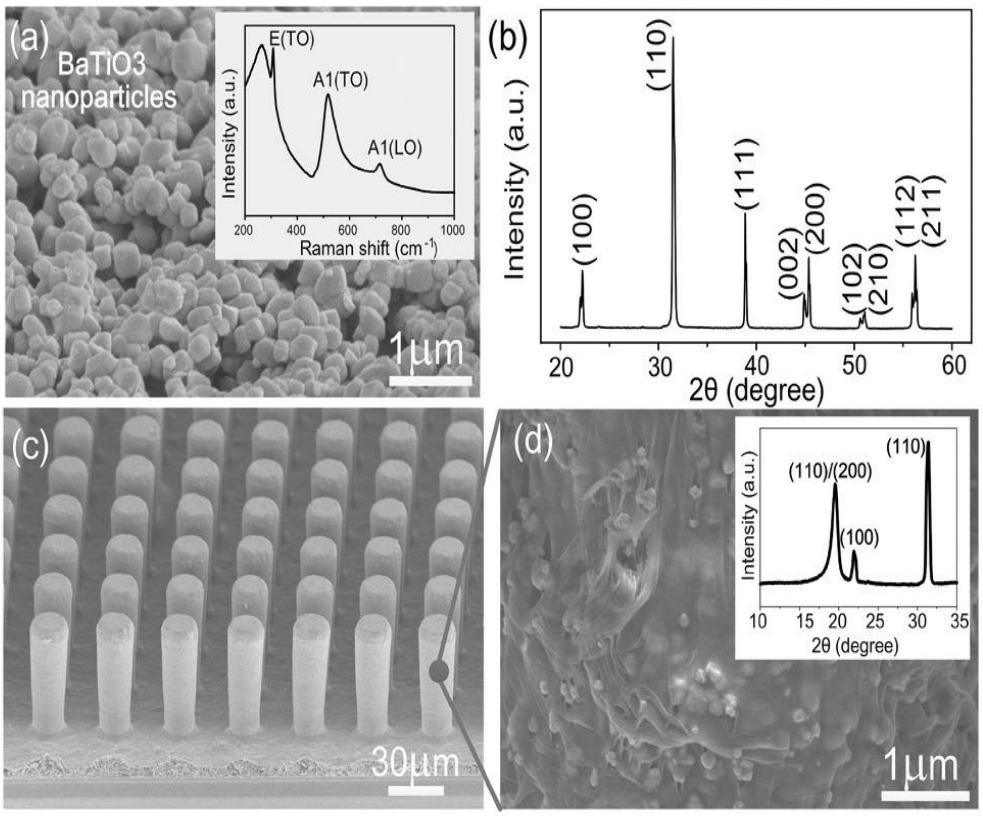

Figure 16. (a) SEM image of BaTiO3 Nanopillars. Raman spectrum of the micropillar pattern of the BaTiO3 NPs (inset), (b) XRD patterns of BaTiO3 NPs, (c) SEM image of PVDF-TrFE/BaTiO3 nanocomposite micropillar array, (d) The magnified view of SEM image of the micropillar arrays. The XRD spectrum of nanocomposite (inset)

The nanocomposite nanogenerator was later tested with vertical presses. The enhanced voltage of 13.2V and a current density of 0.33μA cm^{-2} were found. Switching the polarity test also confirmed the enhanced performances of the nanocomposites. The nanogenerator was also tested with different frequency of load and showed a mechanically stable result [80].

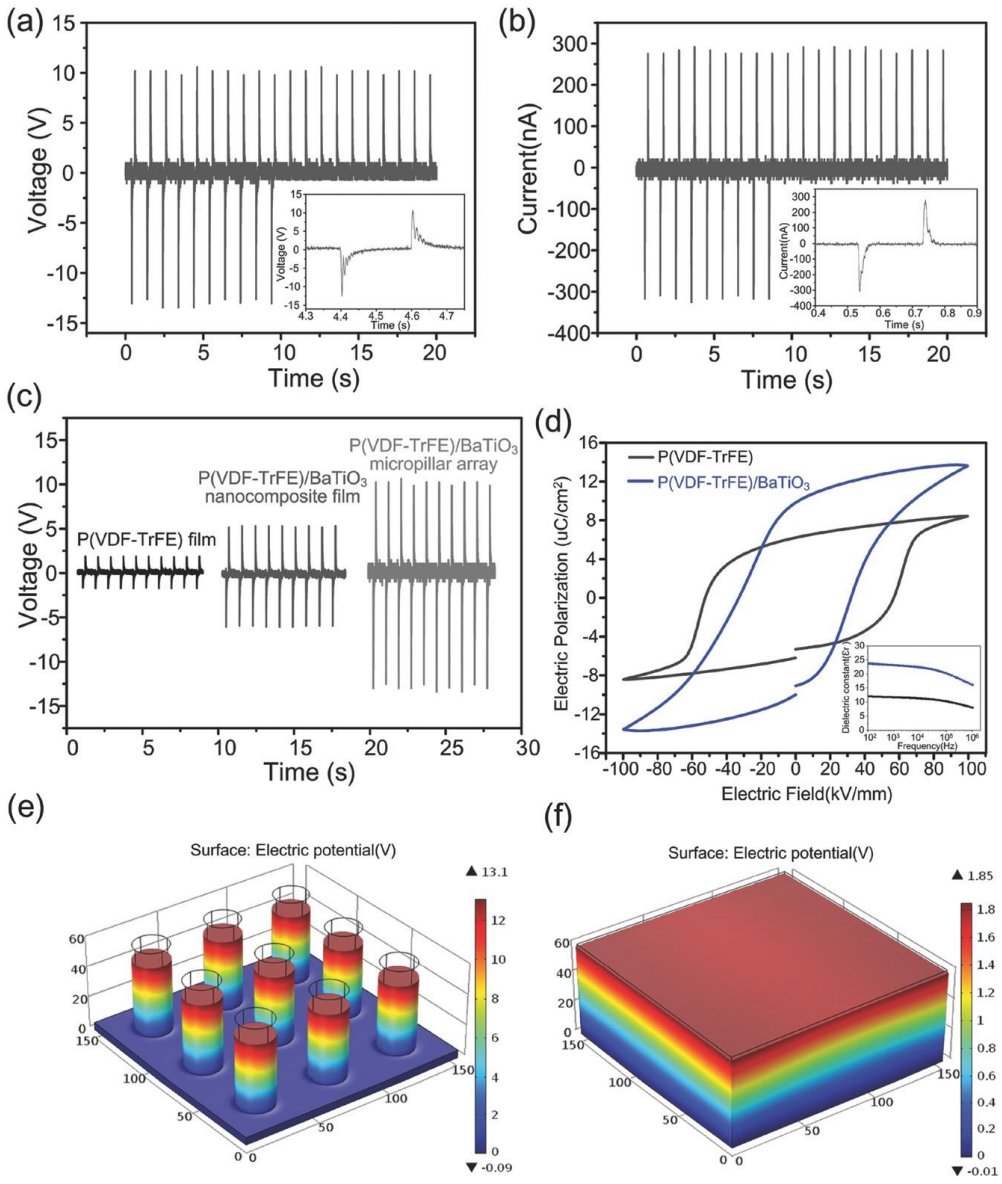

Figure 17. (a,b) Output Voltage and current of device under stresses; (c) A comparison of output voltages for the piezoelectric devices based on P(VDF-TrFE)/BaTiO3 micropillar array, P(VDF-TrFE)/BaTiO3 nanocomposite film and for a bulk P(VDF-TrFE) film, (d) P–E loops of P(VDF-TrFE) film and P(VDF-TrFE)/BaTiO3 nanocomposite film. ε value of P(VDF-TrFE)/BaTiO3 nanocomposite film and P(VDF-TrFE) film(inset) (e,f) Simulation result of the generated piezopotential distribution of two unit blocks, as obtained for **[80]**.

Dahiya *et al*. have demonstrated one-dimensional ZnO encapsulated in parylene C polymer matrix produced excellent results of open circuit voltage ≈10 V, short circuit current density ≈0.11 μA cm^{-2} with relatively higher peak power of ≈3 μW [81].

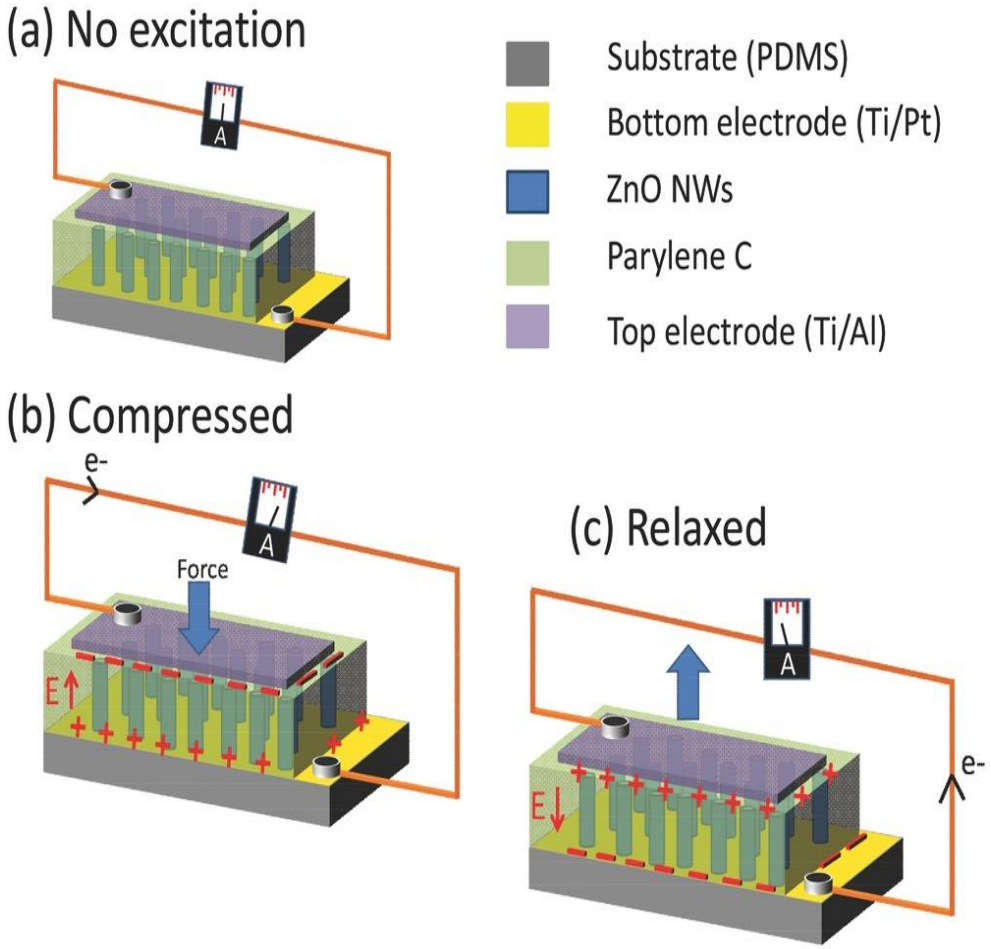

Figure 18: The working mechanism of the fabricated nanogenerator devices: a) No external force. b) The piezoelectric-induced flow of the electrons through external compressive force from the top. c) reverse electron flow with the relaxation of the force **[81]**.

ZnO nanowire was grown in Ti/Pt layer on PDMS substrate by hydrothermal following by seeding through a sputtering technique. Later Parylene C deposition on ZnO nanowire was

achieved by vapor-phase deposition process utilizing three-stage deposition systems (sublimation, pyrolysis and polymerization) [81].

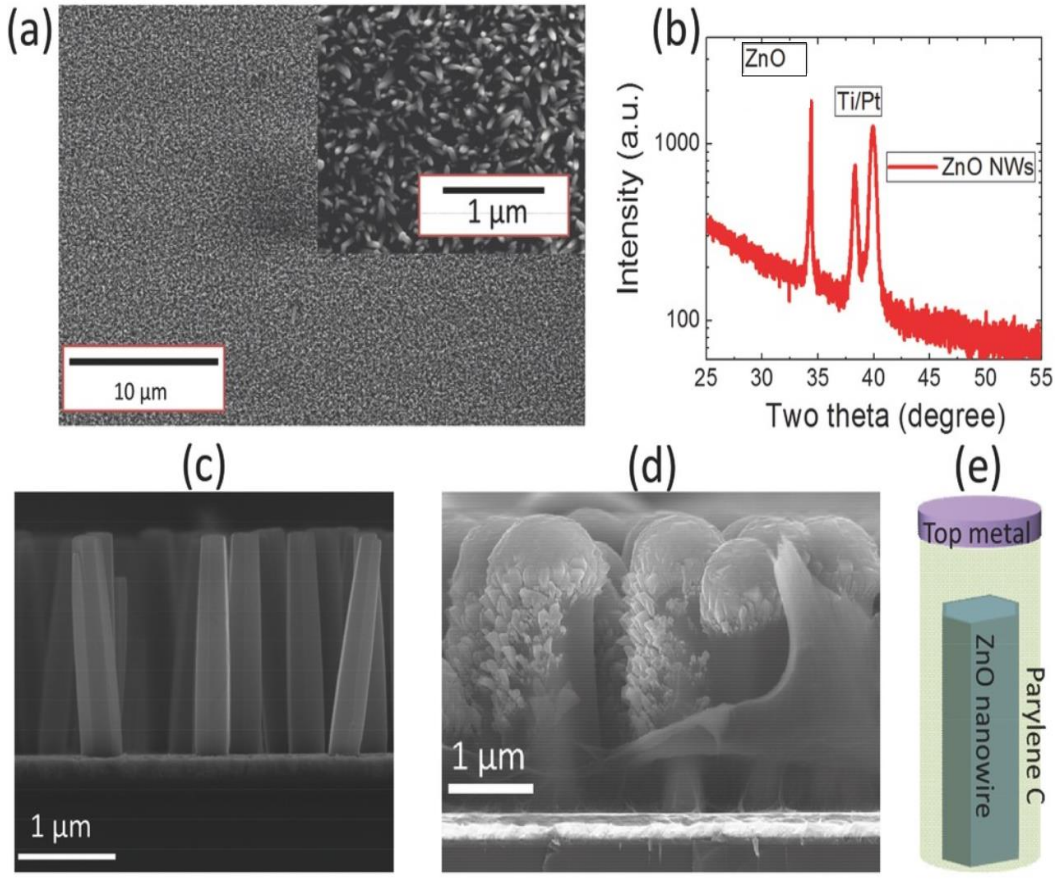

Figure 19: a) SEM image of NWs grown on PDMS. The inset shows the high-magnification SEM image. b) XRD pattern of ZnO NW on Ti/Pt c) and d) SEM cross-sectional views of NWs grown on silicon before and after parylene C/metal deposition. e) Schematic representation of ZnO-parylene nanocomposite **[81]**.

Prepared Piezoelectric nanogenerator as integrated in the back of a flexible bankcard to test device performances (Figure 20). 13N force with 5Hz frequency was applied in an area of

8cm^2. The device showed a rise in voltage output (27 V) with a fall in current output (11 µA) with an increase of load resistance [81].

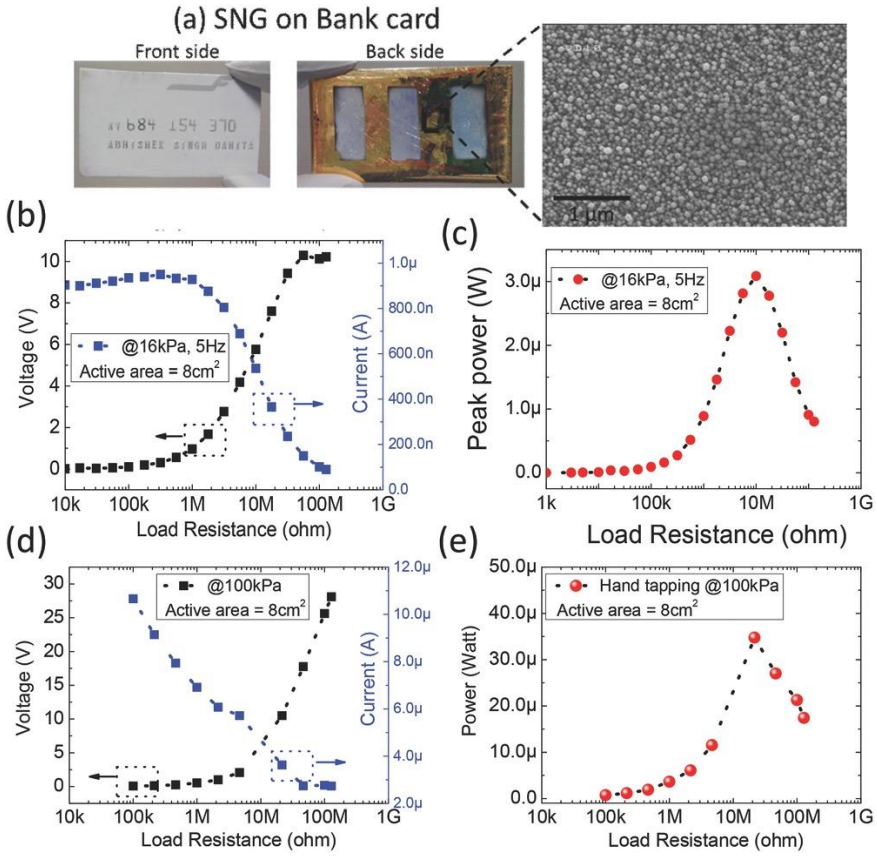

Figure 20: Electric output from large nanogenerator device fabricated on typical bank cards: a) Picture of the bank card and fabricated device at the back side of it. SEM image showing the as-grown ZnO NWs. b) Voltage and current output as a function of load resistance at 16 kPa of applied compressive pressure. c) Peak output power vs. load resistance d) Voltage and current amplitude vs. load resistance at 100 kPa of applied stress. e) Peak output power as a function of load resistance conforming to the hand tapping **[81]**.

The device was later wearable tested by attaching it with the middle of the index finger. The device produced open circuit voltage with bending (positive) and releasing (negative) of the finger [81].

Bisiorek *et al.* made some comparative studies of similar organic-inorganic hybrid materials with 1D anionic structures of $(C_3N_2H_5)[BiCl_4]\cdot H_2O$ (PAC) and $(C_3N_2H_5)[SbCl_4]\cdot H_2O$ (PBC) and showed that a very little change can bring a significant favorable or unfavorable change in piezoelectric properties. Figure 21 shows the dielectric properties comparison of PAC and PBC [21].

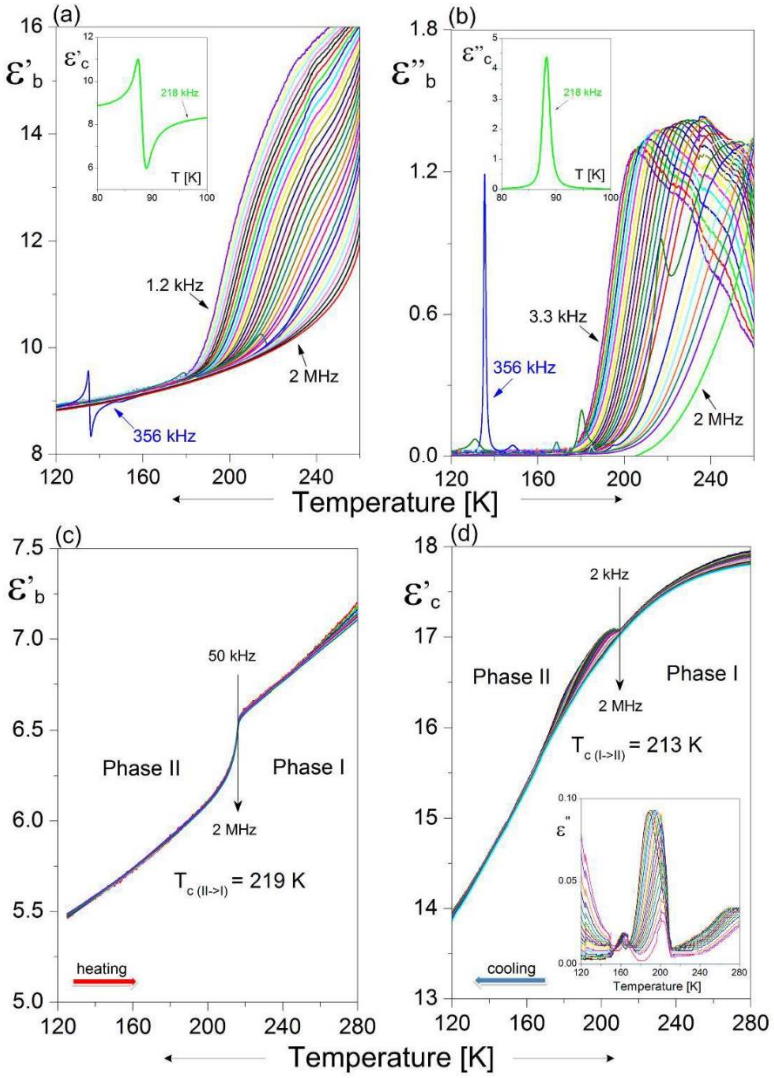

Figure 21: (a-b) Real, ε', and imaginary, ε'' with respect to temperature change, parts of the complex electric permittivity of PAC along with the b-axis; (c-d) Temperature dependence of the real part ε' the complex electric permittivity of PBC crystals along the b- and c-axis **[21]**.

Anomalies of ε' and ε" curves at greater than 200 kHz (Figure 21(a-b)) are found more desirable because of accentric symmetry. They also demonstrated that in 190-230K temperature range contains clear relaxation process in the kilohertz frequency region. For PBC (Figure 21(c-d)) it was found with significant dielectric anisotropy because the dielectric response is radically different along b- and c- direction. In 219K ε' for PBC is found with a step-like an anomaly, which confirms the unfavorable piezoelectric properties of PBC.

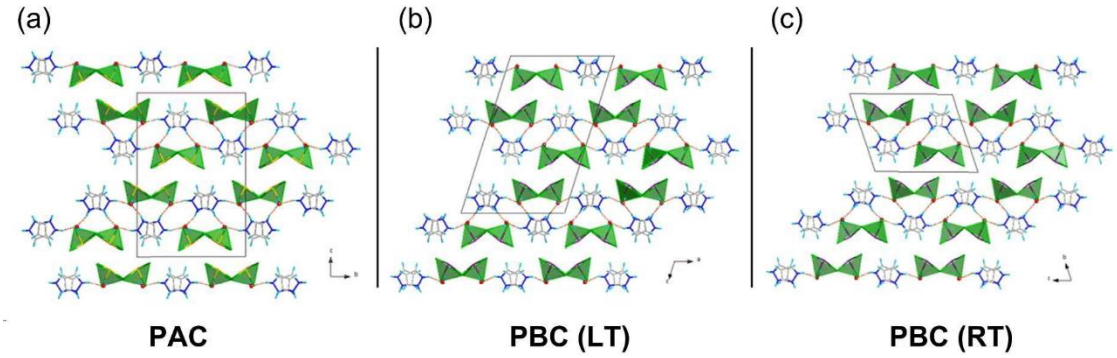

Figure 22: Crystal structure of (a) PAC (100 K) along the a-axis, (b) PBC (100 K) along the b-axis and (b) PBC (240K) along the a-axis **[21]**.

It was found that though both PAC and PBC has almost the same molecular arrangement (Figure 22), their crystal structures are determined by piezoelectric and ferroelectric properties of the materials. PAC shows similar molecular arrangement along a-, b- and c- axis through a large temperature range. While PBC showed a phase transition at 219K along with a- axis, this phase transition is responsible for the change of dielectric constant. Hence PBC shows anomaly for piezoelectric behaviour [21].

Two-dimensional piezoelectric nanogenerators

Two-dimensional (2D) piezoelectrical materials are promising components of nanogenerators due to their typically high electromechanical coupling [82]. They have also garnered interest due to their high roughness factors and large exposed polar basal planes which often lend them better energy efficiency than the more common 1D piezoelectric structures, unique electrical, optical, mechanical and thermal properties, which does not exist in their bulk counterparts [83,84]. Their enhanced energy efficiency can also be partially attributed to their ability to withstand large deformations and generally enhanced nanoscale properties [85]. Moreover, 2D materials are strong, flexible, easier to be analysed at the atomic level, easy to be co-integrated with other materials or electromechanical systems which makes itself a better piezoelectric nanogenerator [86] .

Ahmed Almusallam *et al.* have demonstrated recently that the incorporation of pressed silver nanoparticles in a film like structure in composite materials on flexible plastic and textile substrates can result in a significant increase in the d_{33} value of nanocomposites. This improvement also occurs without the loss of output voltage [87].

Snghoon Park *et al.* have shown that energy efficiency, as well as sensitivity, can be largely increased in the way of application of tensile stress. This clearly indicates that high stress alone cannot provide high energy, but the vertical stress to already stressed surfaces is required. It was also found that free-standing thin film piezoelectric materials have higher energy conversion efficiencies than any other omnidirectional nanogenerator morphologies [88]. Tang Y. L. *et al.* have shown that a ZnO/silicon monoxide bilayer nanofilm can serve as a dependable nanogenerator active layer due to its superior mechanical and chemical properties [89].

While working with polyvinylidene fluoride hexafluoropropylene (PVDF-HFP) and PVDF-HFP/Co-ZnO nanofibers fabricated by electrospinning, Parangusan *et al.* showed that the percent ß phase of polymer, dielectric loss, as well as dielectric constant, largely increases with the increase of the percentage of Cobalt doped Zinc Oxide in nanocomposite film. However, the increase was noticed until the percentage of Co-ZnO reached up to 2%. The nanocomposite film reached a voltage of 2.5V with 2% Co-ZnO [90]. Guo *et al.* also have demonstrated that PVDF fibre on conductive fabric can reach a voltage up to 80V. He also tested PVDF fibre on conductive fibre with triboelectric action with silk fibroin fibres. This hybrid action of (piezo-tribo) reached up to 500V and 12 µA [91]. While most of the piezoelectric nanogenerator has been tested with dual electrode method, Wang *et al.* have demonstrated that single electrode method for electrospun PVDF nanofiber composite film would result in easy sensing of load and release because of steady state sensing of stress while double electrode method appears in pulsing signal. He demonstrated his work with Moravec's paradox which says low-level sensorimotor skills are more difficult than high-level reasoning in artificial intelligence and robotics. It was exemplified by human body nature of single electrode sensing [92].

Jin-Ho Kng *et al. have* experimented on transparent and flexible piezoelectric nanogenerator based on GaN (Figure 23). GaN was grown via metal-organic chemical vapor deposition followed by an electrochemical etching process because of its high selectivity on the electrical conductivity of GaN layer rather than chemical constituent [93].

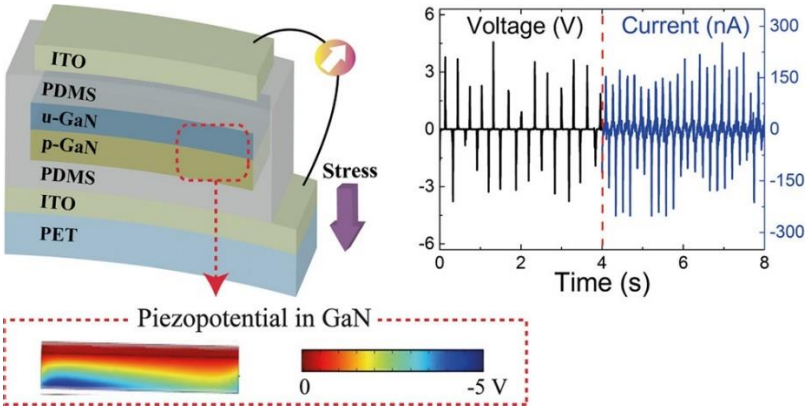

Figure 23. Nanogenerator based on a GaN membrane and its piezoelectric response to ~182 mN force prepared by Kng et al. **[94]**.

Two layers of GaN are generated from these processes, a bottom n-GaN layer, and a top u-GaN layer. The bottom layer of GaN (doping concentration(n) = 2×10^{18} cm^{-3}, 200 nm thick) provided enhanced lateral current flow while the upper layer of GaN was found to be highly n-doped (n^{+}-GaN, doping concentration(n) = 8×10^{18} cm^{-3}, 400 nm thick). This was achieved by growing p-doped GaN p doped-GaN, uniformly doped-GaN to form p-n junctions in the p-n junction, followed by photolithography and chlorine-based reactive ion etching to expose sidewalls in the bottom layer of GaN and open vias with diameters ranging from 4 to 90 μm (Figure 24-(b,c)). After removal of the deposition substrate, the bottom layer of the p-n junction was transferred onto polydimethylsiloxane (PDMS, 2 μm), and sputter coated with indium tin oxide (ITO, 300nm) on a PET substrate (PET, 188 μm) (Figure 24d).

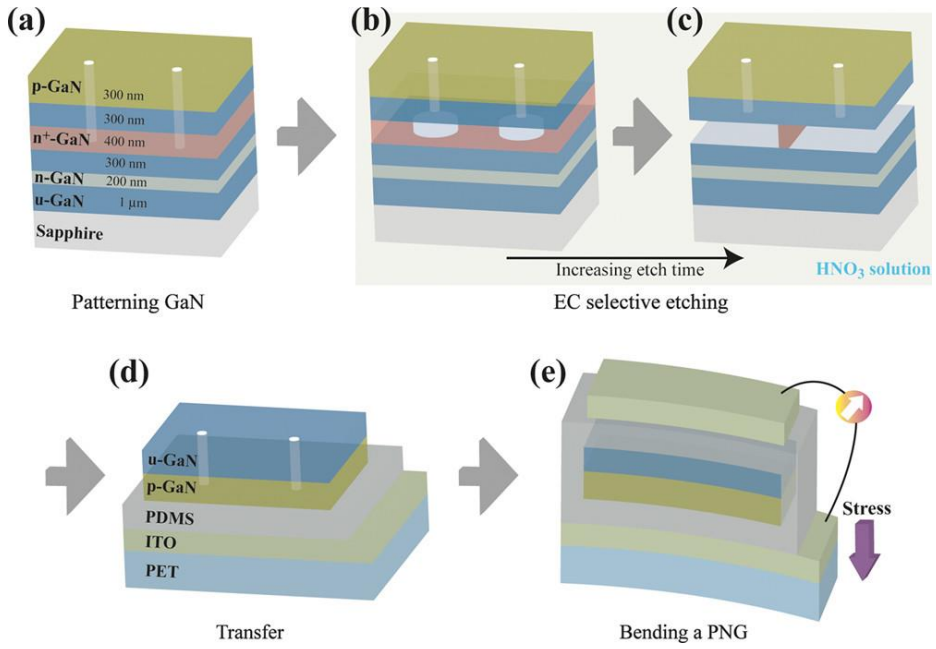

Figure 24. Schematic representation of GaN-based NG fabrication: (a) Patterning GaN structures to expose the sacrificial layer (b) selective electrochemical etching of the sacrificial layer in nitric acid, (c) the loosely bound GaN membrane due to nanoscale etching residues, (d) shifting the GaN membrane onto an ITO/PDMS-coated PET substrate, and (e) electrical output due to stress application **[94]**.

The piezoelectric response of the produced nanogenerator was measured under finger force (~182 mN). As the thickness of the GaN layer was 600 nm, tensile and compressive stresses along lateral and vertical directions resulted in a vertical piezoelectric polarization as shown in the COMSOL simulation result (Figure 25b). The resulting piezoelectric output voltage and current values of 4.2 V and 150 nA, respectively, were measured. P-GaN is responsible for the high output voltage and reduced junction current due to its high resistivity. Further improvement of this nanogenerator architecture to decrease the possibility of unexpected Mg

activation of p doped -GaN which may have occurred during processing and might contribute to the observed fast decay of the output voltage [94].

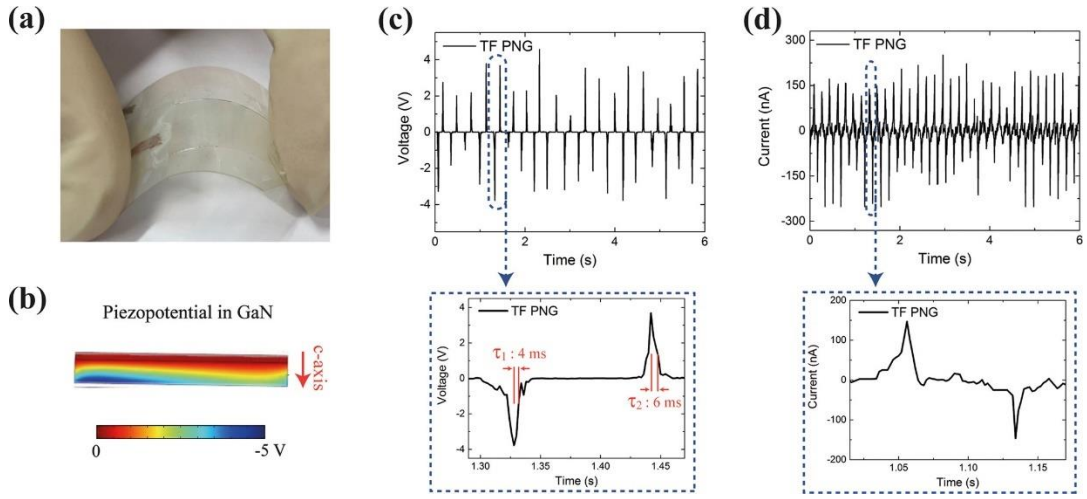

Figure 25. (a) NG prepared by Kng et al, (b) COMSOL-simulated voltage output of NG on two tip (c) piezoelectric output voltage on bending the NG, magnified view of the output voltage (bottom panel) and (d) current output on bending the NG magnified view of current output (bottom panel) **[94]**.

P-GaN is the reason for high output voltage and reduced junction current for its high resistivity. Though this nanogenerator seemed to work perfectly, the improvement opportunity remained in processing to decrease the possibility of unexpected Mg activation of p-GaN which may have occurred fast decay of output voltage.

Kuntal Maitay *et al.* have experimented with a two-dimensional piezoelectric MoS_2 modulated nanogenerator/nanosensor based on PVDF nanofiber webs. The team also prepared a sandwich like piezoelectric nanogenerator [95]. MoS_2 incorporated PVDF nanosheets was prepared [96] [97]. To prepare these MoS_2 incorporated PVDF nanosheets, MoS_2 was exfoliated by addition of 8 mg ml^{-1} MoS_2 to a DMF/brine (3:1) solution followed by stirring and sonication.

After completion of exfoliation, the mass was extracted into ethyl acetate and dried by nitrogen bubbling. It was again re-dispersed in DMF to achieve homogenization by sonication and stirring.

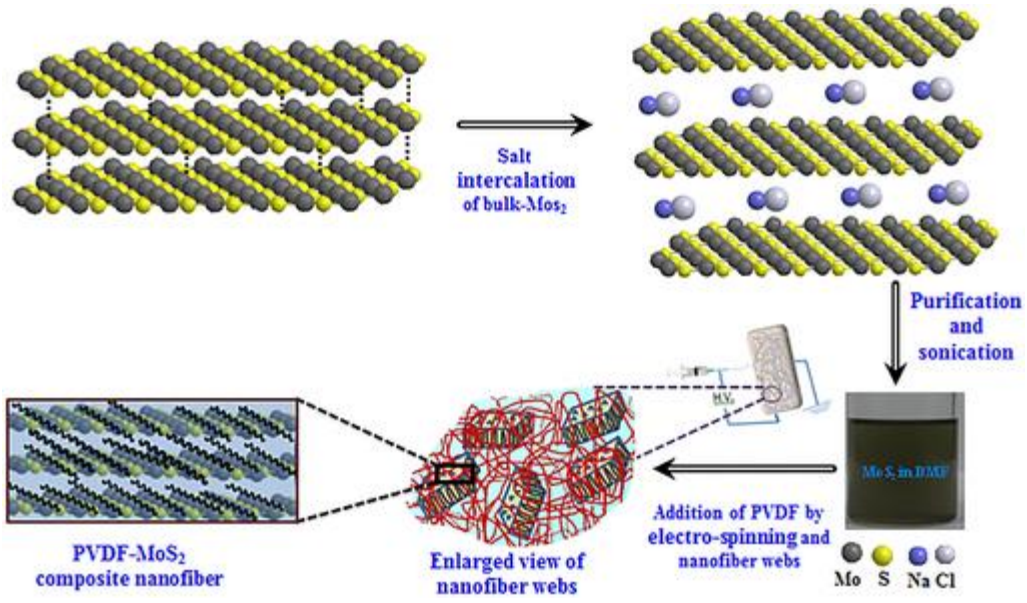

Figure 26: Representation of MoS2 nanosheets dispersion in DMF and the preparation of the PVDF-MoS2 composite nanofiber by Maitay et al. **[98]**.

This piezoelectric nanogenerator was tested with a lightweight material (leaf, 0.68g) dropped from different heights (30 cm, 25 cm, and 20cm). It was also tested with an even lighter matchstick (0.09 mg). Responses were graphed as time vs. voltage (Figure 27). This showed a linear response towards impact intensity; thus, it was determined that the nanogenerator was very much sensitive. It was also capable of generating up to 14V on human touch. The response of the nanogenerator was also tested when subjected to recordings of different English letters; Figure 28 shows the differing responses of the nanogenerator to individual letters. Though this study focused on the piezoelectric nanogenerator's response to determine the usefulness of the material

in a nanosensor role, it can be inferred that a high degree of energy can be harvested with this material, leading to a power density up to (16 nW cm^{-2}) [98].

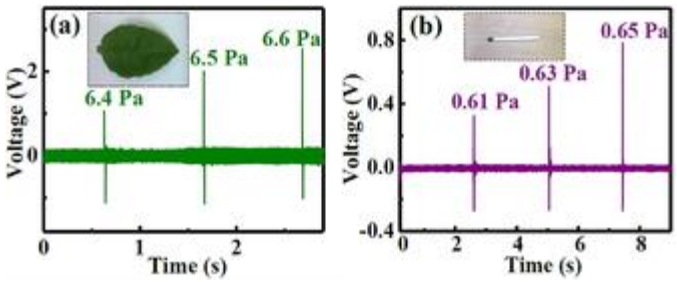

Figure 27. Voltage produced by NG due to different stresses **[98]**.

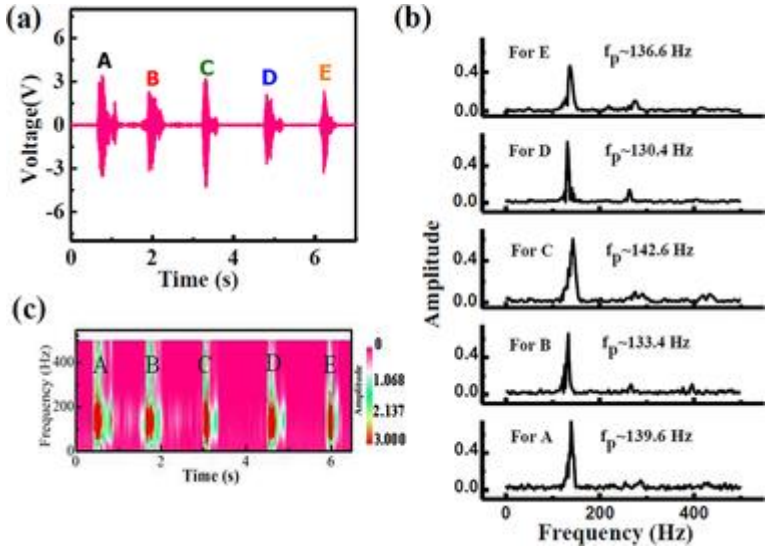

Figure 28. (a) The voltage output of NG as different letters (A, B, C, D, and E) are pronounced, (b) The corresponding fast Fourier transform (FFT) processed frequency spectrum and (c) FFT-processed time-dependent spectrogram (the right side color scale bar denotes the amplitude) **[98]**.

Another study on MoS_2 have been conducted by Han *et al.* They have demonstrated that sulfur vacancy passivated monolayer of MoS_2 has better piezoelectric response compared to MoS_2. This is because the vacancy passivation reduces the charge-carrier density of the

monolayer MoS_2 surface, thus the screening effect of piezoelectric polarization charges by the free carrier is significantly prevented. This passivated MoS_2 is prepared by S treatment (H_2S gas flowing over the subject at 1000°C) of pristine MoS_2 (prepared by chemical vapor deposition method) [99].

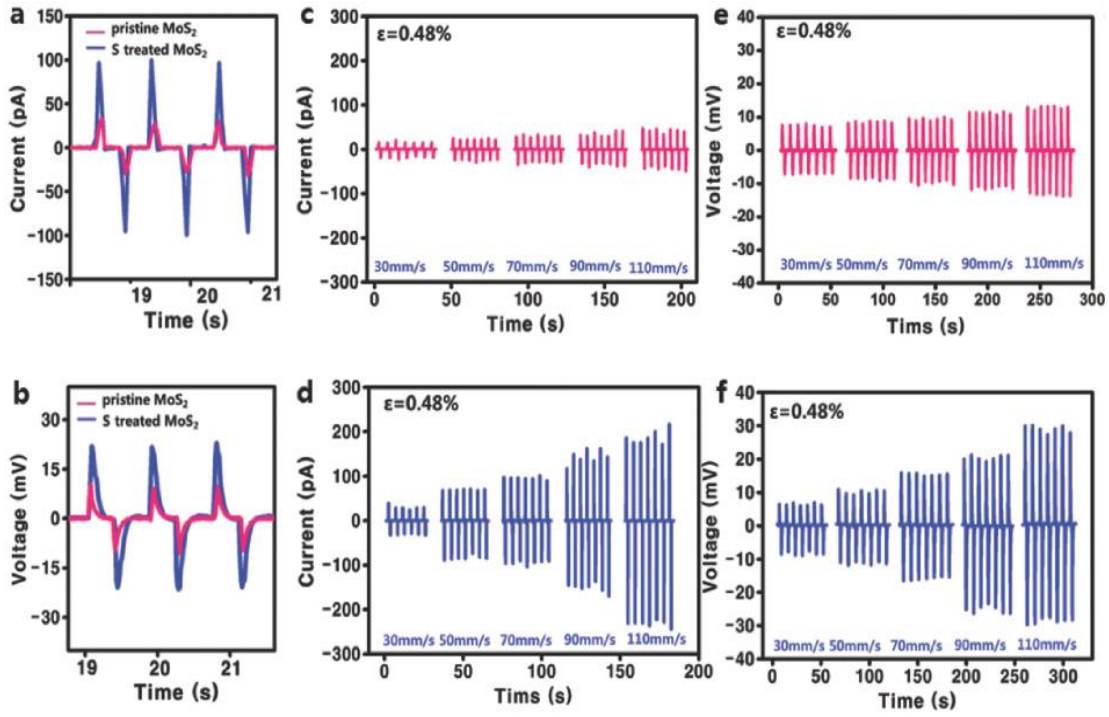

Figure 29: a) Output current difference between the pristine and S-treated monolayer MoS2 NGs.. b) Output voltage difference between the pristine and S-treated monolayer MoS2 NGs. (c) and (e) current/voltage variation of the pristine (untreated) monolayer MoS2 PNGs under 0.48% fixed strain, and different strain rate condition. (d) and (f) show current/voltage variation of the S-treated monolayer MoS2 NGs under 0.48% fixed strain and different strain rate condition **[99]**.

Figure 29 illustrates the comparative piezoelectric output of pristine MoS_2 and S treated MoS_2. The comparative current production shows that S-treated MoS_2 is creating almost three

times more current than pristine monolayer MoS_2. The output voltage of S- treated was also found two times higher than regular pristine MoS_2. Polarity switching test also showed the reliability of the results of MoS_2 [99].

Sanghoon Park *et al.* have experimented with graphene-covered PVDF films and metal-covered PVDF films. Graphene / PVDF / Graphene was prepared with dissolving 15 wt % P(VDF-TrFE) in N, N-dimethylformamide (DMF). Silicon wafer coating was carried out with bar-coating method. It was subsequently dried and annealed at 60°C for 40 minutes. Annealing was followed by removal of excess hydrophobic P(VDF-TrFE) from the substrate with DI water. Later poling was performed on the substrate in an electric field of 50 MV m^{-1} (Figure 30(a)) [88]. Coating with graphene was carried out by dipping the film into DI water covered with a graphene layer supported by PMMA which was removed by acetone (Figure 30 (b)). Also, the PVDF film's surfaces were metalized (50 nm) via coating with aluminium or silver with electron-beam deposition.

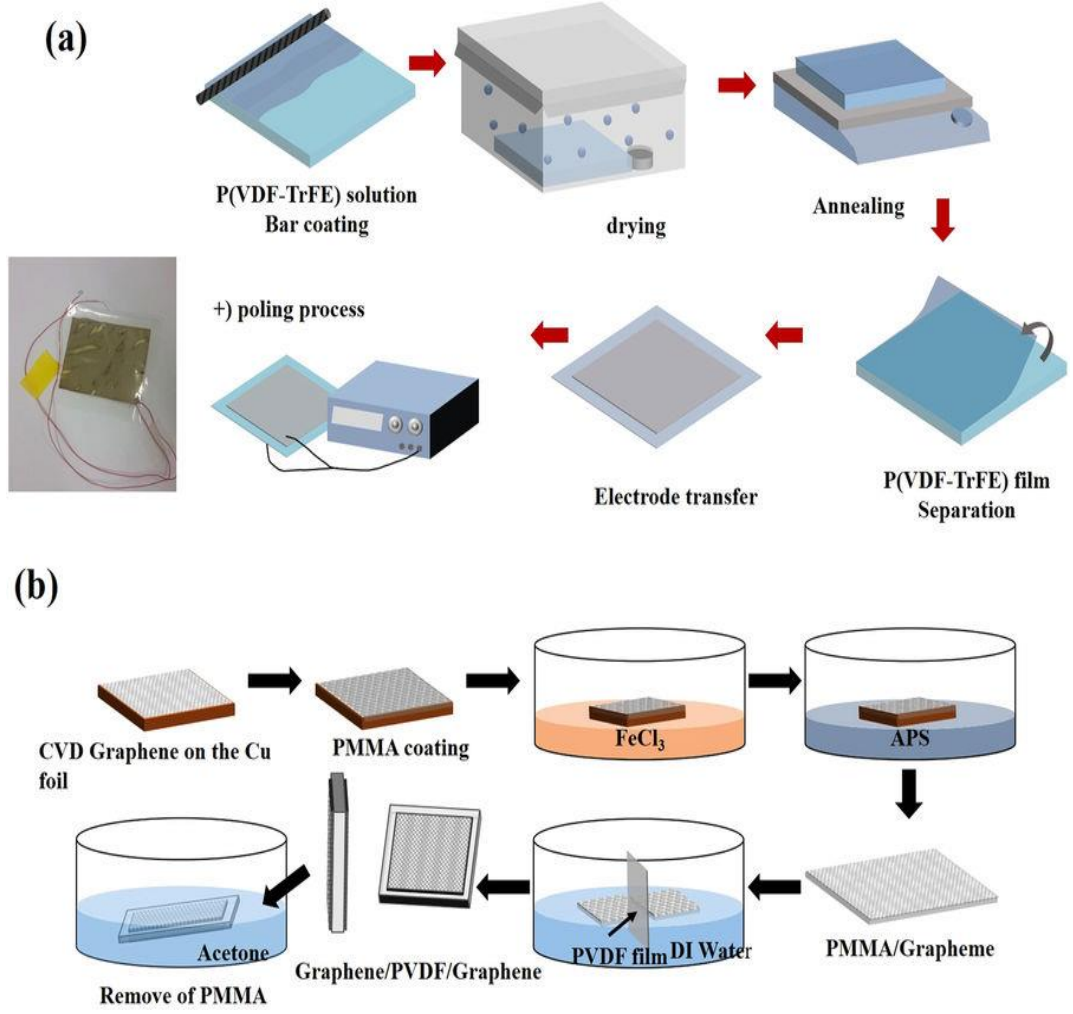

Figure 30. (a) Representation of preparation of P(VDF-TrFE) based thin film generators (the inset shows a photograph of a fabricated device), and (b) a G/PVDF/G generator fabricated by double-sided graphene transfer by Park et al. **[88]**.

The film was stressed in a soundproof chamber, and it was found that there was a peak around 60Hz without any intentional excitation. It was then tested at different loads and applied sound frequencies. The results are described in Figure 32. It can be clearly seen that higher stresses resulted in higher potentials. The maximum voltages at varying resonance frequencies were measured as (e) 1.9 V_{pp} at 185 Hz, (f) 2.6 V_{pp} at 182 Hz, (g) 2.9 V_{pp} at 210 Hz, (h) 7.6 V_{pp} at 280 Hz, and (i) 6.6 V_{pp} at 283 Hz, and the applied masses were 170 g, 370 g, 570 g, 870 g and

1070 g, respectively. It was also found that the measured voltage depended on the load resistance. When the 870g load was applied a maximum 7.6 V_{pp} was found. This voltage data can be converted into power by considering an impedance of 1 MΩ and was found to be 7.2 μW. The effect of the electrodes on piezo films is plotted in Figure 33 (a). The same measurement was carried out for the M/PVDF/M sample (Figure 33b), which indicates that the stress dependencies of both V_{pp} and f_r for G/PVDF/G and M/PVDF/M device are similar. However, the output voltage for M/PVDF/M device was better, likely due to its cleaner surface with good electrical contact. The devices were also tested with different layer thicknesses, and it was found that increased layer thickness made the devices less efficient [88].

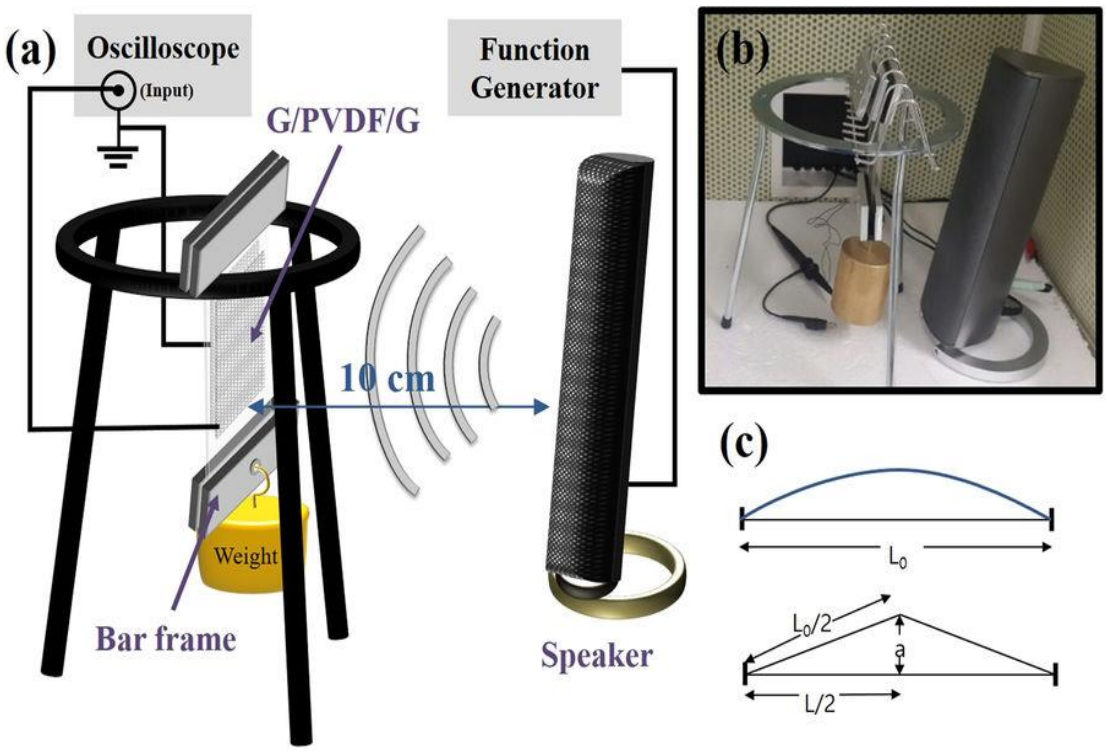

Figure 31. (a) Schematics of the experimental setup applying tensile stress to the generator. and measurement of voltage output due to sound effect, (b) Photograph of the stressed film-based generator and a loudspeaker as a sound source, (c) The illustration of the model of the vibration of the film with fixed ends **[88]**.

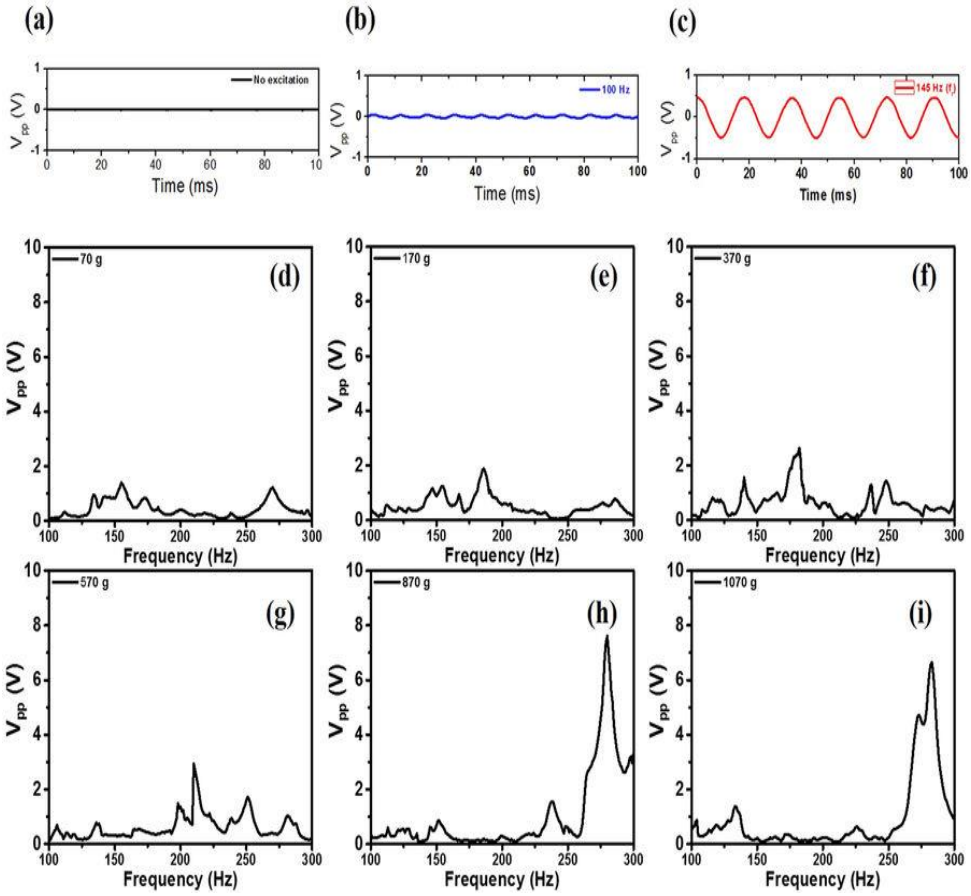

Figure 32. The waveforms of the detected voltages from the stretched G/PVDF/G generator under 1.2 MPa stress were investigated depending on different acoustic environments: (a) No acoustic excitation was applied intentionally, (b) 95 mVpp generation by acoustic excitation (86.7 dB at 100Hz), (c) 1.12 Vpp generation by acoustic excitation (83.7 dB at 220Hz). The peak-to-peak output voltage spectra were measured after input voltage of 5V under tensile stresses by different weights: (d) 70 g, (e) 170 g, (f) 370 g, (g) 570 g, (h) 870 g, and (i) 1070 g **[88]**.

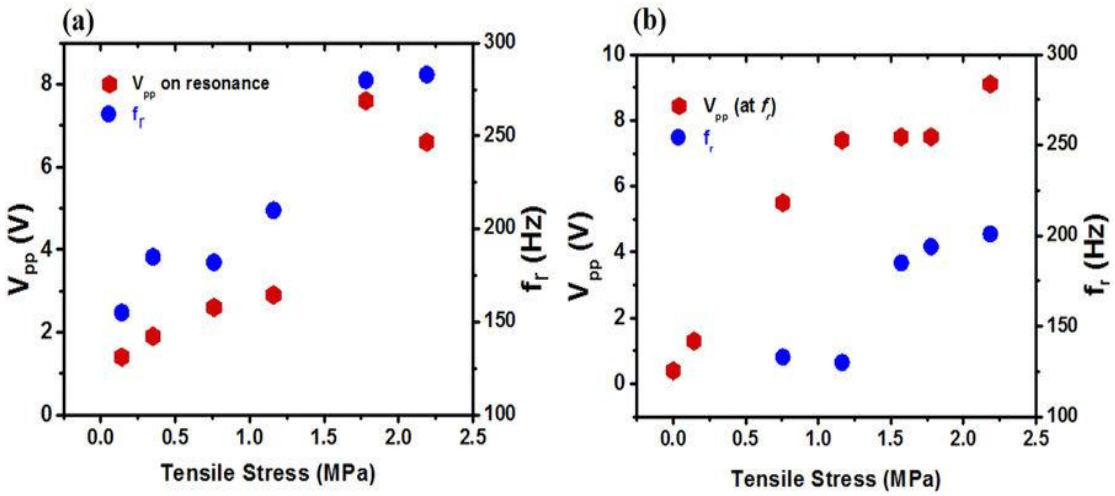

Figure 33. The resonance frequency *f*r and the voltage Vpp vs tensile stresses: (a) G/PVDF/G device and (b) M/PVDF/M device. **[88]**.

Conservation of the piezoelectric response of PVDF polymer films has also been evaluated under irradiation. G. Melilli *et al.* have experimented with 100 nm thick gold sputtered PVDF films irradiated with $_{136}Xe^{48+}$7.46 MeV amu^{-1} under Helium atmosphere at room temperature (Figure 34). Adjusted fluencies were used to account for the number of particles passing through the material / the ion-beam flux. Fluencies were 10^7 cm^{-2}, 10^8 cm^{-2} and 10^9 cm^{-2}. These fluencies were converted into doses absorbed by the polymer (kGy) [100]. The crystallinity of the PVDF polymer film after irradiation was found to be pretty consistent. Nearly full retention of crystallinity was found in 15-20 kGy range. Below this range, chain scissions cause shorter polymer chains and reduce the number of entanglements which in turn increases molecular mobility, which raised the percent crystallinity from 35% to 43% (Figure 35) [100].

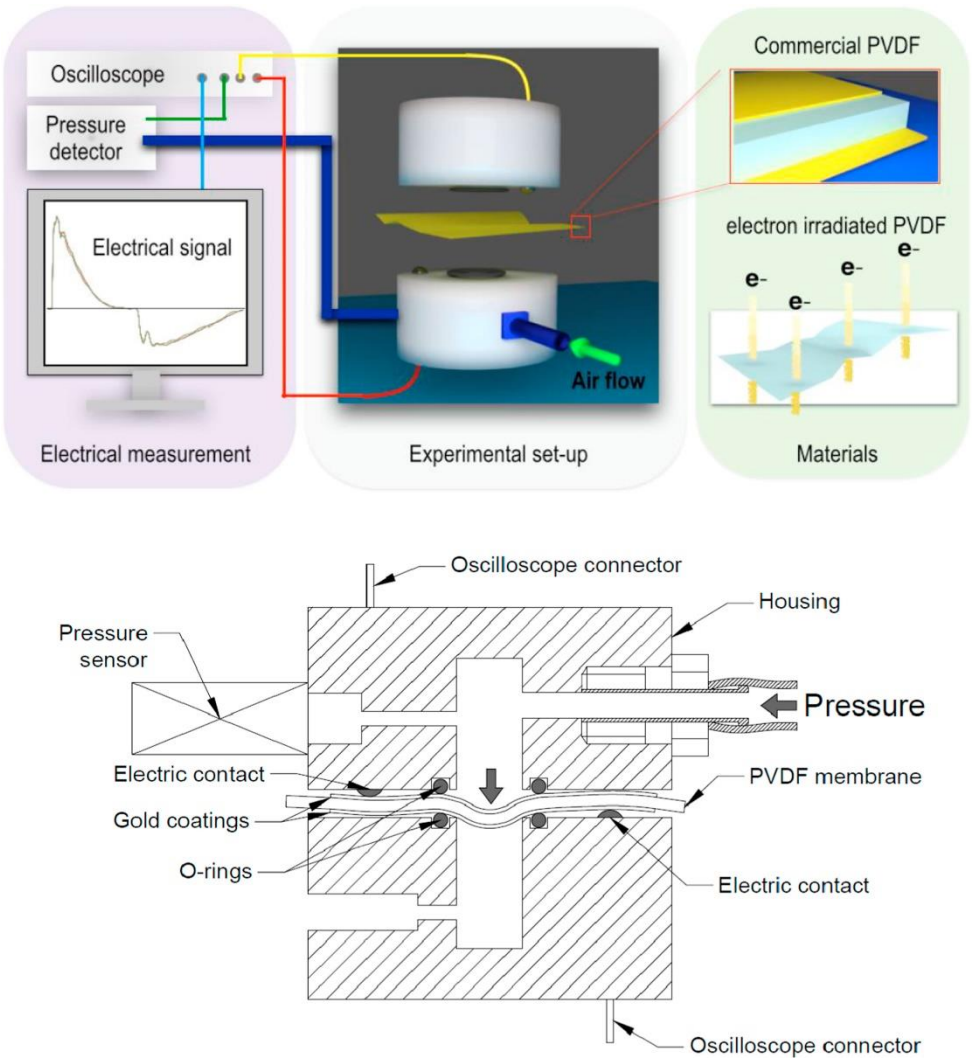

Figure 34. Schematic representation of the experimental set-up (top) and cross-section of the PVDF pressure cell (down) utilized by Melilli et al. **[100]**.

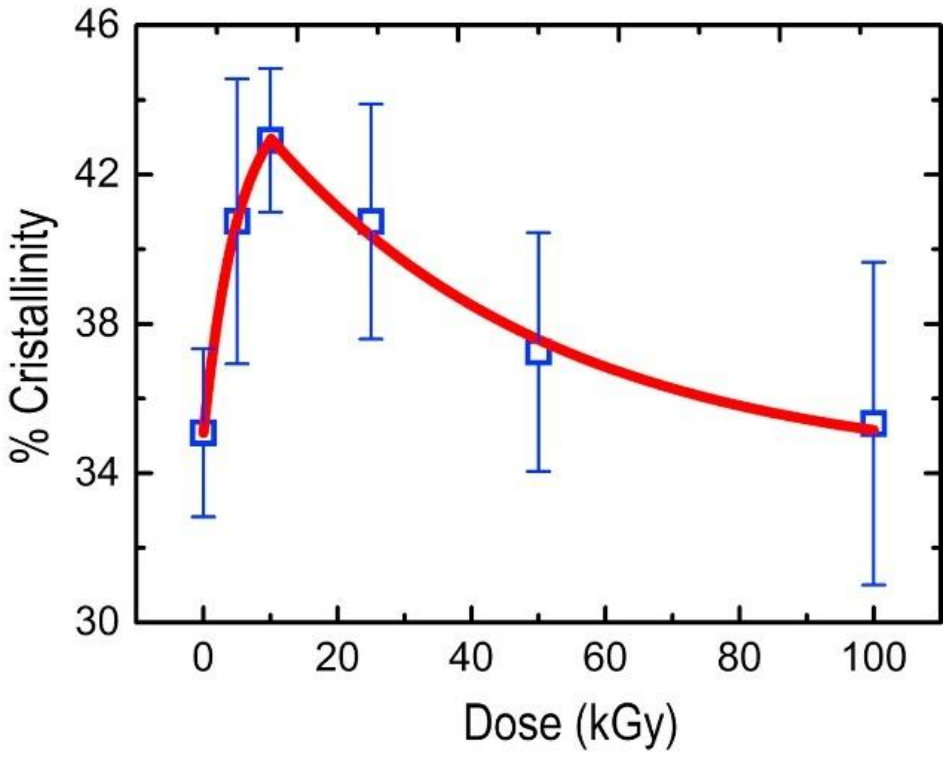

Figure 35. Degree of crystallinity of PVDF polymer versus irradiated doses **[100]**.

Three-Dimensional piezoelectric nanogenerators

Three-dimensional (3D) piezoelectric nanogenerators can include piezoelectric materials in which zero-dimensional, one-dimensional and two-dimensional structural elements form interfaces / come into close contact with each other [44]. It has been observed that 3D piezoelectric nanowire-type materials exhibit piezoelectricity which is enhanced up to six times relative to their bulk counterparts (because of large d_{33} value); 3D piezoelectric materials have been produced with output voltages enhanced up to three times relative to those obtained from bulk materials [101]. 3D nanomaterials containing nanogenerators are also found with the ability to withstand higher compression, stretching, and bending and high mechanical durability which makes it unique in usage in energy scavenging applications [102]. It also has advantages over lesser dimension in designing constraints as well as enabling patterning. [103].

Yiin Kuen Fuh *et al.* have demonstrated that paper-based self-powered sensors (Figure 36) with three-dimensional spatially-stacked fibers were capable of generating up to 4 V and 100 nA of electricity. Figure 36a describes all the processes involved in the experiment in detail [104]. It is notable that this output voltage is nearly five times increased relative to the bulk material, which typically produces piezoelectric voltages of less than 0.3 V [105]. Because the material processing techniques in both experiments were identical, it can be inferred that this large difference in voltage is due to the three-dimensionally structured nature of the former material, which clearly indicates how three-dimensionally structured piezoelectric materials can substantially improve the feasibility of piezoelectric generators.

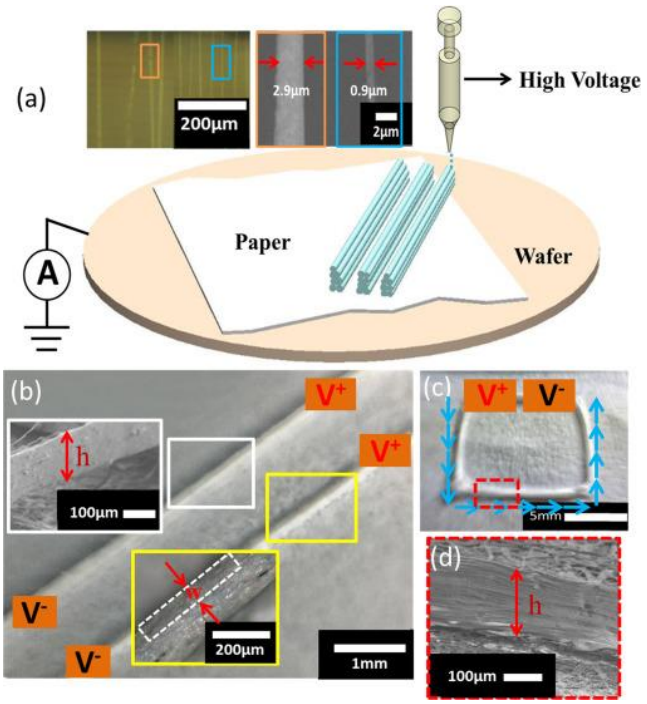

Figure 36. (a) Schematic representation of 3D fiber stacking by electrospinning and SEM image of a direct-write of different diameters. There are diameter variations of fibers as shown at 0.9 and 2.9 μm, respectively, (b) SEM image of two aligned 3D fibers structures constructed on a paper substrate, (electrospinning parameters: applied voltage at 1.5 kV, motion speed of 50 mm/s, initial spinneret-to-collector distance of 1.5 mm) and an enlarged SEM image of sequentially stacked about 600 fibers of 300 μm in height (Inset) (c) A photograph of the 3D square structure of area 1×1 cm2 was fabricated on a paper substrate, (d) SEM image showing the area of the square and micro-wall structure of 600 layer **[104]**.

D.M. Correia *et al.* also demonstrated that three-dimensional PVDF polymers could be very useful for enhancing the proportion of the β-phase and the overall degree of crystallinity towards 45%. This scaffold structure was achieved by freeze-extraction and solvent leaching of the different templates which resulted in near linear response (Figure 37) of strain to applied stress [106]. This clearly indicates that 3D piezoelectric can sustain a significant amount of stress

and remain elastic even over many cycles. This also indicates that when carefully prepared the 3D structured PVDF substrates can have better mechanical properties than bulk PVDF.

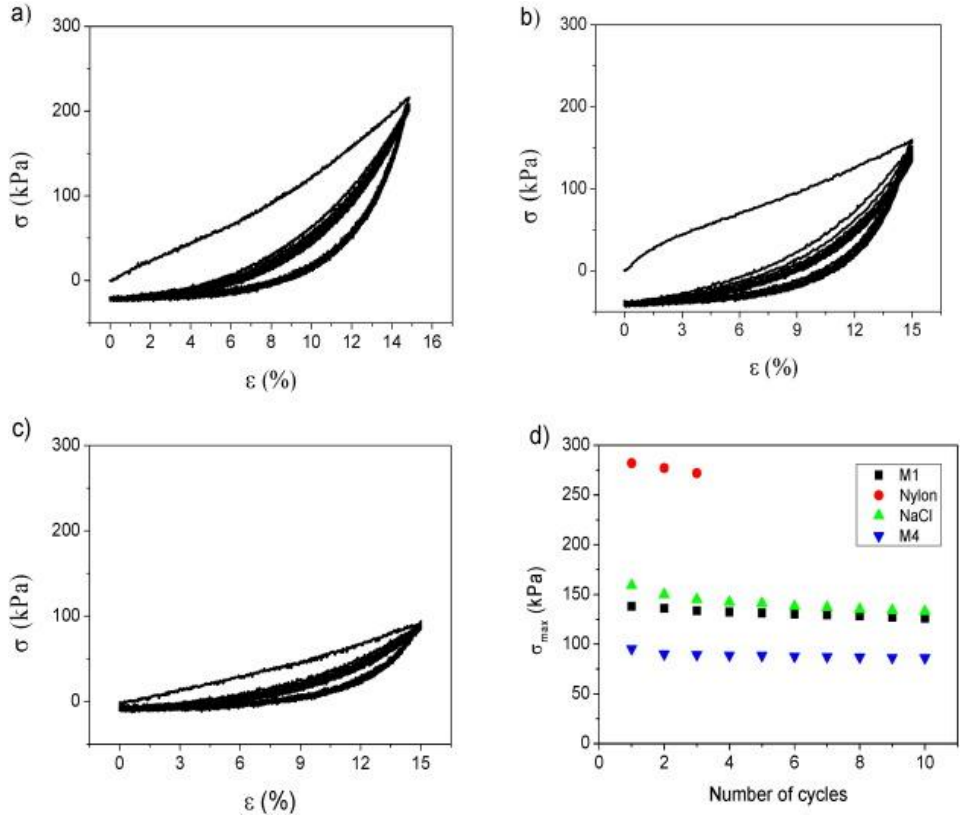

Figure 37. Characteristics stress-strain curves of PVDF scaffolds for compression assays at 15%. PVDF scaffolds obtained by (a) solvent-casting NaCl leaching, (b) freeze extraction with a 0.6nm filament distance template (c) freeze extraction with a 1.2nm filament distance template, (d) evolution of the maximum stress obtained up to 10 cycles **[106]**.

Nonpolymeric materials have also been tested as three-dimensionally structured piezoelectric materials. Microelectronic systems with lead Zirconate Titanate films with multiple degrees of freedom were micropatterned on cantilevers using an electrospinning method by Kensuke Kanda *et al.* [55]. SiN film was formed on (111) surface of the Si surface by chemical vapor deposition method which was subsequently inductively coupled plasma reactive ion

etching (ICP-RIE) to generate the pattern. Later it was wet etched with KOH solution (20 wt%, 80 °C, 120 min) to generate the trenches. After removal of SiN film, radio-frequency magnetron sputtering equipment was used to generate Ti adhesion layer, a Pt bottom electrode, a PZT thin film, another Ti adhesion layer, and a Pt top electrode. It was later characterized using hysteresis loop (Figure 37) fabricated as a cantilever with dimensions of 10 mm in length × 282 μm in width × 200 μm in thickness, and a slope angle of 54.7°. This was then sputtered to laminate with PZT on the surface of the cantilever. Figure 38 shows the fabrication methodology of the triangular column cantilever [55].

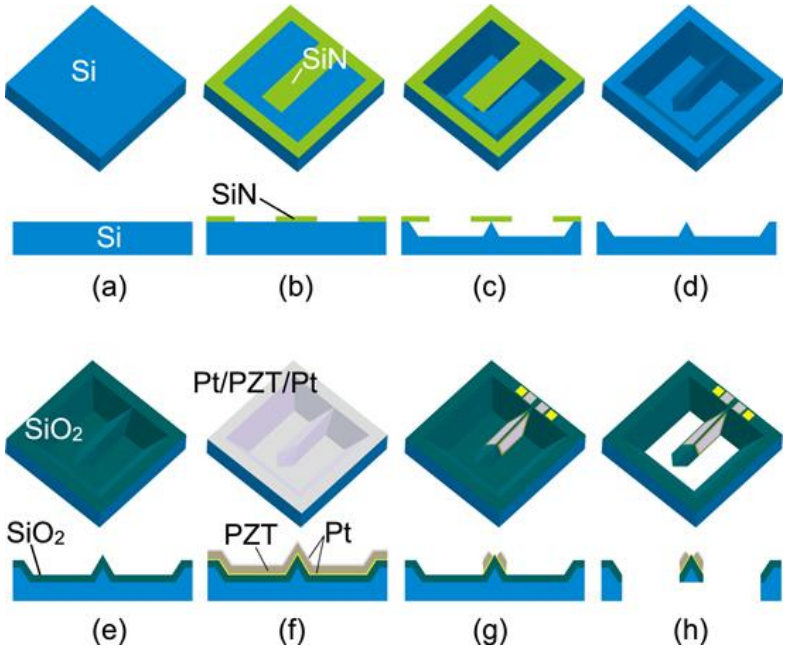

Figure 38. Schematic representation of processing of triangular column cantilever. (a) Si wafer, (b) deposition and patterning of SiN films, (c) anisotropic crystalline etching of Si, (d) removal of SiN thin films, (e) thermal oxidation, (f) sequential deposition of bottom metal of Pt, PZT thin films and top metal of Pt, and (g) sequential dry etching of top Pt, PZT and bottom Pt thin films, and (h) penetration etching of silicon from back surface of the wafer (by Deep reactive-ion etching) and removal of residual silicon oxide films **[107]**.

Sloped cantilever actuation tests were carried out. Figure 39 describes the observed relationship between tip displacement and applied voltage. Both PZT actuation and *X*-directional displacement is much larger than the *Z*-directional displacement. A similar process was followed to investigate the bimorph cantilever laminated with PZT. This was carried out with a half dicing process. A schematic of the bimorph cantilever is presented in Figure 40 [108]. Figure 41 shows the relationship between the poling voltage and bending of the cantilevers to illustrate the piezoelectric effect [108]. Figure 39 and 41 demonstrate the reverse piezoelectric effect of PZT and confirm that three-dimensional PZT can have a large piezoelectric effect compared to its bulk counterpart [109].

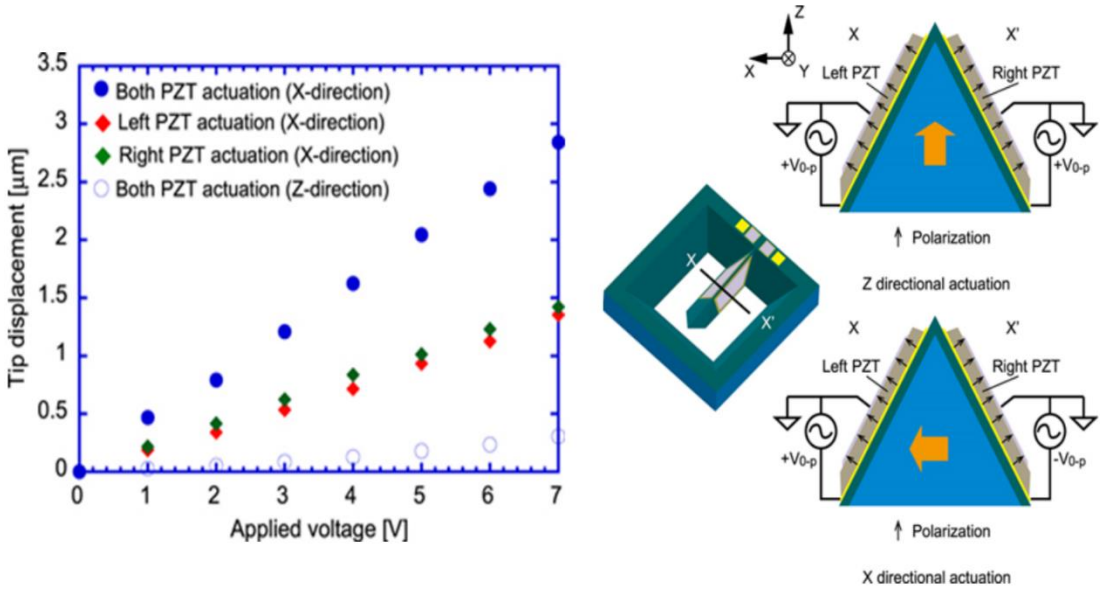

Figure 39. Tip displacement vs. applied voltage for x-directional actuation **[108]**.

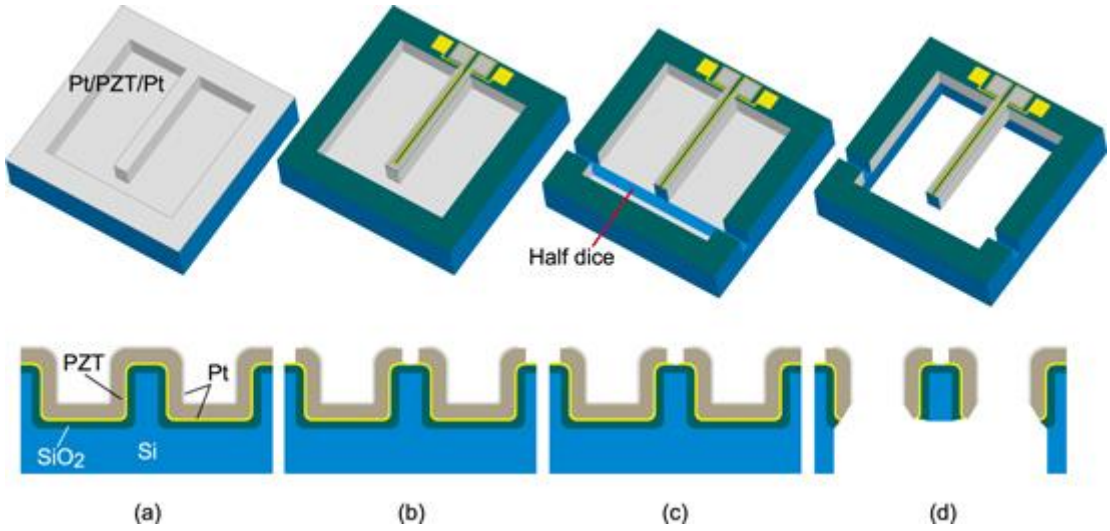

Figure 40. Schematic representation of processing of bimorph cantilever with PZT thin films deposited on the sidewalls (a) After thin film depositions, (b) dry etching the top metal, Pt, PZT thin films, and bottom Pt located on the top surface, (c) half dicing to separate right and left electrodes, and (d) Self standing cantilever **[108]**.

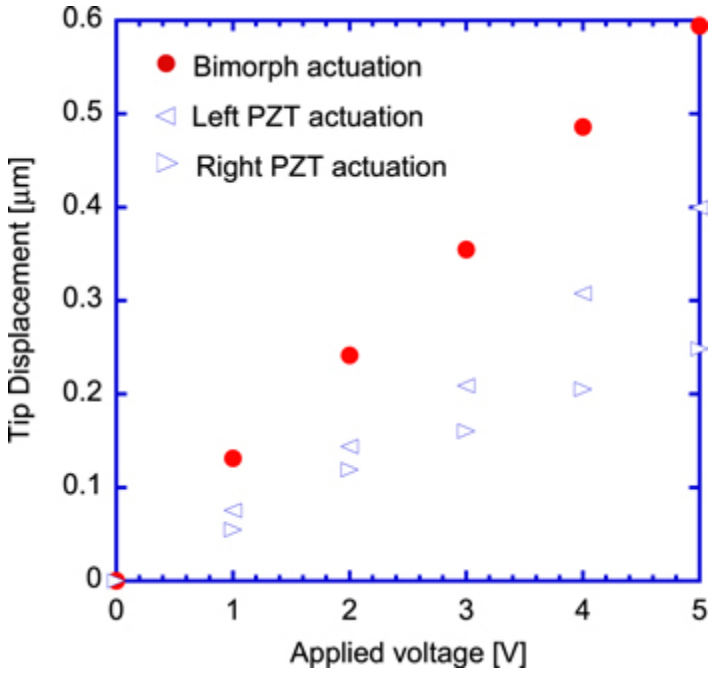

Figure 41. Tip displacement of bimorph cantilevers. Bimorph actuation doubled the tip displacement of the cantilever compared with those of single layer actuations **[108]**.

Bing Yin *et al.* have experimented with ZnO nanoparticles prepared with a thorny ball structure (Figure 42). This nanogenerator was prepared by putting thorny balls prepared by chemical vapor deposition in a controlled environment between two copper sheets. These thorny balls were prepared inside a quartz reaction tube at 550°C under a flow of 70 sccm (standard cubic centimeters per minute) of N_2 followed first by thermal heating up to 950°C under a constant flow of N_2 and O_2 and then cooling to room temperature [110]. Characterization of thorny balls consisted of I-V calculation and output current calculation (Figure 43). This demonstrates antisymmetric non-linear power generation which indicates that it can be treated as a back-to-back Schotty diodes [111].

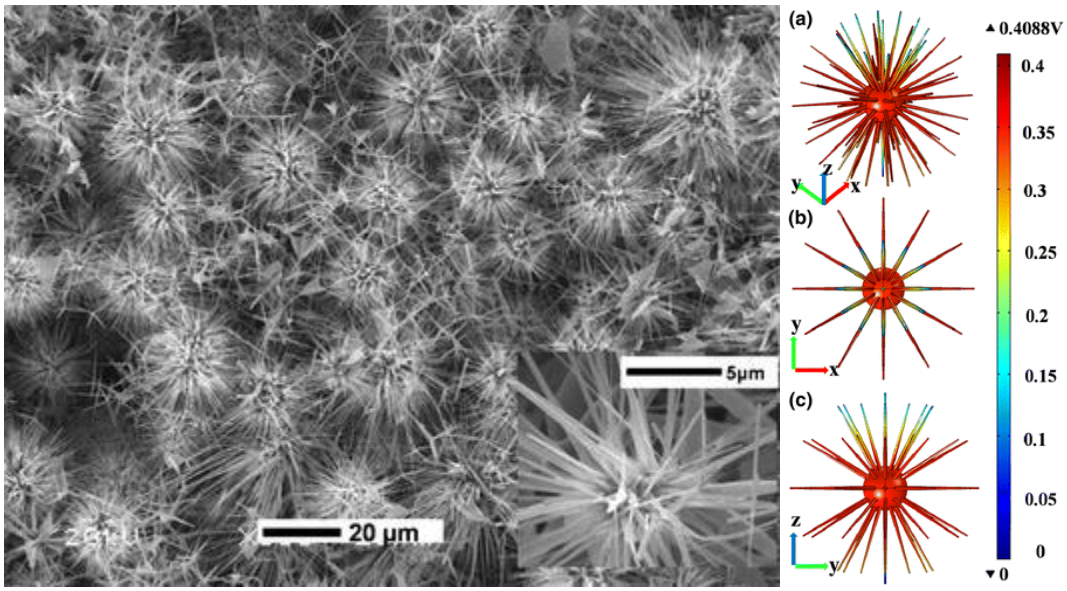

Figure 42. SEM image (Left) of ZnO micro-thornyballs and piezoepotential distribution (right) of ZnO thornyball with is the three-dimensional distribution (a-c) **[110]**.

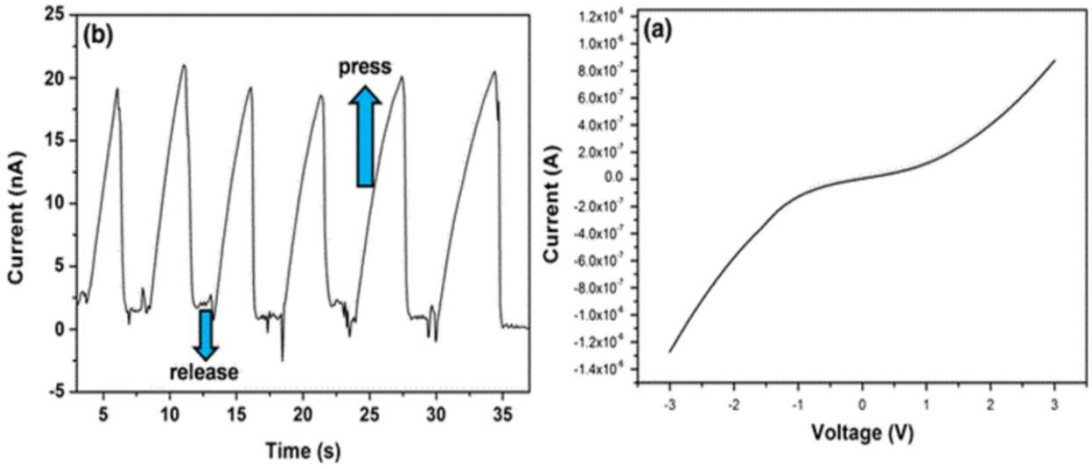

Figure 43**. (a**) I–V curve of the piezoelectric nanogenerator (ZnO micro-thornyballs) with stress and release, **(b)** Output current of the ZnO micro-thorny balls nanogenerator **[110]**.

You *et al.* have discovered an organic-inorganic ferroelectric perovskite based on trimethyl chloromethyl ammonium trichloromanganese (II) (TMCM-$MnCl_3$). The material, prepared at room temperature, showed a crystal packing similar to the $BaNiO_3$ perovskite structure and excellent piezoelectric response (d_{33} = 185 pC/N). The observed thermal variation of the crystal structure of TMCM-$MnCl_3$ is shown in Figure 44 [20].

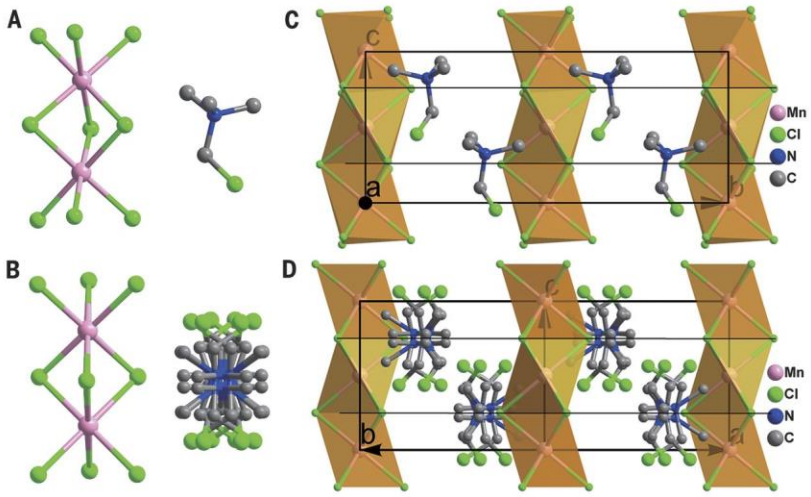

Figure 44: (a) Structural unit of TMCM-MnCl3, demonstrating the coordination geometry of the MnCl6 (octahedron and cationic structure) in low-temperature phase, (b) Structural unit of TMCM-MnCl3 in the high-temperature phase, showing the multi-orientation of the cation, (c) Projection of the low-temperature structure. The lines indicate the pseudo-mirror planes perpendicular to the c axis, which demonstrate the relative ionic displacement due to symmetry-breaking, (d) Projection of the high-temperature structure. The lines indicate the mirror planes perpendicular to the a-axis. Hydrogen atoms are omitted for clarity **[20]**.

In TMCM-$MnCl_3$, the Cl acts as a disruptor in the crystal structures and induces the potential energy barrier tumbling motion. Depending on the relationship between lattice cells molecular tumbling with 12-fold orientation disorder. These effected on d_{33} value a lot. Its stiffness was also found relatively lesser than $BaTiO_3$ which has d33 value of 105 pC/N (compared to TMCM-$MnCl_3$ d_{33} value of 185 pC/N) [20].

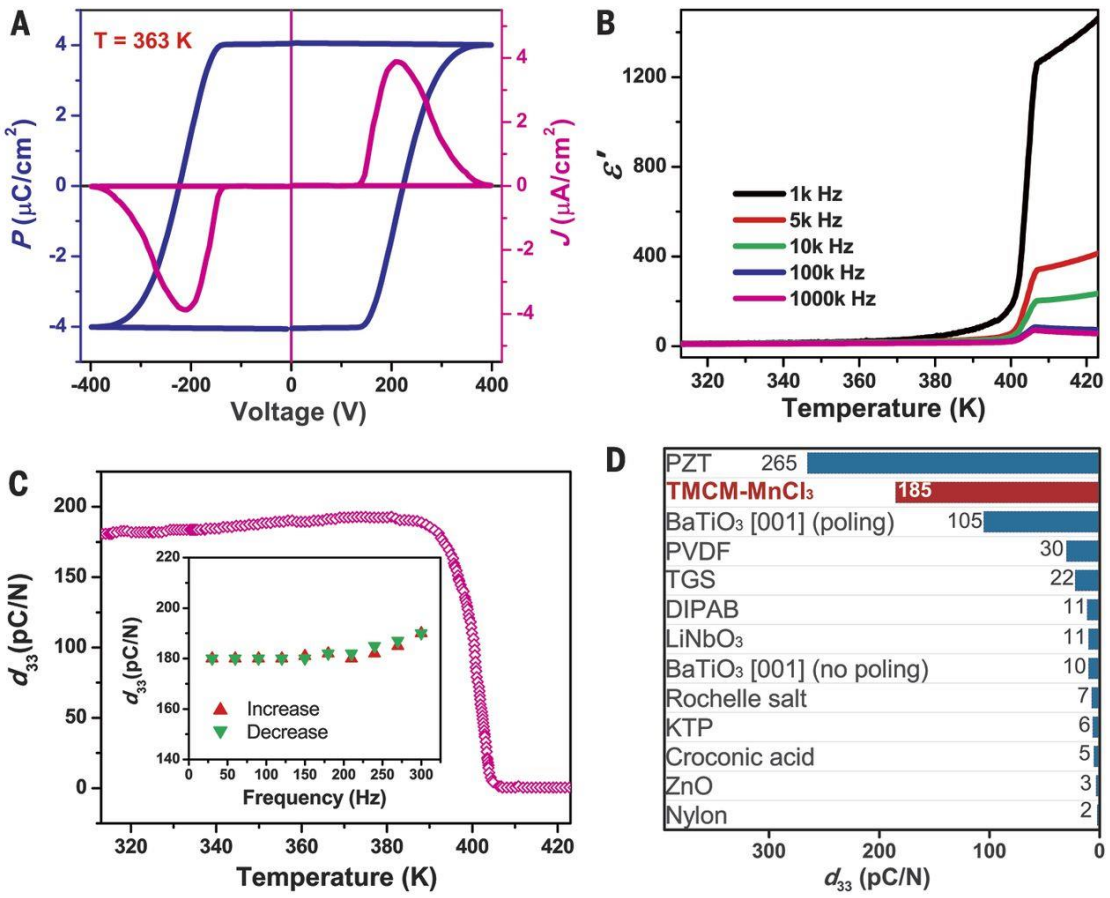

Figure 45. (a) J~V (Current density-bias voltage) curves and P~V (polarization-bias voltage hysteresis loop) Curves of TMCM-MnCl3 , (b) Temperature vs the real part (ε′) of dielectric permittivity (ε = ε′ – iε″) (c) Piezoelectric coefficient (d33) of TMCM-MnCl3 as a function of temperature and frequency (inset) (d) Piezoelectric coefficient (d33) of TMCM-MnCl3 compared with some organic and inorganic materials **[20]**.

Figure 45 shows the performance of the ferroelectricity of TMCM-$MnCl_3$ by observing P-E hysteresis loops. Step like dielectric anomalies was found and revealed the ferroelectric character of the transition. Piezoresponse was also measured along with a comparison to other established material. Piezoresponse was recorded using different frequency as the driving force.

The result showed a very small fluctuation in response (<10 pC/N). The data collected at different frequency indicate that organic-inorganic hybrid perovskite materials can be utilized as flexible piezoelectric materials with high ductility and lower stiffness [20]

Zhang *et al.* have demonstrated that 3D interconnected piezoelectric ceramic foam-based composite has better piezoelectric output compared to other non-connected 3D ceramic and less dimensional materials. They showed with 3D PZT ceramic foam prepared by pouring PZT precursor in PU foam followed by sintering and compositing by PDMS matrix (Figure 46) [102].

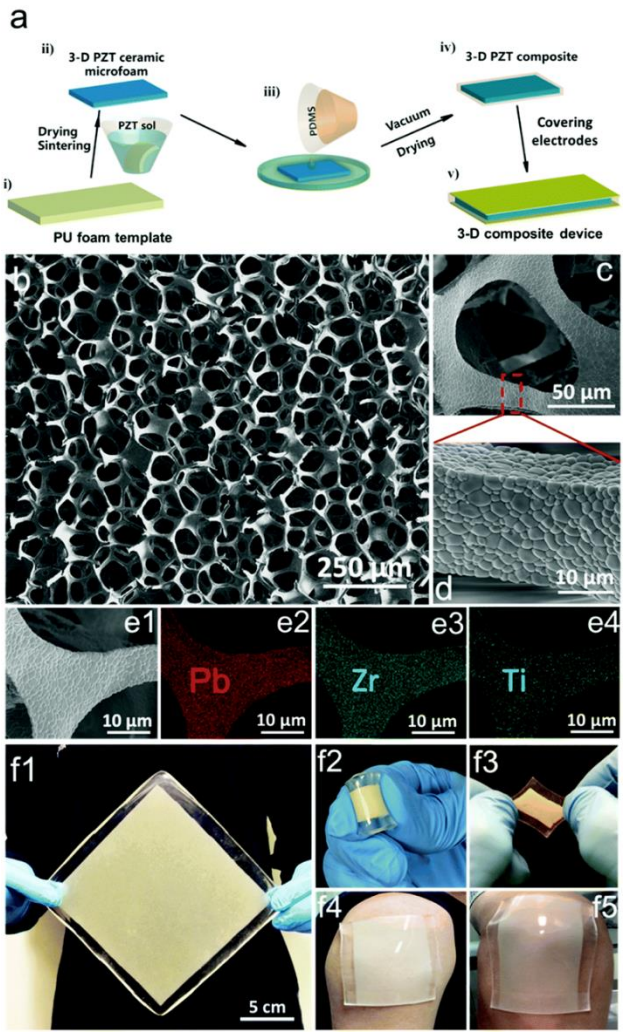

Figure 46: (a) The schematics representation of the preparation procedure of the 3D composites. (b) The SEM image of the 3D PZT ceramic foams. (c) The magnified SEM image of the PZT skeletons. (d) The localized surface morphology of the skeleton. (e) The EDS mappings of the PZT skeleton. The elements of lead, zirconium, and titanium are homogeneously dispersed in the skeletons. (f) The optical images of the 3D composites. (f1) A large-area 3D composite, demonstrating the scalability of the fabrication method for the 3D ceramic composites. (f2 and f3) The 3D composite bent and stretched by fingers. (f4 and f5) The 3D composite attached on the shoulder and knee, **[102]**.

The interconnected ceramic foam was showing excellent results in laboratory experiment as well as in simulated results. It was demonstrated that the foam was generating more current and voltage with increased strain. A similar result was found with bending moment simulation (FigureFigure 47) [102].

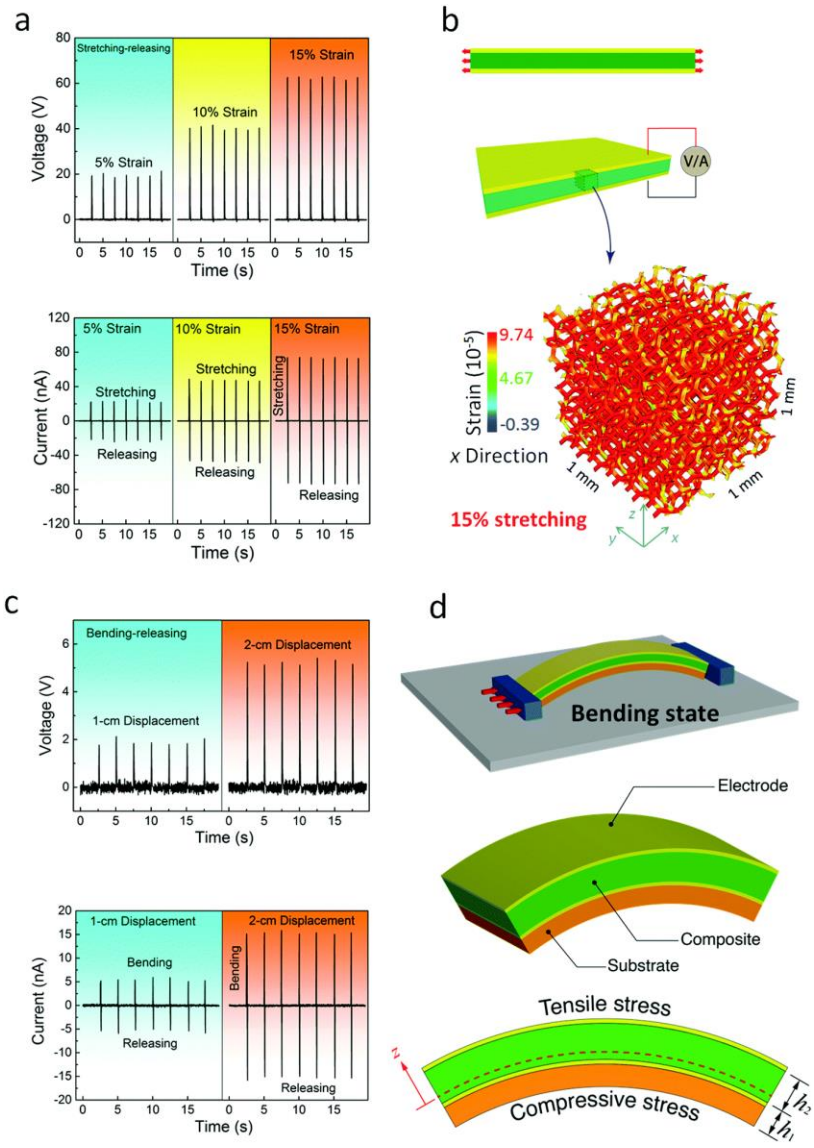

Figure 47: (a) The output voltages and currents of the 3D composites under different amount of strain (b) Modelling of the strain distribution on the PZT foam when the composite is stretched by 15%. (c) The electrical output (voltages and currents) of the 3D composites under bending and change of length (1cm and 2cm) from original size (5cm). (d) Schematic representation of the simulation model. The thickness of the composite (h1) and the thickness auxiliary substrate (h2) are 1 mm and 0.4 mm, respectively. **[102]**.

In Figure 48, PZT NP composite with 1 wt% multiwall carbon nanotubes (CNTs), labeled as the NP-CNT composite. PZT nanoparticles (NPs, 300 nm in diameter) and nanowires (NWs, 100 nm in diameter and 3 μm in length) with the same volume fraction of PZT (i.e., 16 vol%) dispersed in PDMS for the comparative study. A comparative test with other low dimensional composite result (shown in Figure 48) proves that interconnected 3D ceramic has better output voltage as well as current production. This is due to 3D interconnected architecture which creates a continuous pathway for load transfer to break the load-transfer scaling law seen in the conventional composites with low-dimensional ceramic fillers [102].

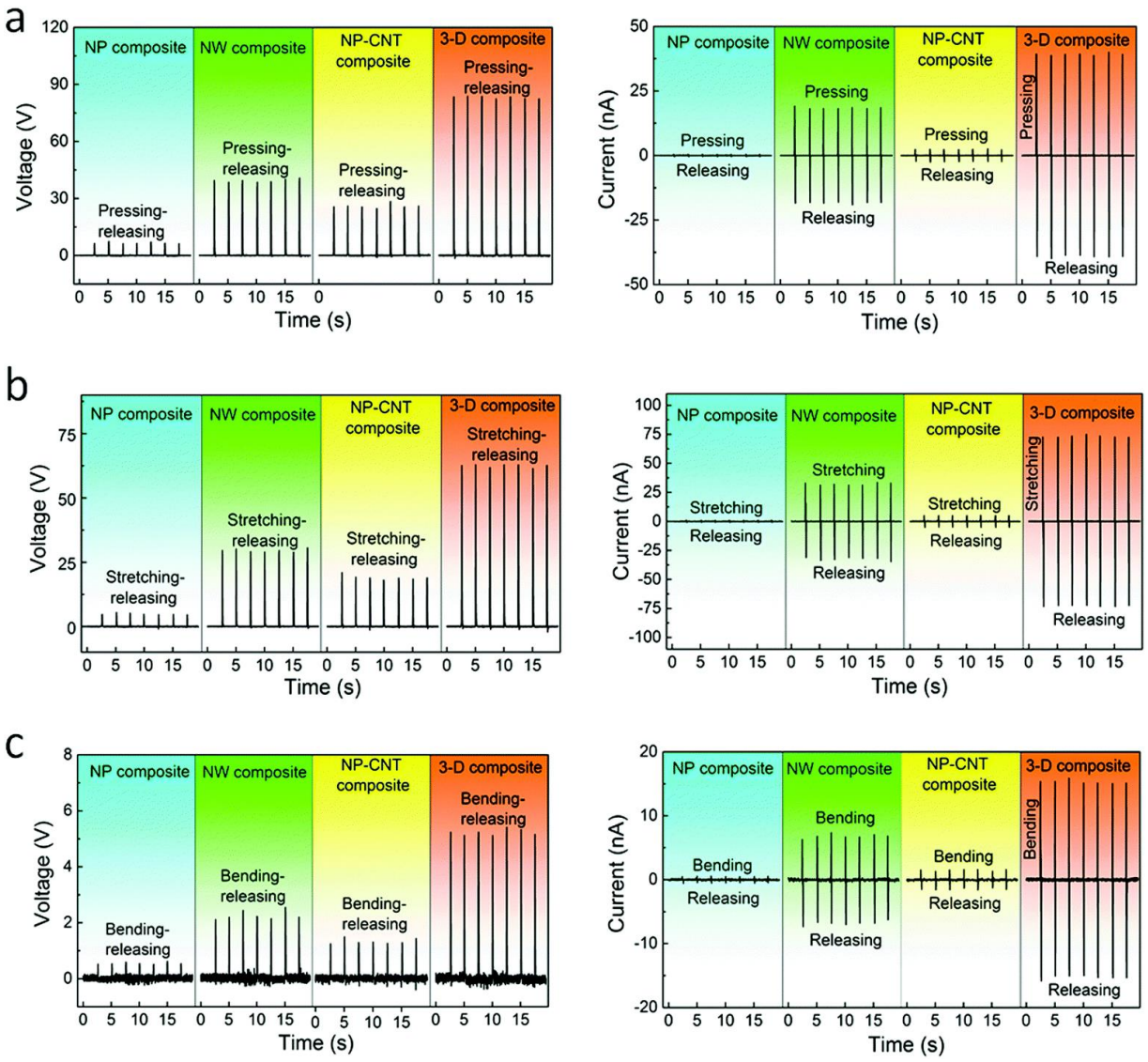

Figure 48: Piezoelectric responses of the NP, NW, NP-CNT and 3D composites with multiple deformation modes. (a) The output voltages and currents of different composites under compressing–releasing mode with 8% strain. (b) The output voltages and currents of the composites under stretching–releasing mode with 15% strain. (c) The output voltages and currents of the samples under bending and length change of length (1cm and 2cm) from original size (5cm). **[102]**.

While working with broccoli structured 3D piezoelectric nanogenerator for biomedicine, Chowdhury *et al.* have demonstrated the use of Li-ZnO grown on poly(styrene-co-divinylbenzene) (PSCDB) followed by exposing to high temperature to burn the PSCDB and surface treatment with polyethylene glycol (PEG) results in higher piezoelectric potential compared to unpoled Li-ZnO. They have reached the piezoelectric potential up to 10.1V in nanogenerators comprising of Li-ZnO in PVDF matrix. However, use of CNT enhanced the conductivity in a large proportion [7].

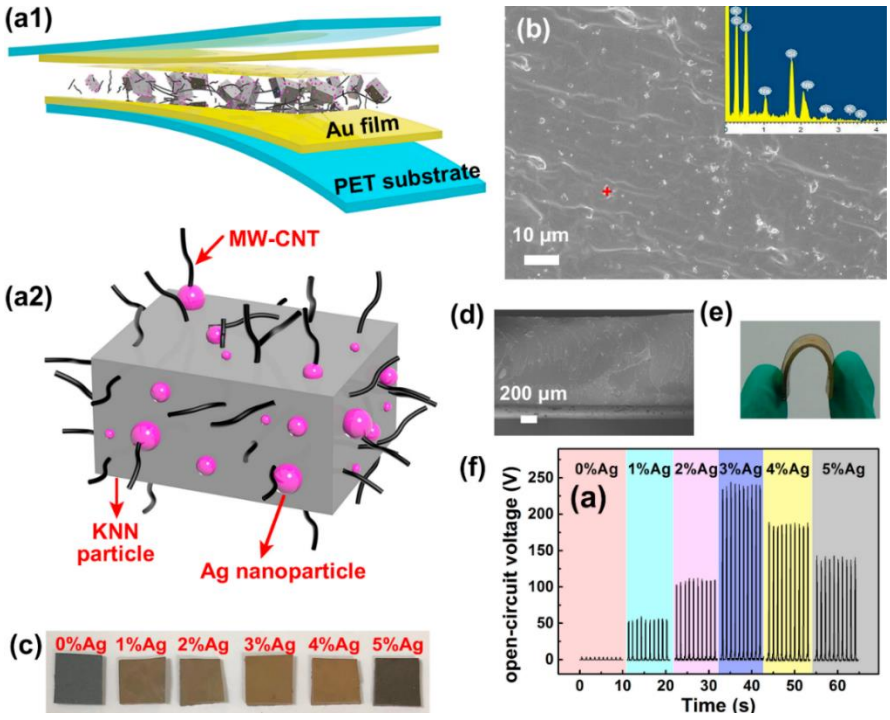

Figure 49: (a1) Schematic diagram of the structure of theconstructed piezoelectric nanogenerator device. (a2) Schematic diagram of Ag/(K,Na)NbO3 particles, Ag nanoparticles and MW-CNTs distribution in PDMS polymeric matrix. (b) SEM image and EDX in the region with a red asterisk for 3% Ag loading (K,Na)NbO3-based composite film. (c) Photograph of the composite film. (d) Cross-section SEM image of the composite film. (e) Photograph of the flexible p-NG device. (f) Open-circuit voltage of piezoelectric nanogenerator under stress **[112]**.

Heterostructured Ag/(K,Na)NbO_3 has been investigated by Huan *et al.* Ag/(K,Na)NbO_3 nanoparticle with CNT were put between Au films and PET substrate and tested with different body motions and found reaching open-circuit voltage and short-circuit current of ~240 V and ~23 μA respectively under the external mechanical stress of 0.1 MPa, which are over 70 times higher than the pure KNN particle embedded p-NG device (~3.5 V and 0.3 μA, respectively). This nanogenerator also showed extensive mechanical stability even after 1000 cycles of loadings. Experimenting with different Ag percentages showed best results with 3% Ag. Figure 49 is demonstrating schematic diagram and performance of sandwich-like flexible nanogenerator [112].

Future Development of Piezoelectric Nanogenerator

This review has focused on multicomponent piezoelectric nanogenerators and the recent developments of multicomponent piezoelectric nanogenerators. Piezoelectricity are already used in our daily life and have become well established energy generators, especially when compared to other types of nanogenerators (e.g. triboelectricity or pyroelectricity). Although it is hard to predict the future, nonetheless piezoelectric nanogenerators will be utilized as energy scavenging as well as energy generation for self-powered systems. However, there are many challenges to be addressed before the complete utility of piezoelectric nanogenerators can be realized. Considerable research has been and is currently ongoing with the focus of developing new piezoelectric materials and enhancing the performance of current piezoelectric nanogenerators. In this advance the trend is towards a multidisciplinary approach from the point of view of the chemistry, material science, physics, electronics to better clarify fundamental relationship between structure and properties for better taking advantage of these materials. Yet, performance and durability need to be optimized and many uncertainties are still unanswered and much

remains to be explored. Current research has been focused on addressing the following challenges [18]:

(i) The increase of power output density

(ii) The integration of energy storage units with the nanogenerators

(iii) The optimization of harvesting efficiency of mechanical energy from varying working conditions,

(iv) The optimization of electromechanical conversion efficiency through structural design,

(v) The long-term stability, mechanical strength, and chemical stability of the nanogenerators,

(vi) The development of a simple process to prepare single crystal piezoelectric materials,

(vii) The development of piezoelectric nanogenerators for specific use in the practical field

(viii) The integration of piezoelectric nanogenerators with triboelectric and pyroelectric nanogenerators [113].

It is also desirable to develop solutions for the following issues [18]:

(i) The long-term stability and mechanical strength of the active chemical sensors,

(ii) The development of piezoelectric nanogenerator as well as materials with lower noise production and higher signal

(iii) The generation of a stable output voltage for active sensors, which is crucial for the accuracy of the sensing results

(iv) The integration and packaging of nanogenerator with sensing units for self-powered sensor systems

(v) Accounting for temperature drift during the sensing process for active/self-powered sensors

(vi) The integration and development of nanogenerators for use in bionic and Artificial Intelligence

(vii) The development of materials for multipurpose use such as pyroelectricity, triboelectricity and piezoelectricity generation

(viii) The development of multicomponent piezoelectric materials which can be easily processed

(ix) The integration of active or self-powered systems with data processing and transmitting systems

(x) The growth mechanism of the piezoelectric materials for nanogenerator [45].

(xi) The development of more nontoxic piezoelectric materials like ZnO for biomedical application

(xii) Development of nanogenerator for replacement of batteries from biomedical implants.

Conclusion

The ever-increasing demand for multicomponent piezoelectric materials for nanogenerators is driving fervent research. Energy harvesting and utilization as sensors have been the prime uses for piezoelectric materials. In addition to these potential applications, large-scale energy harvesting remains a promising application for piezoelectric. Futuristic large-scale deployment of nanogenerators could be a viable solution to meet ever-growing energy demands. With proper development, the use of nano and microscale piezoelectric nanogenerator can be transformed into a large-scale use of electromechanical devices. It is an arduous work to

summarise all the development in piezoelectrical energy generation, yet we tried to do the summary of selected works on a very small scale. Hybrid nanogenerators are also a matter of study for scientists [114]. Piezoelectric materials combined with triboelectric, pyroelectric, solar energy harvesting, and other energy scavenging or energy transforming materials/techniques can open up a more extensive array of novel applications. Through hybridization, enhanced nanogenerators can be a new way to meet humanity's energy demands. Although many composite piezoelectric nanogenerators have been developed for advanced and niche scientific uses, commercialization of these technologies could be very beneficial in the future. Optimization studies also remain essential for enhancing the efficiency of existing device architectures. After all these years, many avenues of research and development are open for researchers to develop novel and practical ways to harvest electromechanical energy.

CHAPTER III

PIEZOELECTRIC DEVICE AS COST-EFFECTIVE TRANSDUCER FOR ENERGY AND BIOMEDICINE

Introduction

Harvesting energy from the environment and sensing environmental stresses are both potential motivations for the fabrication of novel, high-yield piezoelectric materials.[115,116] Among the various sources of energy available, mechanical energy is perhaps the most abundant in daily life through like human motion,[117] walking,[118] vibration,[119] fluid flow,[120] and respiration.[65] Piezoelectric nanogenerators are the most straightforward and cleanest method of scavenging this energy, and they have the ability to act as sensors which generate an electrical signal from mechanical action upon the substrate.[80,121] Ung-ho Shin *et al.* has experimented with lithium doped zinc oxide nanowire polymer composites, and it was found a significant change in the voltammetric response with doping of the piezoelectric material.[122] Moreover, most piezoelectric nanogenerators require costly treatments, such as electrical poling at a high temperature in a strong electromagnetic field.[123] However, discovery of piezoelectricity by Curie *et al.* was done without any use of electrical poling machine.[124] Cauda *et al.* have demonstrated dimensional nanoconfinement and oriented crystallization by processing PVDF into arrays of oe-dimensional nanowire can led to enhanced piezoelectric response without any external poling action[75]. Kim *et al.* also have reported achievement of high dielectric constant

of surface treated $BaTiO_3$ with poly(vinylidene fluoride-co-hexafluoro propylene) and phosphonic acid of the nanoparticle without electromagnetic poling. [16] Which means surface modification can lead to increase in piezoelectric properties without costly poling operation. It was reported by Chinya *et al.* that increasing of the polar phase can be achieved with the surface treatment of filler ceramics. Their experiment with PEG coated Zinc Ferrite reached up to 92% polar phase without any external poling action.[65] These studies have led to increasing the interest in piezoelectric nanogenerators/sensors comprised of Lithium doped zinc oxide and PVDF polymer. Indeed, surface treated zinc ferrite has shown output voltages of up to 18 V which is very promising without any poling action.[65,122] Thus surface treatment seems to be an increasingly viable solution for avoiding costly poling operation to transform PVDF to beta phase. However, the development of a piezoelectric device which can generate very high current flux as well as a response in a linear for to applied force still remains a matter of study.

Thanks to the presence of ß phase, PVDF and its copolymers are considered the best polymeric materials for piezoelectric applications, but enhancement of the polymer piezoelectric properties through the transformation of the α into the ß phase requires high-field electrical poling (several hundred MV m^{-1}), which, in turn, is cost-intensive, inconvenient, and tedious, thus being a major hindrance to large-scale production. To overcome these issues, modification of the interface of the nanostructured filler material and the bulk matrix has been tested with a number of different surface-modifier agents. [16,125–128] The dipole interaction between the surface of nanoparticles and surface-modifiers has been shown to increase in-situ ß phase PVDF growth. This has led to an increase in the performance of nanocomposites due to an increased proportion of the ß phase, as well insertion of metal oxide has increased percentages of ceramic or metal oxides in nanogenerator/sensors. The conductivity of polymer has been another major

bottleneck for polymer-based piezoelectric devices. Incorporation of carbon nanotubes is a promising pathway to overcome this issue of low innate conductivity. [129] Ranvijai Ram *et al.* has experimented with multiwalled carbon nanotube (MWCNT) incorporated PVDF in an attempt to improve the electrical conductivity of the composite material. It was demonstrated that the threshold percolation limit (defined as the point at which the vast majority of the MWCNTs are connected and form a conductive network throughout the polymer) for a PVDF/MWCNT is 1 wt%. At over 1 wt% MWCNT conductivity does not increase further due to the insignificant additional improvement of the conductive network. [130]

In this work, a simple and cost-effective Li-ZnO/PVDF nanocomposite piezoelectric device architecture (for both power generation and sensing of mechanical stresses) was developed and evaluated. The piezoelectric devices were prepared by hydrothermal growth of three-dimensional (3D) Li-ZnO on the surface of poly(styrene-co-divinylbenzene) microspheres (6.0-10.0 μm average particle size) followed by a coating of polyethylene glycol(PEG; 20000 g mol^{-1}) on the surface of the 3D structured Li-ZnO. Finally, the piezoelectric devices were assembled via the incorporation of the 3D structured Li-ZnO and MWCNTs into a PVDF matrix. The devices were thoroughly characterized and analyzed with different body motions and in different environments.

The development of inexpensive piezoelectric devices which are both mechanically flexible and electrically conductive could promote the use of transducers and energy scavengers into daily life applications, thus making energy harvesting and biomedicine needs more affordable also by poor Countries.

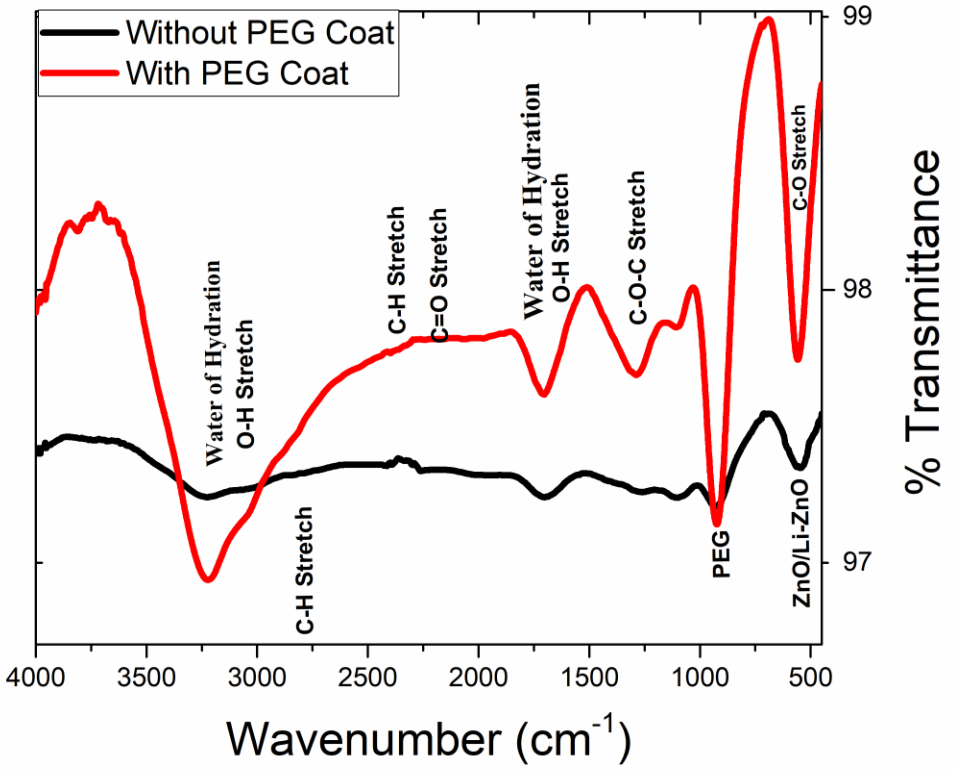

Figure 50. Fourier-transform infrared spectroscopy (FTIR) spectra of coated and uncoated PEG Li-ZnO.

The first objective has been to study the effects of polyglycolation to assess that PEG is bond to the Li-ZnO. In this view, Fourier-Transform Infrared (FTIR) spectroscopy analysis was carried out on the Li-ZnO, and PEG coated Li-ZnO. Figure 1 shows the FTIR transmission spectra of Li-ZnO and PEG coated Li-ZnO. The peak at 532 cm^{-1} corresponds to Li-ZnO. There are other peaks in the PEG free Li-ZnO spectra due to broad -OH vibration at 3214 cm^{-1} and 1766 cm^{-1}. This absorption is due to residual water coexisting with the nanoparticles. PEG-

coated Li-ZnO shows C=O stretches at 547 cm^{-1}. Furthermore, the PEG-coated sample shows a strong absorbance at 917 cm^{-1}, likely due to a C-O-C stretch at 917cm^{-1}, with tetrahedral bridges evident at 1281cm^{-1}. The water of hydration shows a good absorbance in 1714 cm^{-1} and 3246 cm^{-1}. Two small peaks are notable has at 2117 cm^{-1} and 2356 cm^{-1} for C=O and C=H stretching respectively. These FTIR spectra qualitatively indicate that the PEG completely and robustly bound Li-ZnO.

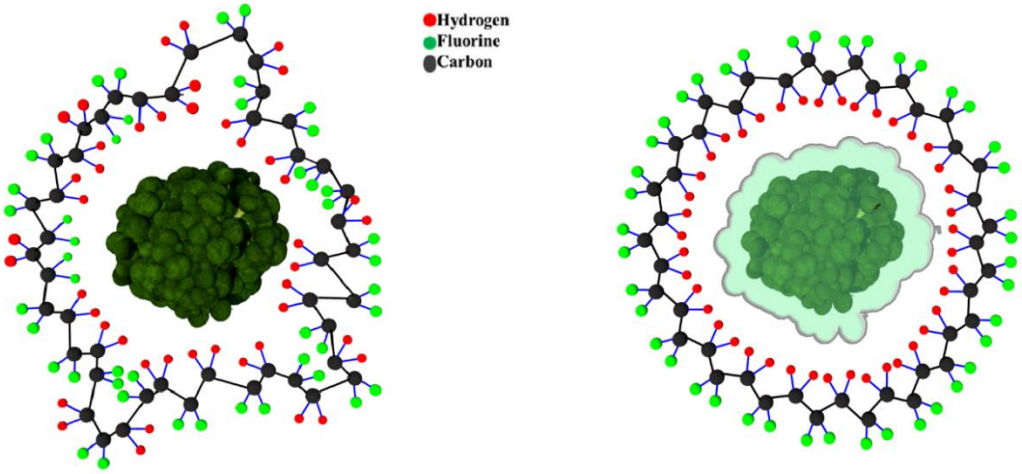

Figure 51. Schematic representation of the interaction between untreated and surface treated Li-ZnO with PVDF.

According to previous studies,[65] we can assume that, after polyglycolation, the Li-ZnO has become more negatively charged, which promoted interaction with the -CH_2 groups of PVDF via local electrostatic interactions (shown Figure 51). This promotes and stabilizes the bipolar ordering in PVDF. Thus, it can be seen that both -OH from PEG as well as -CH_2 and -

CF_2 from PVDF play an important role in inducing self-polarization. These actions generated dipoles of PVDF around the PEG coated Li-ZnO. It is already proven that the PEG coating can improve the piezoelectric response while attributing mechanical properties.

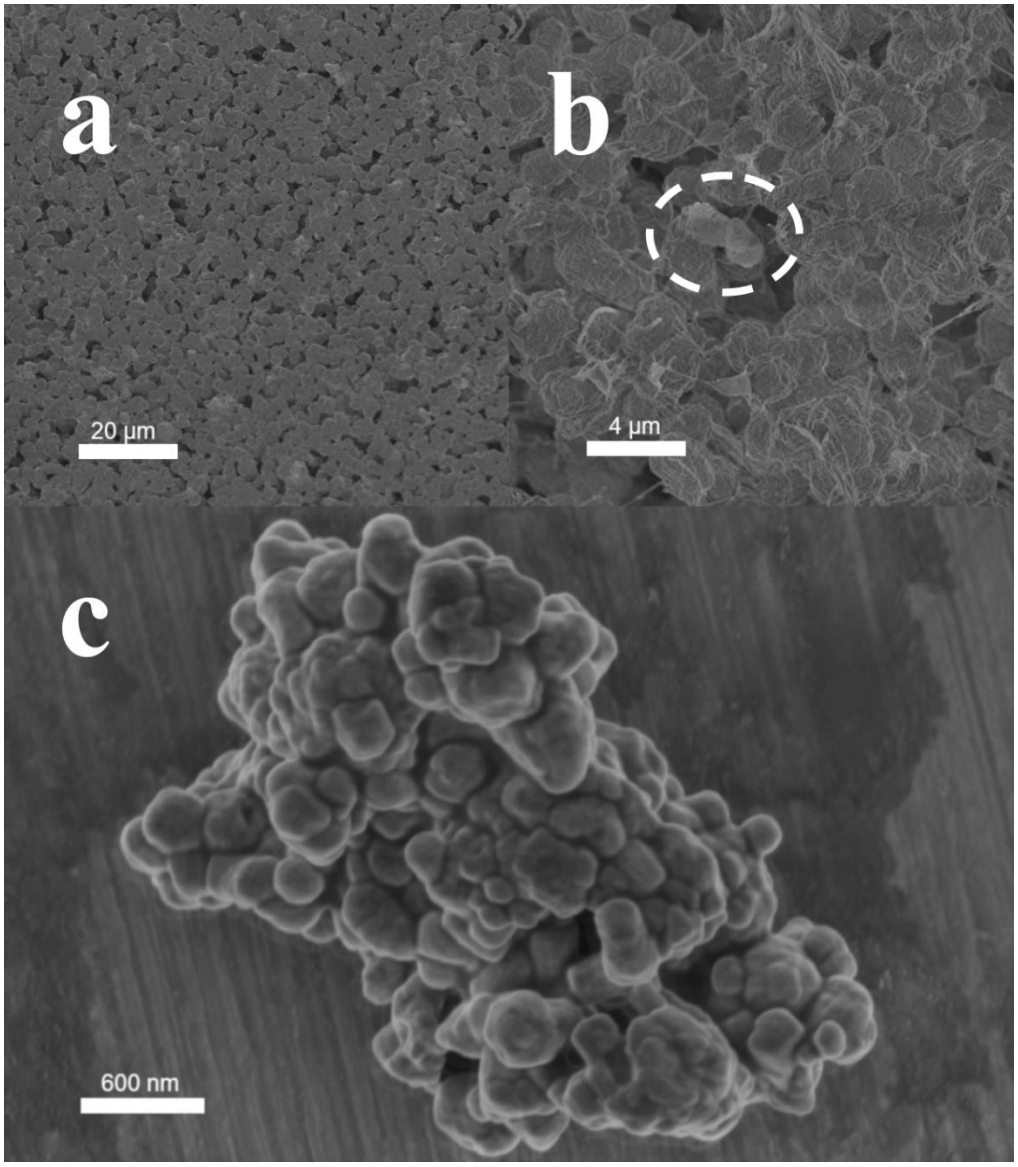

Figure 52. (a) SEM images of the Piezoelectric device. (b) a High-resolution SEM image (zoom on image a) of the piezoelectric device. PEG coated Li-ZnO inside white dashline (c) Sem image of PEG-coated Li-doped ZnO

The Scanning Electron Microscopy (SEM) images of the piezoelectric device reveals a high degree of homogeneity and prove a high degree of insertion of its component (Figure 52). PEG-coated 3D Li-ZnO is visible as small flock floating (white dashed marked) in the surface along with MWCNT as a fibrous structure in Figure 3b. Porosity in the piezoelectric device enhances amenability towards applied stresses. Figure 3c demonstrates the formation of PEG-coated Li-ZnO, and reveals a very high surface area. This high surface area and nonuniformity in structures help to increase the piezoelectric response due to a higher amount of flexibility at the surface compared to the lower amount of flexibility and hence lower movement deep inside the structures.

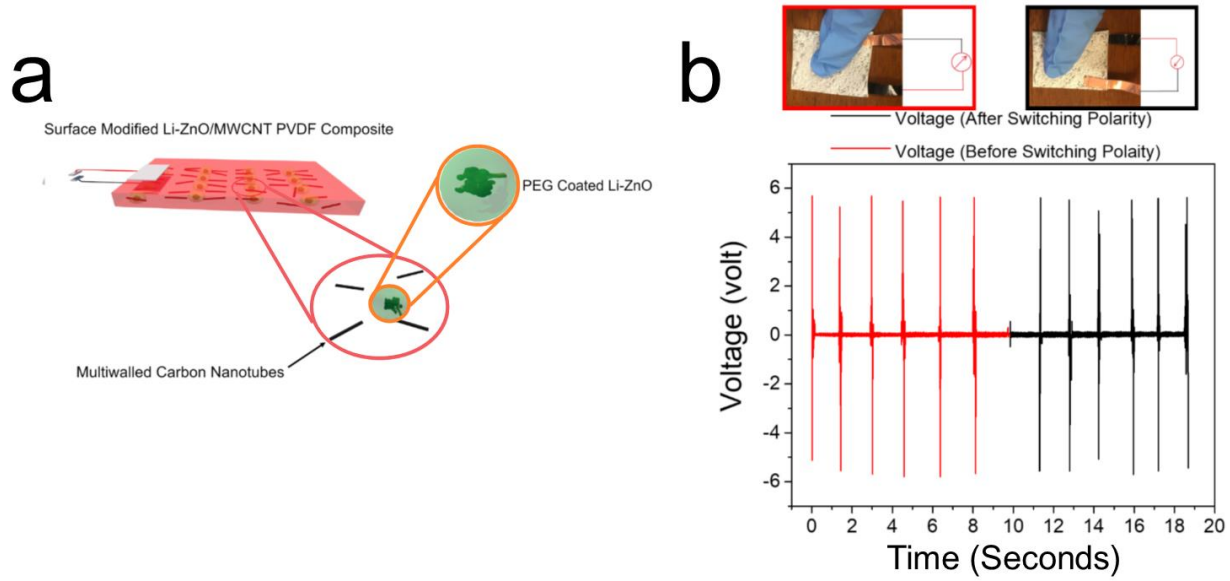

Figure 53. (a) Schematic diagram of the piezoelectric nanogenerator and (b) piezoelectric device's electrical response to finger presses

A schematic representation of the piezoelectric device architecture, as well as the electrical response of the device to applied finger-strength stress are presented in Figure 53. The response of the piezoelectric device was investigated by applying firm and quick finger presses and measuring the response by the oscilloscope (Tektronix Td-1001B). An open circuit voltage (V_{OC}) of 6 V was obtained. To verify the piezoelectric polarity of the composite, a switching polarity test was also performed (the device connection was switched after first 10 seconds of the test), and it was observed that switching the connections did not affect the response of the device. As the piezoelectric device was pressed with a finger, a stress was applied on the surface comprised mostly of PVDF polymer, which transferred the stress to surface modified Li-ZnO incorporated in the piezoelectric device. Finger press stressed the outer layer of the piezoelectric device which then transferred it to inner parts including the incorporated surface modified Li-ZnO. These stresses affect the composite piezoelectric device by transforming the regular structure and enhance the piezoelectric responses. Surface-activated Li-ZnO acts as a piezoelectric response enhancer because of its high dielectric constant, as well as a ß phase transformer for PVDF. In this way, an unpoled piezoelectric device response could reach a value nearly to a poled piezoelectric device.[131]

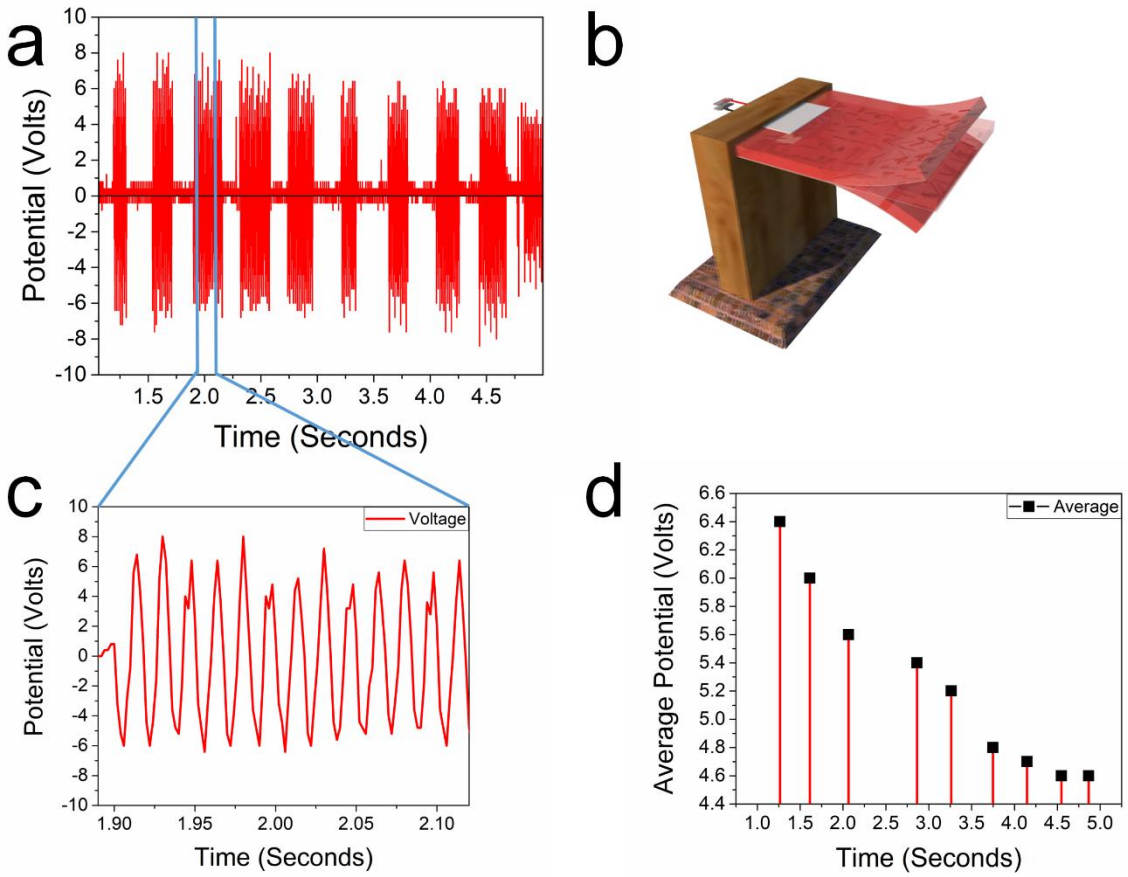

Figure 54. (a) Response on cantilever action of the reinforced piezoelectric device; (b) Schematic Representation of reinforced Piezoelectric Device in cantilever motion during oscillation; (c) Enlarged electrical response of cantilever oscillated motion; (d) Average potential drop on a timely basis in oscillated motion.

The performance of the piezoelectric sensor was tested with different body motions. Figure 54 shows the cantilever body motion (Figure 54b) of the piezoelectric sensor. In this case, the sensor film was cast on the surface of an aluminum sheet (thickness 0.3 mm) to mechanically support the film during oscillations. The piezoelectric device was connected to an oscilloscope to

measure alternating current (AC) voltage being formed due to electromechanical action. Figure 5a shows the cantilever's response to finger action, which clearly displays consecutive responses due to vibrations even after removal of the initial force. The accumulated response is due to repetitive vibration of the cantilever that creates consecutive contraction and relaxation. It is also worth mentioning the gradual decrease of voltaic response with time due to the slow mechanical failure of the aluminum sheet as well as deterioration of the interface between thin-piezoelectric film/Al foil leading to reduced conductivity. Figure 54c highlights an enlargement (zoomed) of a small portion of Figure 54b. It can be inferred from the data that piezoelectric device shows a continuous response with absolute amplitude difference value of around 2 V. Ups and downs in the graph are due to micro-vibration due to relaxation and stress of the film during cantilever motion. As long as vibration goes, it shows a decrease in the absolute amplitude production which is described in Figure 54d. The decrease in the response potential of the mechanical failure of aluminum foil due to its punch penetration. [132] Such a voltage decrease is not due to any piezoelectric device component which is described in Figure 9.

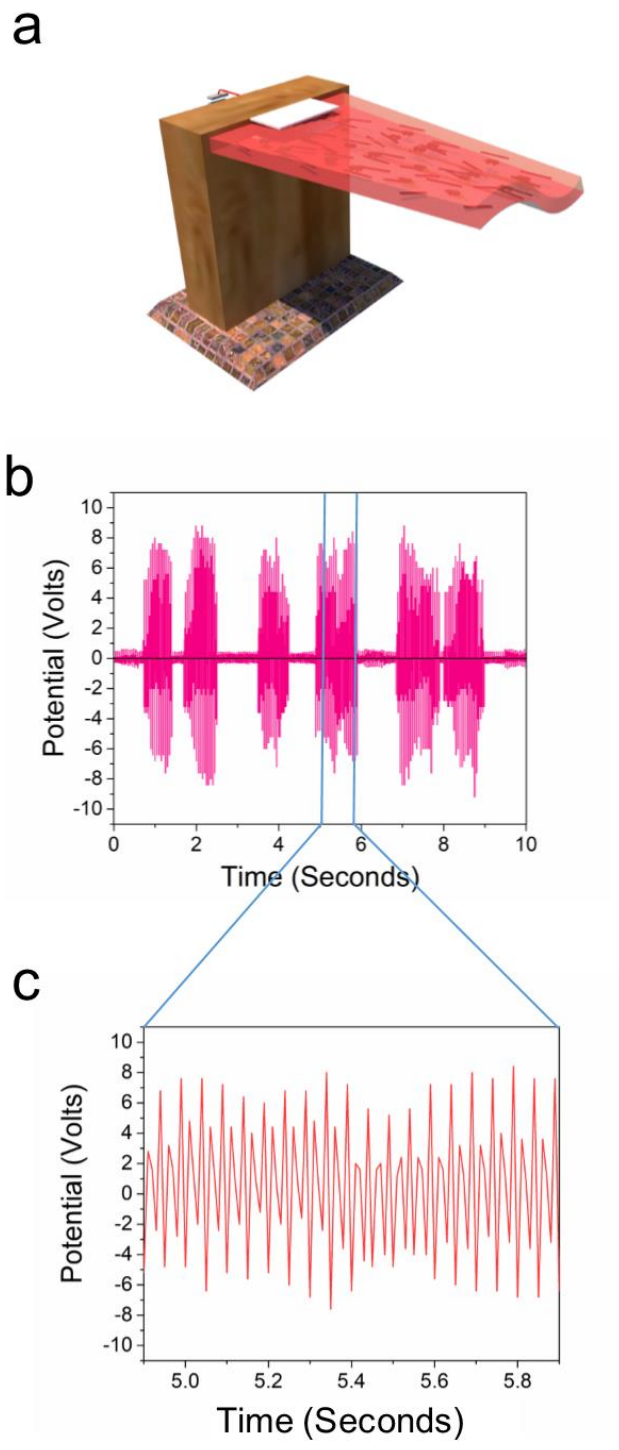

Figure 55. (a) Schematic representation of the piezoelectric device in torsion; (b) The electric response of the device to torsion motion; (c) An enlarged view of the response.

The piezoelectric device was also tested with a rapid 90° twisting (torsion). Twisting carried out in the clockwise direction and rapid release let the film return to its original position. The sensor returns to its previous shape immediately after the release of the applied twisting force. A schematic representation of the torsional characterization as well as the electrical response of the device to torsional stress are presented in Figure 55. Twisting generated amplitudes of AC voltage of up to 8 V (Figure 55b). Under continuous torsion up to 90° relative to its original orientation, the piezoelectric device shows continuous responses. The irregular breadth of response voltage was likely due to discontinuous mechanical relaxation of the thin film. This torsion response is quite different from the cantilever response due to consecutive voltage generation. The breadth of the response is seen to be larger for twisting due to greater stresses on the device compared to cantilever action, as twisting requires a greater applied force to counter the innate resistant to flexing of the device. Figure 6c shows an enlarged view of the response from 4.8 s to 6.0 s. Indeed, 20 peaks and dips are found to be present per second during torsion and relaxation. These rapids peaks and drops are followed by relaxation peaks and dips. Both relaxation and torsion were found identical. This finding indicates equal response and proves linear outcome during action and reaction as well as rapid response. It is clearly seen that average absolute amplitude fluctuates within 2 V, which proves that the response is very consistent. Such a 2 V fluctuation is due to micro-relaxation and stresses as well as the interaction between surface modified Li-ZnO.

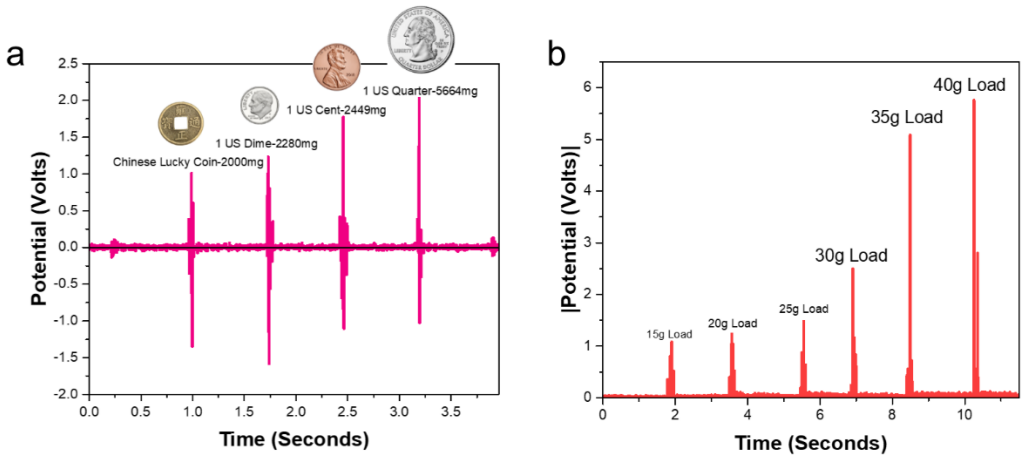

Figure 56. Electrical response of the piezoelectric device to the (a) coin drop and (b) different load tests.

Figure 56 shows the electrical response of the piezoelectric sensor film to various loads being dropped on it from a 5 cm height. It is clear that the absolute open-circuit voltage (V_{OC}) value was showing a linear response between 15 g (0.735 mN) to 40 g (1.960 mN) of the load (Figure 56a). In addition, to demonstrate the quick response of this type of device architecture, rapid forces were applied. Although the applied stress and recovery of the device were generated potential simultaneously, the signal was linear when considering the absolute voltage. The linearity of the response of the piezoelectric sensor (1 layer) was also tested with several kinds of coins (Figure 56b).

There are several peaks on every signal during different weight drop tests. These are the results of non-instantaneous impact and reaction. This peaks and dips are thinner than the response from Figure 54 and Figure 55 because of low thickness and small impact area. The

smaller thickness of the film made lesser non-homogeneity of Li-ZnO and CNT in the device, the higher the chance of impacting on the smaller surface area. Signal linearity with impact force has been tested in different sections of the device. It is also self-proving that interaction between surface activated nanoparticles and PVDF polymer is well working even after infliction done by stressing components. The linearity of response demonstrates the efficiency of the piezoelectric device as a stress sensor.

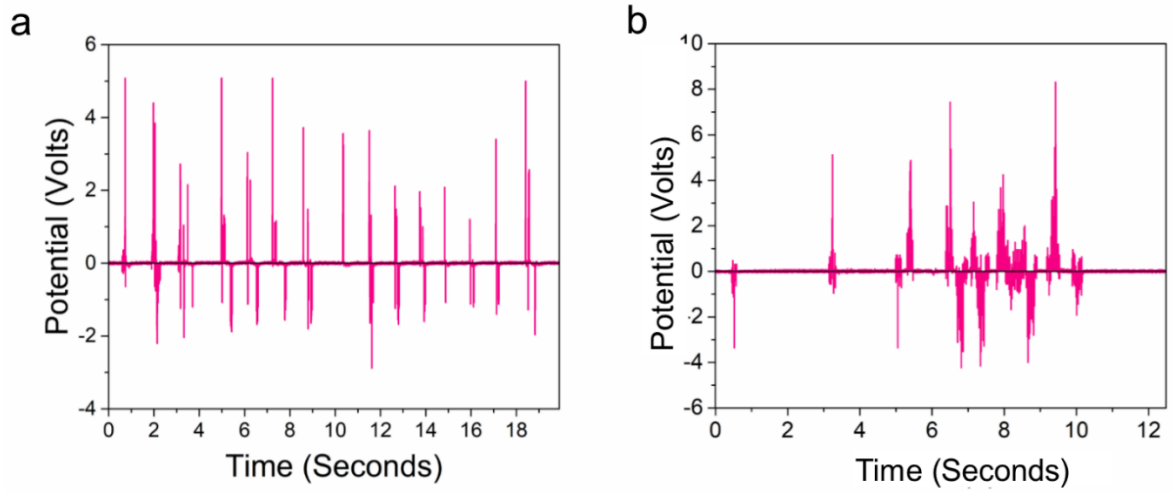

Figure 57. The electrical response of the piezoelectric device in different environments: (a) stressed underwater and (b) stressed under silicone oil.

The piezoelectric device was tested with finger-strength stresses in different environments to gauge its reliability underwater and under silicone oil (Figure 57). When placed under deionized water (DI) the device shows almost equivalent voltage amplitude responses (Figure 8a) compared to in-air, while when placed under silicone oil the sensor showed nearly

identical voltage responses (Figure 8b). However, due to the high penetration of PVDF in silicone oil and greater difficulty in applying mechanical stress to the device, the piezoelectric device shows signs of mechanical failure. The high viscosity of the silicone oil is also responsible for slow relaxation of film and hence somewhat decreased voltage under silicone oil. The underwater test also demonstrated less negative AC voltage due to the relatively high viscosity of DI water compared to air, which leads to a slower relaxation of the device from the stressed state. But the voltage output is quite similar. Hence it indicates that voltage production is largely dependent on surface activated Li-ZnO because under silicone oil device is getting destroyed by dissolving of PVDF while device was intact under deionized water.

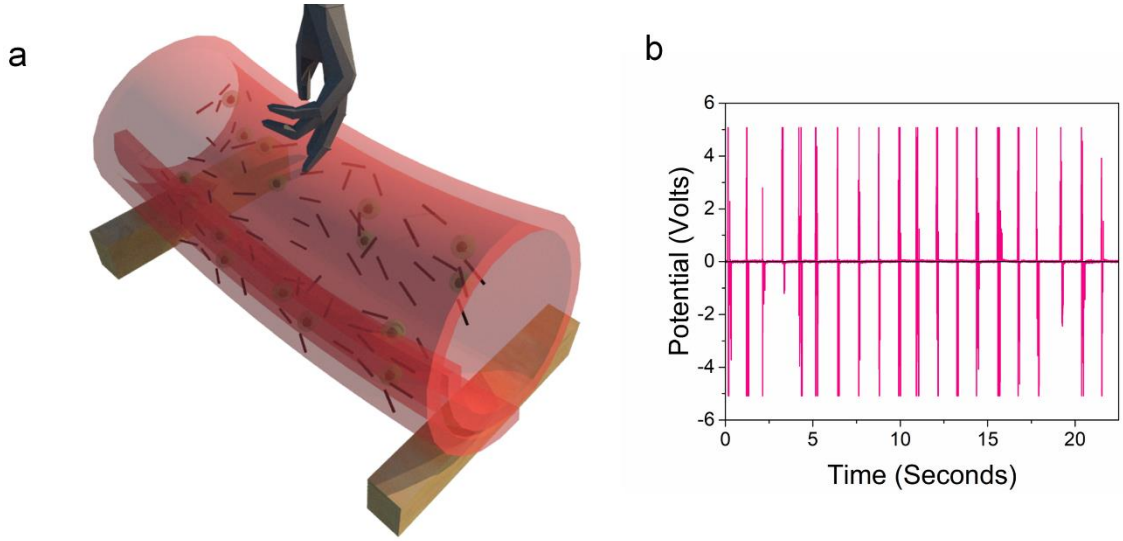

Figure 58. (a) Schematic representation of pressing of the rolled piezoelectric film; (b) Electrical response of pressing of rolled piezoelectric film.

The rolled film reveals a more consistent response (Figure 58) when stressed with a finger than any other test (Figure 58b). This consistent result is likely due to the rolled film more easily relaxing to its original state, since the rolled film took the shape of a cylindrical tube, which could sustain much larger stress in any direction perpendicular to surface and recover instantly. PVDF reinforced with MWCNT and Li-ZnO acts as highly ductile material when pressed from the top in rolled condition. In this condition (rolled), the device is tensed in the outer surface and compressed in the inner surface which enhances piezoelectric response during stress. This is carried out by releasing the tensile stresses on outer surface while and releasing the compressive stresses on inner surfaces. The release of stresses makes a quick recovery and hence makes a straight line as an output signal. From the Figure 58, it is easily inferred that positive voltage is initially created due to finger press and negative voltage is due to the release of the fingers press. It can also be seen that there is no more than one peak and dip in every press and release which can because of PVDF response and surface activated Li-ZnO response to press altogether. The rolled piezoelectric device is giving less noise than other body options like Figure 55 and Figure 56. This less noisy response is due to rolled up piezoelectric device returns to its original position quickly and efficiently without transmitting motion to stationary parts of the device. It is self-proving that rolled piezoelectric device can generate response more consistently with lesser response to noise ratio.

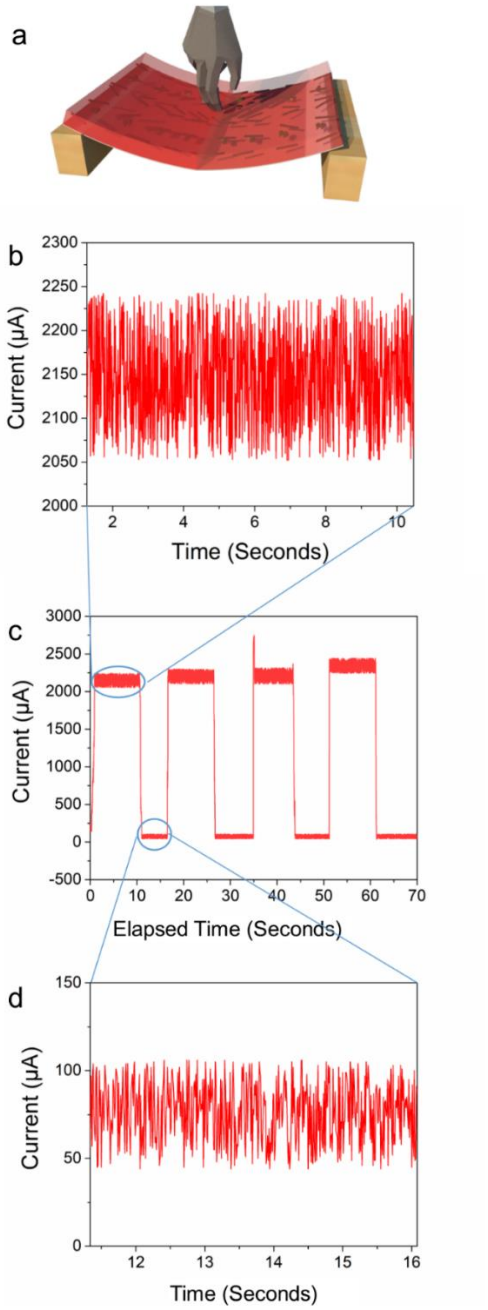

Figure 59. (a) Schematic representation of holding stress to the piezoelectric film; (b) Zoomed in the amperometric response of finger pressed substrate; (c) Amperometric response of finger pressed and released substrate; (d) Zoomed in the amperometric response of the released substrate.

The device was tested under constant stress and release cycle under an amperometric condition with potentiostat (VersaSTAT3) to find out the true potential of drew current due to change in the innate resistance (shown in Figure 59). The highest peak of 2740 µA found with constant stress (Figure 59c). It also evident from the figure that drew current is impressively stable under constant stress. The small fluctuation in peaks and humps because of micro relaxation and stress. Stress and release for an extended period did not affect the mechanically or by any other means to the device because the response is similar even after extended period of stressing and bending. Response peaks show the flux of current fluctuation within 200 µA amplitude during bending and hold (Figure 59a). Dips during the release of the bending show a fluctuation of 50 µA. It can also be seen in Figure 59a and Figure 59c that fluctuation is merely following any pattern which because of constant tension and compression largely affects the drew of current. This huge flux of current is much more dependent on MWCNT than any other components. Differently, surface activated Li-ZnO and PVDF is responsible for the current generation. The micro short circuit was not present due to a high degree of branching of MWCNT while shortcircuit requires smaller branching. High concentration of MWCNT increased the ability to turn the device into more electrically conductive. This highly conductive and reinforced piezoelectric device has a very high potential to be used as nanogenerator. The harvesting of energy is possible by using this piezoelectric device to convert deflections or displacements by applied forces such as mechanical vibration, body motion, air flow etc.

It has also to be noticed that PVDF and PEG are FDA-approved biomaterials for medical applications. Moreover, in recent years many studies are proposing the use of carbon nanotubes

and nanoceramics in medical devices, even as PVDF-based composites. [28,29] Therefore, this and other studies are paving the way to future biomedical exploitation of this type of hybrid piezotransducers.

All in all, the fabricated nanoceramic-filled polymer-matrix composite hybrid device combines multi-scale features (from nano-to-macro), including surface features, which act synergistically to induce robust and versatile piezoelectric performance. Surface modification represents a lower cost option as an alternative to energy treatments towards the achievements of smart transducers of easier transfer to daily life, which could represent breakthrough options for energy and medicine. [29]

Conclusion

In conclusion, we have demonstrated a self-polarizing piezoelectric device architecture that can serve as a robust and versatile sensor/nanogenerator by combining MWCNT with PEG-coated Li-ZnO in the PVDF matrix. The output performance is greatly enhanced compared to other unpoled nanogenerators due to the induced self-polarization. In addition to the avoidance of cost-intensive poling, the linearity of the output voltage (up to ~10 V) and high drew of current flux (~2800 μA) due to innate resistance change were made possible by the incorporation of MWCNTs to increase the conductivity of the PVDF matrix. Our approach provides a simple and cost-effective way to enhance the performance of Li-doped ZnO based piezoelectric nanotransducers, using a facile synthetic method that is well-suited for large-scale piezoelectric device fabrication for green energy scavenging and sensory utilization. Formed piezoelectric device has also been tested with different body motion which has proved potentiality of the device as stress sensor as well as nanogenerator with high mechanical stability.

Experimental Section

Surface Activated 3D Li-Doped ZnO Synthesis:

The 50 mM of zinc nitrate ($Zn(NO_3)_2$, Sigma-Aldrich), lithium nitrate ($LiNO_3$, Sigma-Aldrich) and 50 mM of hexamethylenetetramine (HMTA, Sigma Aldrich) was prepared, and to 100mL of this solution was added to 20 ml of ethanol (Sigma-Aldrich) treated 500 mg poly(Styrene-co-divinylbenzene) microspheres, (6.0-10.0 µm average particle size, Sigma-Aldrich). This solution was stirred on a hot plate for 60°C for 2 hours followed by holding in oven temperature at 95°C for 10 hours. After this growth process, the remaining liquid was decanted, and the solid product was dried in an oxygen rich environment at 600°C for 2 hours. After 2 hours the temperature was reduced to 450°C and substrate was held at this temperature for 3 hours for annealing. For even coating of the surface of the microparticles, they were then added to a 0.01 g ml^{-1} ethanolic solution of PEG (Alfa Aesar, 20000 g mol^{-1}) and stirred for 1 hour until a brown suspension was obtained. This suspension was allowed to sit for 2 hours. The suspension was then filtered, and the solids washed with ethyl alcohol for removal of excess PEG. The PEG-coated Li-ZnO was dried at room temperature under vacuum overnight.

Preparation of free PEG coated Li-ZnO/PVDF Composite:

The thus prepared PEG-coated Li-ZnO along with PVDF pellets (Sigma-Aldrich, ~180,000 g mol^{-1} by GPC) was added to MWCNTs suspended in anhydrous N, N-Dimethyl formamide (Sigma-Aldrich) and stirred for 48 hours. This mixture was drop-cast and pressed between the glass substrates, and the solvent was evaporated at 120°C for 6 hours to generate the

thin films. The thin films were collected, heated (at 120°C) and pressed (8 tons) to form thin film composites. Both sides of the device were painted with a silver paste for electrical measurements.

Measuring of Output:

Electrical contacts were made by attaching wires to the device with conductive Ag paste, and the device was connected to the VersaSTAT3 machine to measure the piezoelectric output voltage as well as amperometric electricity . Results were confirmed by the measurement with Tektronix TDS 1001B.

Morphological Characterization:

SEM characterization of the Ag/Au-TiO2 cotton fiber samples was performed using a JEOL 7800 F Field Emission Scanning Electron Microscope, equipped with an Electron Dispersive X-ray Spectroscopy system (EX-37270VUP).

FTIR Characterization:

Fourier-transform infrared spectroscopic analysis was carried out using a Perkin Elmer Frontier FTIR spectrometer, and data was collected in absorbance mode over the full range of the instrument (4000–450 cm^{-1}). Samples for FTIR analysis were prepared by thoroughly mixing equal amount of lithium doped zinc oxide working samples with 25 mg of optical grade potassium bromide(purchased from International Crystal Labs), and pressing the mixture into a thin, one-inch diameter pellet using a hydraulic press. The pellets were very fragile and

were directly transferred onto copper tape (to act as a rigid backing) with a hole such that the IR beam was obstructed by only the pellet. The procedure was repeated for working sample of PEG coated Lithium doped zinc oxide.

CHAPTER IV

PIEZOELECTRIC-TRIBOELECTRIC HYBRID NANOGENERATOR

Introduction

The world has seen a drastic increase in the global population, economic activity and technological development in recent years. This progress is creating an increasing demand for energy. By the end of 2035, this demand will almost be doubled. At the moment, we are majorly dependent on fossil fuels as an energy source. About 86% of the generated energy of the World is coming from fossil fuels which are not only severely harmful to the environment but are also being depleted with time[8,9,133,134]. Thus, experts are promoting renewable energy for energy generation as a solution for present and future energy scarcity problem. Mechanical energy can be one of the alternatives to existing energy crisis and can contribute significantly in solving the problem. There are several sources for mechanical energy, including ocean wave energy, wind flow energy, water flow energy, human motion energy, etc. [135,136]. In 2006, Wang *et al.* made a nanogenerator based on the piezoelectric effect which was a revolutionary invention towards the goal of mechanical harvesting energy[137]. Later in 2012 Wang and his group introduced the concept of Triboelectric Nanogenerator (TENG)[138]. From there on several attempts have been made to build Piezo-Triboelectric Hybrid Nanogenerators (PTENGs) which can be solution to our global energy issues [139–145]. Device fabrication from the combination of the triboelectric and piezoelectric nanogenerator does not

require any substantial changes due to hybridization [146,147]. Recently several hybrids nanogenerator has been developed to scavenge energy and sensory application. Despite these vast amount of research has been conducted in hybridization of nanogenerators, the practical application and cost effectiveness is still a matter of consideration in the field of hybrid nanogenerator [91].

In this work, we have developed and fabricated a novel, cost effective tribo-piezo hybrid nanogenerator with PVDF/MWCNT/Li-ZnO as the piezoelectric component and PTFE/PDMS as the triboelectric component. Polyvinylidene Fluoride (PVDF) is very well known material used in such nanogenerator due to its piezoelectric response [146,148,149] and accordingly it forms a major part of the piezoelectric panel. Previously surface modification of 3D nanoparticles has been reported as a good solution for avoiding costly polishing action [7]. Hence, we induced surface modified Li-ZnO nanowires into PVDF to increase its piezoelectric response and avoid the need for polishing. Furthermore, MWCNT was doped into the composites of Li-ZnO/PVDF to improve its conductivity [150,151]. For the Triboelectric action, PTFE on Al was used as the electronegative material and PVDF as the electropositive material, which are reported to yield high triboelectric output [152,153]. To further improve the triboelectric effect and increase electrical conductivity; PDMS was introduced into PTFE [153,154]. Also, the effect of applied force in variable frequencies on the PTENG was carried out to see its response under applied stress.

Experimental Procedures

2.1. Surface Activated Li-ZnO Nanowire Synthesis: The 50 mM of zinc nitrate ($Zn(NO_3)_2$, Sigma-Aldrich), lithium nitrate ($LiNO_3$, Sigma-Aldrich) and 50 mM of hexamethylenetetramine (HMTA, Sigma Aldrich) was prepared, and to 125 ml of this solution was stirred on a hot plate for 60°C for 2 hours followed by holding in oven temperature at 95°C for 12 hours. After this growth process, the remaining liquid was decanted, and the solid product was dried and annealed in an oxygen rich environment at 600°C for 2 hours following by cooling to 450°C and substrate was held at this temperature for 3 hours for annealing. For even coating of the surface of the Li-ZnO, they were then added to a 0.01 $g \cdot ml^{-1}$ ethanolic solution of PEG (Alfa Aesar, 20000 g mol-1) and stirred for 1 hour until a brown suspension was obtained. This suspension was allowed to sit for 2 hours. The suspension was then filtered, and the solids washed with ethyl alcohol for removal of excess polyethylene glycol (PEG). The PEG-coated Li-ZnO was dried at room temperature under vacuum overnight.

2.2. Preparation of free PEG-coated Li-ZnO/PVDF Composite: The prepared PEG-coated Li-ZnO along with PVDF pellets (Sigma-Aldrich, ~180,000 g mol-1 by GPC) and MWCNT was added with anhydrous N, N-Dimethyl formamide (Sigma-Aldrich) and stirred for 48 hours. This mixture was drop-casted in the glass substrates, and the solvent was evaporated at 120°C for 6 hours to generate the piezoelectric film. Both sides of the device were painted with a silver paste for piezoelectric response measurements. For hybrid nanogenerator, one side of the Piezoelectric film was painted with silver paste, and other surface was kept as it was for triboelectric action.

2.3. Preparation of PDMS/PTFE Copolymer triboelectric Layer on Aluminium Film: 2 g Polydimethylsiloxane (PDMS) (Sylgard 184, Silicone Elastomer base) and 0.2 g Curing Agent

(Sylgard 184, Silicone Elastomer Curing Agent) was added to hot (85°C) 2 g tert-Butanol (Sigma Aldrich) in a 20 ml Disposable Scintillation Vials. The mixture was mixed in a vortex mixer to ensure well mix. The mixture was placed and spread by doctor blade technique using a smooth surface glass rod on the clean surface of Aluminum foil (thickness of 0.01mm) following by drying in room temperature for 24 hours.

2.4. Preparation of Hybrid nanogenerator: The hybrid nanogenerator was prepared by placing two PTFE spacer on both ends of the piezoelectric copolymer following by placing the triboelectric film on top of PTFE spacer facing the polymer surface towards piezoelectric copolymer.

*2.5.Measuring of Output:*Electrical contacts were made by attaching wires to the device with conductive Ag paste and uncoated aluminum foil, and the device was connected to the VersaSTAT3 machine to measure the piezoelectric output voltage as well hybrid nanogenerator's electrical output. Results were confirmed by the measurement with Tektronix TDS 1001B.

2.6. Morphological Characterization:

Scanning Electron Microscopy (SEM) characterization of the samples was performed using a JEOL 7800 F Field Emission Scanning Electron Microscope, equipped with an Electron Dispersive X-ray Spectroscopy system (EX-37270VUP).

2.7. Photoluminescence measurement:

Photoluminescence (PL) measurement was carried out on an Edinburgh made FLS980 spectrometer which was equipped with steady-state Xenon lamp with variable frequency.

2.8. FTIR Characterization:

Fourier-transform Infrared Spectroscopic analysis was performed using a Perkin Elmer Frontier FTIR Spectrometer. Relative transmittance was collected in absorbance mode over a full range of (4000-450 cm^{-1}). Samples for FTIR analysis were prepared by mixing equal amount of optical grade potassium bromide (International Crystal Labs) following by pressing the mixture to 8-ton force and making one-inch diameter pellet using a hydraulic press. The pellets were directly transferred onto copper tape to act as rigid mechanical support with a hole in it to let IR beam pass only through pellet. The procedure was repeated for working sample of Lithium doped zinc oxide NW, and PEG-coated Lithium Doped Zinc Oxide NW.

Results and Discussion

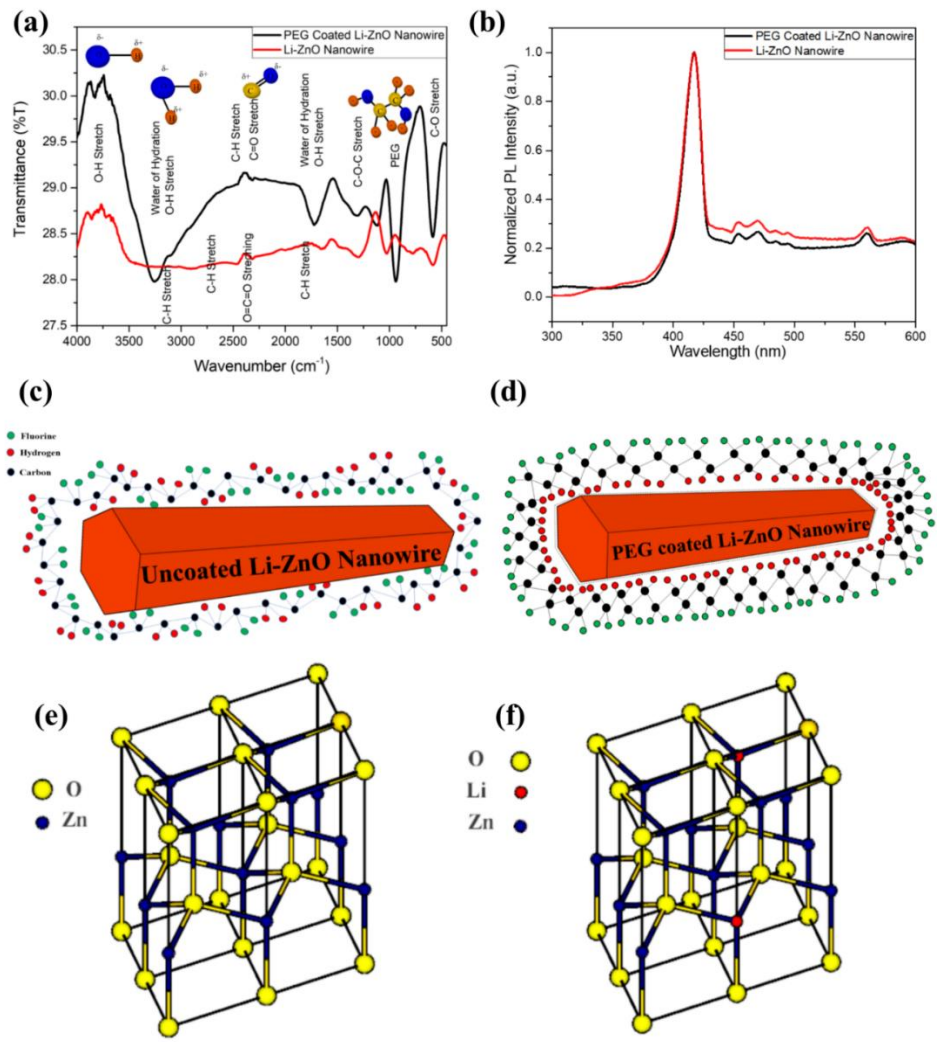

Figure 60: (a) Fourier-transform infrared spectroscopy (FTIR) spectra of PEG-coated and uncoated Li-ZnO. (b)Photoluminescence spectra of PEG-coated and uncoated Li-ZnO NW (c) Uncoated Li-ZnO NW without ß phase of PVDF (d) PEG Coated Li-ZnO with ß phase of PVDF polymer (e) Wurtzite Structure of Zinc Oxide (f) Wurtzite Structure of Li-ZnO.

To demonstrate the effectiveness of PEG coating on Li-ZnO nanowire for ß phase development, FTIR and PL study was conducted.

FTIR spectroscopy gives information related to interaction of PEG to the surface of the Li-ZnO nanowires. According to Figure 60(a), the absorption band located around 3600 cm^{-1} indicates the presence of hydroxyl group. The absorption peak around 2842 cm^{-1} in the spectrum of Figure 60(a) is attributed to C-H stretching which is the signature of PEG being efficiently coated/adsorbed on Li-ZnO NWs [155]. The hydroxyl absorption in case of PEG coated Li-ZnO is shifted to low wavenumber which suggests that PEG adsorbed on surface of Li-ZnO nanowires through H-bonding though other interaction can't be ruled out [156]. However, presence of O-H band peak in PEG coated Li-ZnO is not only dependent on hydration as well as presence of O-H from PEG. C=O stretching is confirmed by small rise on 2395 cm^{-1} on the spectra of PEG-coated Li-ZnO. C-O-C stretch is represented by the peak at 1341 cm^{-1}. The characteristic peak of PEG is shown at 931 cm^{-1} which supports presence of PEG in the surface of Li-ZnO. This presence is also confirmed by other organic stretching like C-O-C, C-H, C-O, and C=O.

Figure 60(b) shows the normalized PL spectra of the Li-ZnO and PEG-coated Li-ZnO synthesized at room temperature. Emission in such cases can arise due to recombination of photoinduced charge carriers (electron, holes etc.). The spectral profile, position and emission intensity and can provide variety of information such as presence of surface defects, oxygen vacancies, charge carrier trapping efficiency and their recombination kinetics [157]. The emission spectra shown in Figure 1b depicts various narrow peaks around 420, 456, 472, 485, 496 and 561 nm. Such multiple emission peaks in zinc oxide is ascribed to presence of intrinsic defects such as surface states, oxygen vacancies and interstitials [158]. The violet-blue emission is attributed to presence of zinc interstitial (Zn_i) defect [159] whereas green emission is attributed

to lithium induced generation of singly ionized oxygen vacancies (SIOV) in ZnO nanowires [160,161].

Moreover, surface modification through PEG coating on Li-ZnO does not showed drastic influence on PL profile except slight reduction in PL intensity mainly in the zone beyond 430 nm. This can be attributed to reduction in defects in Li-ZnO after modification using PEG. The fact that there is not much altercation in spectral profile of Li-ZnO on PEG coating suggested that effect of surface modification on the Li-ZnO nanowire's PL behavior is almost negligible except slight reduction in defects. Most interestingly the absence of a usual broad defect induced luminescence band is evidence of the lower amount of surface defects in existing Li-ZnO due to careful synthesis [162]. Because of high formation energy needed; lithium is not able to replace oxygen ion rather it diffuses into ZnO lattice and occupy interstitial position. This leads to the formation of both interstitial as well as substitutional defects which are compensated by co-existence O_i and V_O in ZnO lattice [163,164]. Following these studies and studies previously conducted, it can be inferred that the ß phase of PVDF development was largely initiated along the surface of PEG-coated Li-ZnO. This ß phase development of PVDF is demonstrated in Figure 60(c-d). As surface of the NW became more negatively charged because of the actively interaction between -CH_2 dipoles of PVDF via local electrostatic interactions, this enhanced the bipolar ordering in PVDF. In this composite O-H group of PEG and H-C group of PVDF reduced the necessities of utilising costly electromagnetic poling for ß phase attaining. This ß phase attaining due to chemical groups interactions enhanced magnetic dipole towards the direction of applied stress to composites. [7,8,65].

Possible defects on ZnO lattice is represented by Figure 60(e) and Figure 60(f). It is already proven that hydrothermally grown Li-ZnO exhibits better ferroelectric properties (e.g.

piezoelectricity) than ZnO. This is due to the induced defects which results in lesser band gaps. It was also found that crystallinity gets better by Lithium doping on ZnO lattice [165–167].

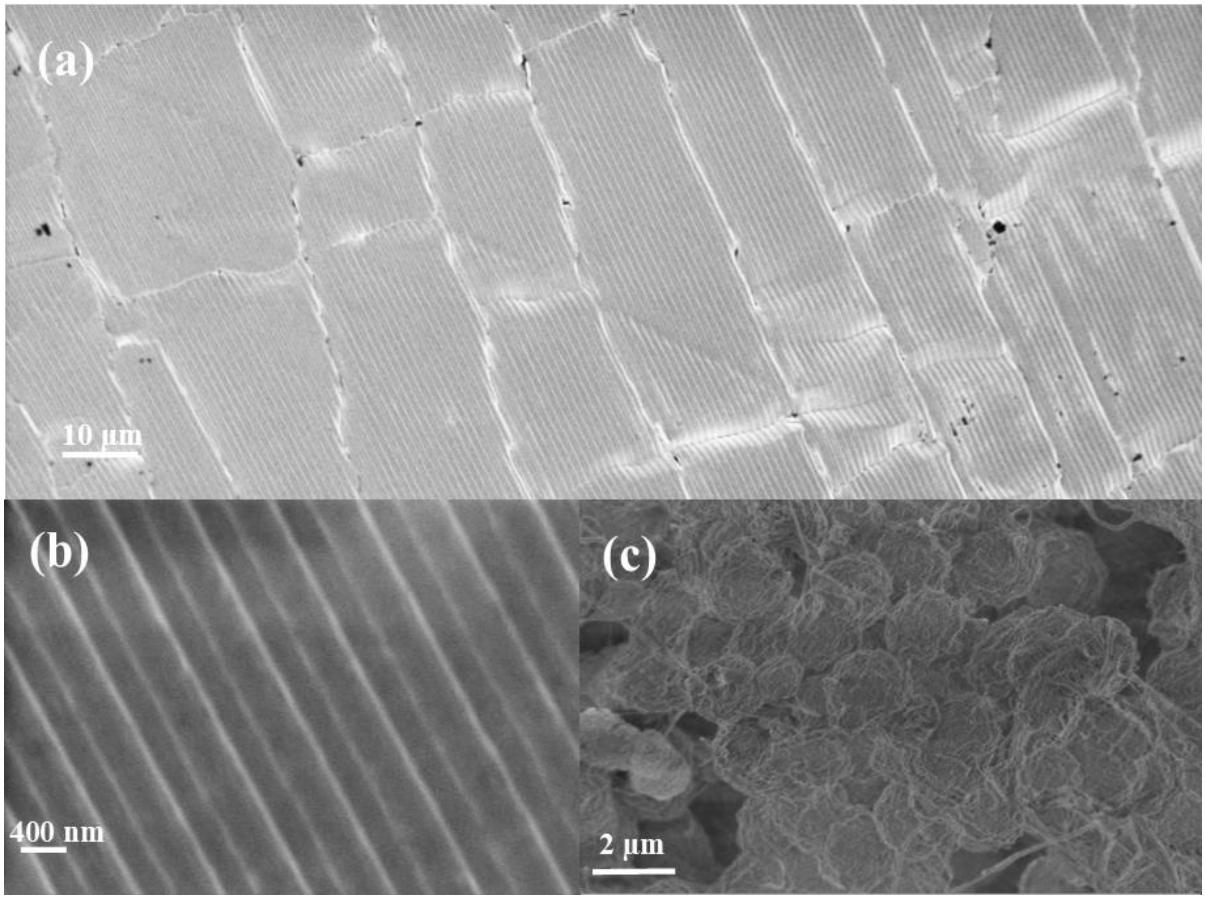

Figure 61: SEM micrographs of (a) triboelectric layer, (b) enlarged view of the triboelectric layer (c) piezoelectric film surface.

SEM images of the piezoelectric and triboelectric layer in Figure 61 show the uniform morphological structure of PDMS/PVDF triboelectric layer in Figure 61(a). Figure 61(b) is the closer view of the triboelectric layer. Parallel lines demonstrate the effect of doctor's blade

technique on the synthesis of the triboelectric layer which confirms equal applied stress all along the layer during synthesis. However, grain-like structures in Figure 61(a) are good evidence of uniform drying as well as even surface morphology. Figure 61(c) reveals the surface morphology of the piezoelectric surface of PEG-coated Li-ZnO/PVDF/MWCNT. SEM image shows microvoids due to the evaporation of DMF. These microvoids lead to the high surface area which increases better contact triboelectric layers and more triboelectric response and non-uniformity in structure to help to increase piezoelectric response and higher amount of flexibility during applied external stress due to its soft structure. The fiber-like portion in the image is evidence of the MWCNTs. Yet, the absence of any surface modified Li-ZnO in SEM image confirms well insertion of metal oxides in the polymer matrix, hence its maximum efficiency bosting in hybrid nanogenerator.

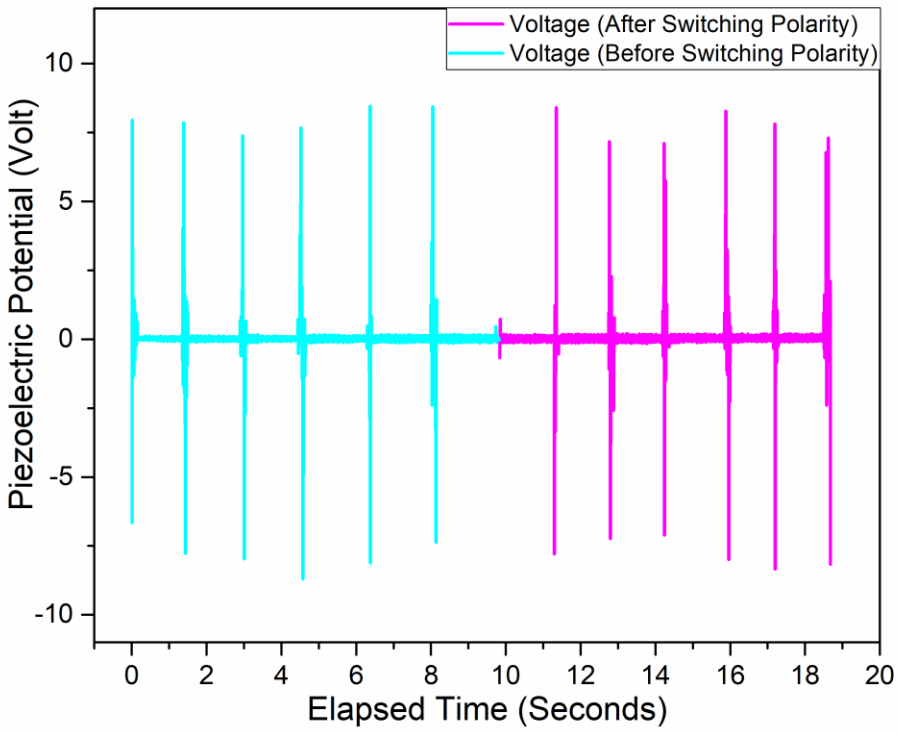

Figure 62: Piezoelectric Response on finger press of drop casted piezoelectric film.

Formed drop cast piezoelectric film was tested with finger pressing to see the usefulness of piezoelectric layer as a potential energy producer. The finger press test yielded a voltage response to 8.1 open circuit voltage (V_{oc}). This response is due to the transfer of stress from the top surface to PVDF polymer matrix as well as MWCNT and Li-ZnO NW. Stress applied to the piezoelectric nanogenerator transfers to nanowires along with Li-ZnO NW which deforms them from their original shape. This initiate production of charge from piezoelectric two-dimensional nano-objects. This is largely depending on the d_{33} values of the nanowires. The more deformation turns more charge production from the nanogenerator. As nanowires are more ductile considering other dimensional nanomaterials, more charge generation is achieved. This

piezoelectric film was also tested with switching polarity to understand the effectiveness of piezoelectric film as an energy-producing component of PTENG. Switching polarity shows that the voltage production remained same which means the production of energy is reliable under any axial stressing conditions. It can also be seen in Figure 3 that the produced noise is much smaller compared to the response which indicates the high response timing as well as higher conductivity in the film due to MWCNT effect. As soon as the charge is produced instantly after the stress is applied to the piezoelectric device, it transfers immediately to the measurement equipment, hence the response is quick enough to avoid any noise production. Rapid response caused by rapid release of strain from piezoelectric nanogenerator [168].

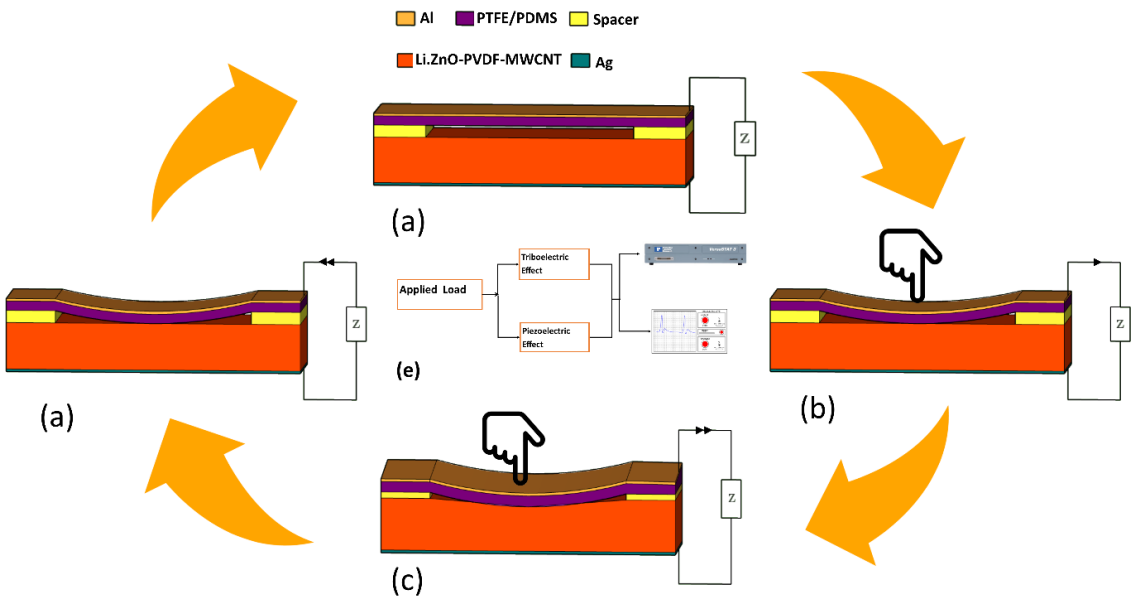

Figure 63: Load Cycle (clockwise) of TPENG during test conditions: (a) no applied stress (b) initiation of contact between triboelectric layers (c) piezoelectric action due to stress on the piezoelectric layer (d) release of stress (e) Block diagram of measuring piezoelectric and triboelectric response.

The Load cycle of PTENG has been demonstrated in Figure 4 along with clockwise direction. Figure 63(a) shows the relaxed condition of TPENG. Triboelectric action, as well as initial stress transfer from the triboelectric layer to the piezoelectric layer, is demonstrated by Figure 63(b). Figure 63(c) demonstrates the deflection of the piezoelectric layer as well as the transfer of load to the piezoelectric layer. Figure 63(d) demonstrates the release of load from PTENG.

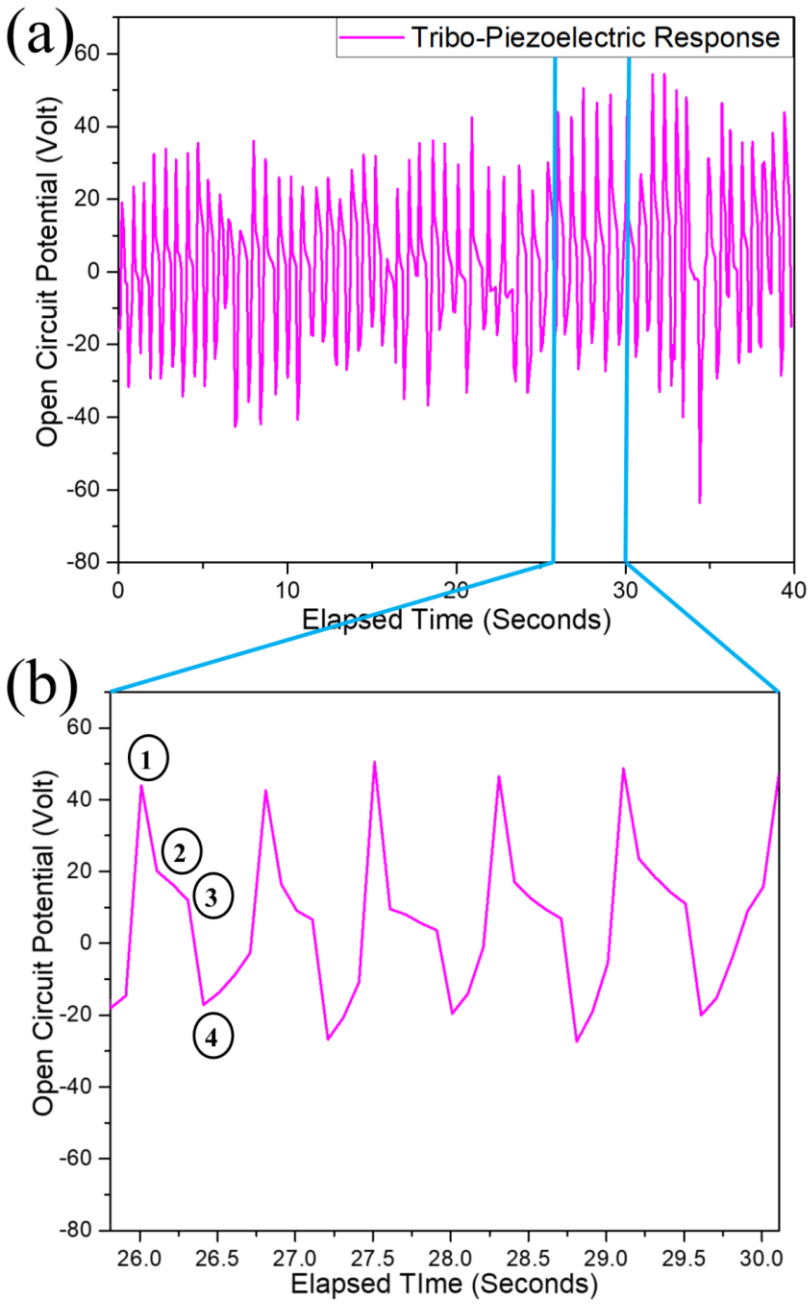

Figure 64: (a)Response (Open Circuit Voltage) of PTENG with Finger press (b) Enlarged view on PTENG Response.

The effectiveness of PTENG was tested with finger presses and showed in Figure 64. Figure 64(a) reveals response of PTENG on finger press action while Figure 64(b) reveals a closer look at open circuit voltage response of finger press. It can be easily inferred from Figure 5 that the produced voltage is reaching up to 60.1 V while most of the noise diminishes. Figure 64(b) shows a closer look at response which identifies response to finger press varies from surface to surface. While stress is applied to the aluminum surface, the stress is transferred to the triboelectric layer immediately under the aluminum surface which comes closer to the piezoelectric layer, and the triboelectric mechanism is initiated. Asa consequence, the voltage reaches a higher point (point 1, shown in Figure 64(b)). As long as the triboelectric layer completes its action, the piezoelectric mechanism is initiated by stress on the piezoelectric layer which takes much longer time to termination of response because of the higher thickness of the piezoelectric film. This piezoelectric response is shown from point-2 to point-3. As stress is released from the PTENG, piezoelectric and triboelectric mechanism work vice versa but in a much faster period, therefore, the response reaches from point-3 to point-4 as negative potential. This cycle is repeated along applied finger presses. This response to applied stress is very much representing the level of applied stresses to the nanogenerator. The level of applied stresses (as load) vs voltage response is represented in following figures.

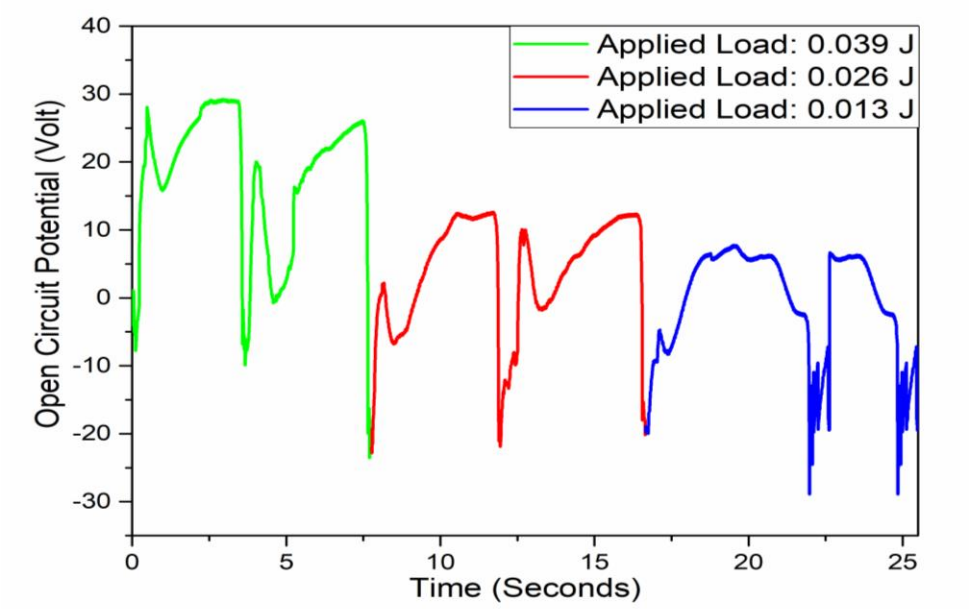

Figure 65: Open Circuit Voltage (Voc) vs. time for the different load (J)

The electrical response of the PTENG for variable applied load was observed experimentally. Figure 6 shows the value of V_{oc} with time for the variable applied load (J) on the PTENG. With the application of the load, the triboelectric upper layer (Al/PDMS/PVDF) moves gradually towards the lower layer from its initial position. Due to this movement, triboelectric potential occurs in the device. Thus, the V_o of the devices increases. As the upper layer touches the lower surface, the stress transmits to the lower surface. The lower surface shows a repulsive force to prevent itself from getting deflected. Thus, the overall voltage reduces a little. But the applied load is sufficient to deflect the Li. ZnO-MWCNT-PVDF layer. In turn, the voltage gets increased towards its peak. After the load is released the PTENG moves towards its initial position. Also, the triboelectric charges transfer towards the opposite direction. So, the voltage decreases gradually. The output V_o of the device increases with the increment of the applied load. During the load test, the voltage increased from 9.5 V to 29.2 V when the applied load

increased from 0.013 J to 0.039 J. Higher load creates higher stress on the microstructure which causes higher deflection of the piezoelectric layer. Higher deflection of the piezoelectric device leads towards the larger value of V_{oc}. This character of the device promotes hybrid PTENG as an effective transducer or stress/pressure sensor.

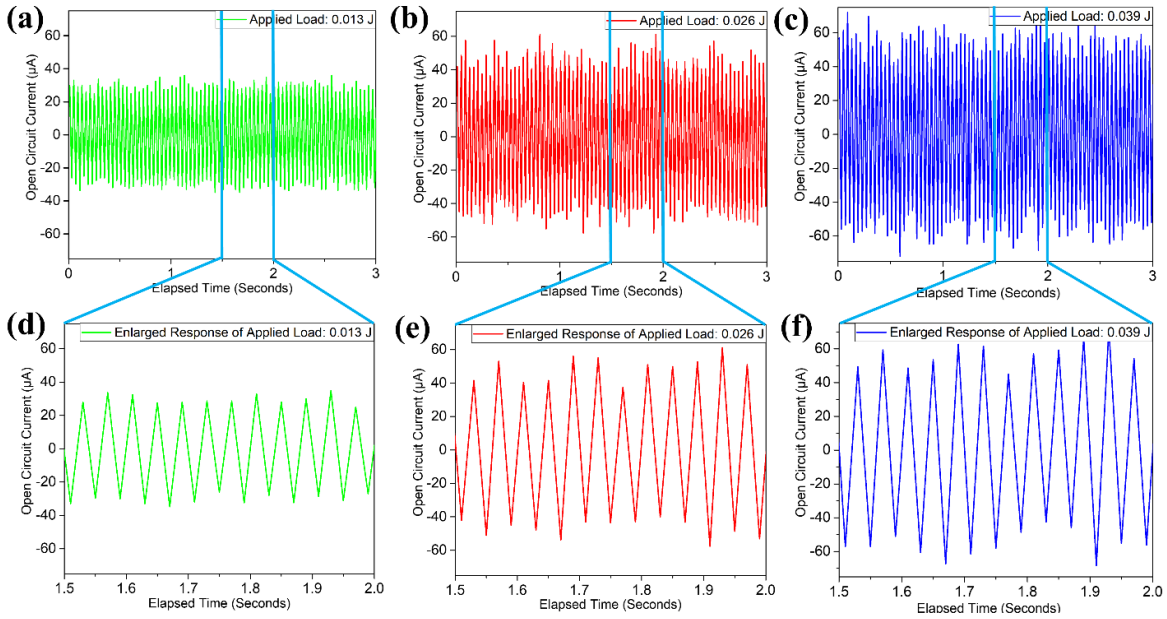

Figure 66: Open Circuit Current of PTENG under (a) Applied Load 0.013J (b) Applied Load 0.026J (c) Applied Load 0.039J (d) Enlarged Response of Applied Load 0.013J (e) Enlarged Response of Applied Load 0.026 J (f) Enlarged Response of Applied load 0.039 J.

Open circuit potential of PTENG is measured under different applied load to measure its productivity in current production. It can be easily inferred from Figure 66(a), (b) and (c) that current production is largely increased under higher load conditions. Under an applied load of 0.013 J open circuit current was reached on an average of 31 μA. However, this value reached 50 μA and 65 μA under 0.026 J and 0.039 J, respectively. It is also clearly evident that fluctuation

in current production is higher while PTENG is under higher load. Still, the current production is considerably analogous towards the applied load. Under the load of 0.013 J in Figure 66(a), electricity plateaued towards the value of 35.2 µA. Whereas under 0.026 J load in Figure 66(b), it reached up to a value of 65 µA. PTENG showed the highest open circuit current value of 75 µA under a load of 0.039 J. This is mostly due to the d_{33} values of composite. Same d_{33} values but different electrical output, resulted as a consequence of different applied loads, hence different charge production from piezoelectric portion of the nanogenerator. Enlarged view of electrical response of PTENG in 0.013 J, 0.026 J and 0.039 J is demonstrated respectively in Figure 66(c), 66(d) and 66(e). It can be easily inferred from the graphs that the amplitude of the response did not vary much during lower applied force (0.013 J). However, this amplitude started to alter up and down with higher applied load (0.026 J, and 0.039 J). This alteration is due to residual load from the last hit to the composite. Triboelectric and piezoelectric effect was acting simultaneously, therefore the combination of the number of responses is higher than the number of applied load.

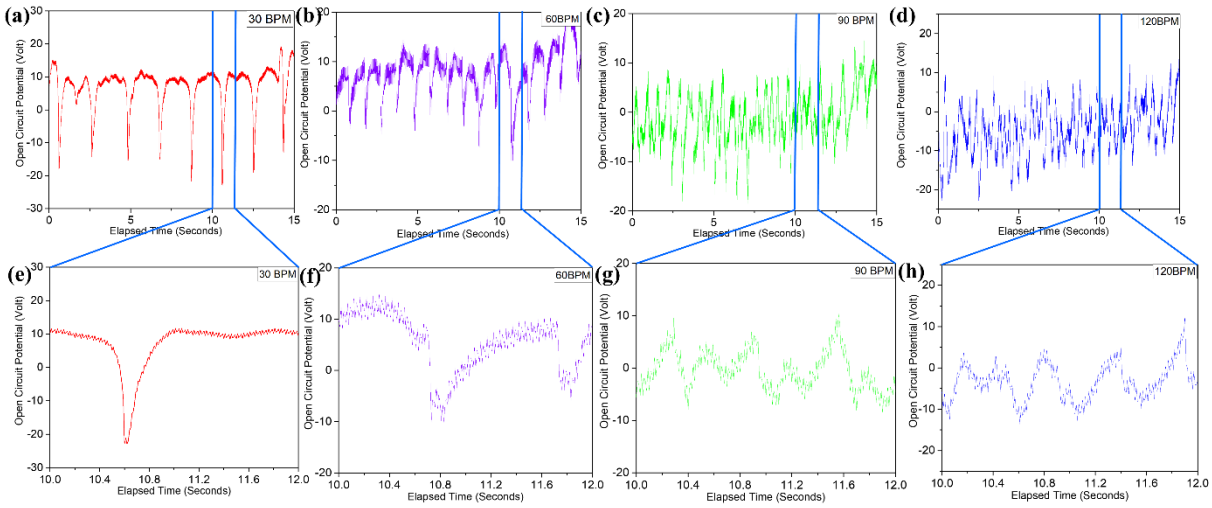

Figure 67: Output response of PTENG with variable load frequency in beats per minute (BPM): (a) 30 BPM (b) 60 BPM (c) 90 BPM (d) 120 BPM.

The hybrid PTENG was characterized for the output response with different application frequency-beats per minute (BPM) of 0.7 N force. Figure 8 shows the Output voltage of the device for constant force with 30 BPM (Figure 67(a)), 60 BPM (Figure 67(b)), 90 BPM (Figure 67(c)) and 120 BPM (Figure 67(d)) at 0.5 Hz, 1.0 Hz, 1.5 Hz and 2.0 Hz respectively) frequencies. Figure 67(e-h) shows an enlarged view on a response from 10.0 s to 12.0 s. The graph demonstrates that the peak-to-peak distance of the signal reduced with the increment of frequency. The inset of each graph provides detailed information about the voltage response. It is clear from the insets that with the increase of frequency, the response shows more fluctuation of voltage. This increment of fluctuation depends on the inconsistency of the stress release of the homogenous stress on the surface film. This homogenous stress all over the surface can be addressed as the micro-stress of the film, which depends on the film thickness [169,170]. Whenever the upper layer strikes the piezoelectric layer due to the applied force, a micro-stress is

generated throughout the surface of the layer. This stress gets released with the withdrawal of force from the device. While the frequency was 0.5 Hz (Figure 67(a)), there was adequate time for the stress to be released. An enlarged view of the response of 30 BPM in Figure 67(e) shows a lesser amount of noise due to the higher period to return to the original stage after an applied stress. With the increment of frequency from Figure 67(a-d), the available stress release time got reduced. So, generation and release of micro-stress became more recurrent with an increased frequency, which showed the inconsistency of voltage response. The device displayed less variation of voltage with a variable frequency of force. The conductivity of the device amplified due to the application of MWCNT, which resulted in a faster transportation of electrons, thus making the variation of voltage lower.

Conclusion

An innovative, flexible PTENG by coupling Li-ZnO/PVDF/MWCNT with PDMS-PTFE film was developed for energy harvesting and stress sensing applications. A linear response was obtained, able to work undervariable load along with 75 μA electricity and 60.1 V voltage. Such findings are promising in measuring pressure and power generation. The high performance of PTENG is due to the enhanced piezoelectric property of ZnO/PVDF after incorporation of MWCNT in the PVDF matrix as well as the triboelectric property of PDMS-PTFE composite film. The enhancement and combination of piezoelectric and triboelectric properties offer an effective way to improve the performance of nanogenerators. This lightweight, flexible, highly efficient, low-cost, and innovative fabrication process of PTENG will be a promising power source for next-generation wearable and portable devices.

REFERENCES

[1] G. Gautschi, Piezoelectric Sensorics: Force Strain Pressure Acceleration and Acoustic Emission Sensors Materials and Amplifiers, Springer Science & Business Media, 2013.

[2] S. Katzir, THE DISCOVERY OF THE PIEZOELECTRIC EFFECT, in: Begin. PIEZOELECTRICITY, Springer, Dordrecht, 2006: pp. 15–64. doi:10.1007/978-1-4020-4670-4_2.

[3] K.S. Ramadan, D. Sameoto, S. Evoy, A review of piezoelectric polymers as functional materials for electromechanical transducers, Smart Mater. Struct. 23 (2014) 033001. doi:10.1088/0964-1726/23/3/033001.

[4] Web of Science [v.5.27] - Web of Science Core Collection, (n.d.). http://apps.webofknowledge.com/RAMore.do?product=WOS&search_mode=GeneralSearch&SID=6AyTNYaTQQhzTTPY1A1&qid=1&ra_mode=more&ra_name=PublicationYear&colName=WOS&viewType=raMore (accessed January 13, 2018).

[5] J. Briscoe, S. Dunn, Piezoelectric nanogenerators – a review of nanostructured piezoelectric energy harvesters, Nano Energy. 14 (2015) 15–29. doi:10.1016/j.nanoen.2014.11.059.

[6] S. Dunn, C.P. Shaw, Z. Huang, R.W. Whatmore, Ultrahigh resolution of lead zirconate titanate 30/70 domains as imaged by piezoforce microscopy, Nanotechnology. 13 (2002) 456. doi:10.1088/0957-4484/13/4/303.

[7] A.R. Chowdhury, J. Jaksik, I. Hussain, P. Tran, S. Danti, M.J. Uddin, Surface Modified Nanostructured Piezoelectric Device as Cost-Effective Transducer for Energy and Biomedicine, Energy Technol. 0 (n.d.). doi:10.1002/ente.201800767.

[8] A.R. Chowdhury, J. Jaksik, I. Hussain, R. Longoria III, F. Faruque, F. Cesano, J. Parsons, M.J. Uddin, Multidimensional Multicomponent Nanostructured Materials for Piezoelectric Devices, Nano-Struct. Nano-Objects. (2018).

[9] I. Hussain, A.R. Chowdhury, J. Jaksik, G. Grissom, A. Touhami, E.E. Ibrahim, M. Schauer, O. Okoli, M.J. Uddin, Conductive glass free carbon nanotube micro yarn based perovskite solar cells, Appl. Surf. Sci. 478 (2019) 327–333. doi:10.1016/j.apsusc.2019.01.233.

[10] A.R. Chowdhury, A.M. Abdullah, I. Hussain, J. Lopez, D. Cantu, Y. Mao, M.J. Uddin, Lithium Doped Zinc Oxide Based Flexible Piezoelectric-Triboelectric Hybrid Nanogenerator, Nano Energy. (2019).

[11] H.D. Espinosa, R.A. Bernal, M. Minary-Jolandan, A Review of Mechanical and Electromechanical Properties of Piezoelectric Nanowires, Adv. Mater. 24 (2012) 4656–4675. doi:10.1002/adma.201104810.

[12] H. Feng, C. Zhao, P. Tan, R. Liu, X. Chen, Z. Li, Nanogenerator for Biomedical Applications, Adv. Healthc. Mater. 7 (2018) 1701298. doi:10.1002/adhm.201701298.

[13] Q. Jing, S. Kar-Narayan, Nanostructured polymer-based piezoelectric and triboelectric materials and devices for energy harvesting applications, J. Phys. Appl. Phys. 51 (2018) 303001. doi:10.1088/1361-6463/aac827.

[14] M. Salim, D. Salim, D. Chandran, H.S. Aljibori, A.S. Kherbeet, Review of nano piezoelectric devices in biomedicine applications, J. Intell. Mater. Syst. Struct. 29 (2018) 2105–2121. doi:10.1177/1045389X17754272.

[15] Novel Ferroelectric Polymer Composites with High Dielectric Constants - Dang - 2003 - Advanced Materials - Wiley Online Library, (n.d.). https://onlinelibrary.wiley.com/doi/abs/10.1002/adma.200304911 (accessed October 17, 2018).

[16] P. Kim, N.M. Doss, J.P. Tillotson, P.J. Hotchkiss, M.-J. Pan, S.R. Marder, J. Li, J.P. Calame, J.W. Perry, High Energy Density Nanocomposites Based on Surface-Modified BaTiO3 and a Ferroelectric Polymer, ACS Nano. 3 (2009) 2581–2592. doi:10.1021/nn9006412.

[17] W.P. Mason, Piezoelectricity, its history and applications, J. Acoust. Soc. Am. 70 (1981) 1561–1566. doi:10.1121/1.387221.

[18] Z. Wang, X. Pan, Y. He, Y. Hu, H. Gu, Y. Wang, Piezoelectric Nanowires in Energy Harvesting Applications, Adv. Mater. Sci. Eng. (2015). doi:10.1155/2015/165631.

[19] U. Ozgur, Y.I. Alivov, C. Liu, A. Teke, M.A. Reshchikov, S. Dogan, V. Avrutin, S.J. Cho, H. Morkoc, A comprehensive review of ZnO materials and devices, J. Appl. Phys. 98 (2005) 041301. doi:10.1063/1.1992666.

[20] Y.-M. You, W.-Q. Liao, D. Zhao, H.-Y. Ye, Y. Zhang, Q. Zhou, X. Niu, J. Wang, P.-F. Li, D.-W. Fu, Z. Wang, S. Gao, K. Yang, J.-M. Liu, J. Li, Y. Yan, R.-G. Xiong, An organic-inorganic perovskite ferroelectric with large piezoelectric response, Science. 357 (2017) 306–309. doi:10.1126/science.aai8535.

[21] A. Piecha-Bisiorek, K. Mencel, V. Kinzhybalo, A. Szota, R. Jakubas, W. Medycki, W. Zawrocki, Ferroelasticity and piezoelectricity of organic–inorganic hybrid materials with a one-dimensional anionic structure: so similar, yet so different, CrystEngComm. 20 (2018) 2112–2119. doi:10.1039/C8CE00140E.

[22] C.A. Randall, A. Kelnberger, G.Y. Yang, R.E. Eitel, T.R. Shrout, High Strain Piezoelectric Multilayer Actuators—A Material Science and Engineering Challenge, J. Electroceramics. 14 (2005) 177–191. doi:10.1007/s10832-005-0956-5.

[23] W. Li, Q. Meng, Y. Zheng, Z. Zhang, W. Xia, Z. Xu, Electric energy storage properties of poly(vinylidene fluoride), Appl. Phys. Lett. 96 (2010) 192905. doi:10.1063/1.3428656.

[24] G.M. Sessler, Piezoelectricity in polyvinylidenefluoride, J. Acoust. Soc. Am. 70 (1981) 1596–1608. doi:10.1121/1.387225.

[25] A. Vinogradov, F. Holloway, Electro-mechanical properties of the piezoelectric polymer PVDF, Ferroelectrics. 226 (1999) 169–181. doi:10.1080/00150199908230298.

[26]M. de Jong, W. Chen, H. Geerlings, M. Asta, K.A. Persson, A database to enable discovery and design of piezoelectric materials, Sci. Data. 2 (2015) 150053. doi:10.1038/sdata.2015.53.

[27]P. Dineva, D. Gross, R. Müller, T. Rangelov, Dynamic Fracture of Piezoelectric Materials: Solution of Time-Harmonic Problems via BIEM, Springer Science & Business Media, 2014.

[28]C. Mota, M. Labardi, L. Trombi, L. Astolfi, M. D'Acunto, D. Puppi, G. Gallone, F. Chiellini, S. Berrettini, L. Bruschini, S. Danti, Biomaterials, Tissue Engineering and Regenerative Medicine/Biomaterials and Tissue Engineering, Materials & Design. 206 (2017) 122.

[29]G. Ciofani, S. Danti, G.G. Genchi, B. Mazzolai, V. Mattoli, Boron nitride nanotubes: biocompatibility and potential spill-over in nanomedicine, Small Weinh. Bergstr. Ger. 9 (2013) 1672–1685. doi:10.1002/smll.201201315.

[30]C. Falconi, G. Mantini, A. D'Amico, V. Ferrari, Modeling of Piezoelectric Nanodevices, in: Piezoelectric Nanomater. Biomed. Appl., Springer, Berlin, Heidelberg, 2012: pp. 93–133. doi:10.1007/978-3-642-28044-3_4.

[31]J.F. Tressler, Piezoelectric Transducer Designs for Sonar Applications, in: Piezoelectric Acoust. Mater. Transducer Appl., Springer, Boston, MA, 2008: pp. 217–239. doi:10.1007/978-0-387-76540-2_11.

[32]C. Dagdeviren, B.D. Yang, Y. Su, P.L. Tran, P. Joe, E. Anderson, J. Xia, V. Doraiswamy, B. Dehdashti, X. Feng, B. Lu, R. Poston, Z. Khalpey, R. Ghaffari, Y. Huang, M.J. Slepian, J.A. Rogers, Conformal piezoelectric energy harvesting and storage from motions of the heart, lung, and diaphragm, Proc. Natl. Acad. Sci. 111 (2014) 1927–1932. doi:10.1073/pnas.1317233111.

[33]Z. Li, P.M. Bainum, Vibration Control Of Flexible Spacecraft Integrating A Momentum Exchange Controller And A Distributed Piezoelectric Actuator, J. Sound Vib. 177 (1994) 539–553. doi:10.1006/jsvi.1994.1450.

[34] S. Tadigadapa, K. Mateti, Piezoelectric MEMS sensors: state-of-the-art and perspectives, Meas. Sci. Technol. 20 (2009) 092001. doi:10.1088/0957-0233/20/9/092001.

[35] S. Roundy, P.K. Wright, A piezoelectric vibration based generator for wireless electronics, Smart Mater. Struct. 13 (2004) 1131–1142. doi:10.1088/0964-1726/13/5/018.

[36] J. Gao, D. Xue, W. Liu, C. Zhou, X. Ren, Recent Progress on BaTiO3-Based Piezoelectric Ceramics for Actuator Applications, Actuators. 6 (2017) 24. doi:10.3390/act6030024.

[37] E.F. CRAWLEY, J.D. LUIS, Use of piezoelectric actuators as elements of intelligent structures, AIAA J. 25 (1987) 1373–1385. doi:10.2514/3.9792.

[38] J.R. Vig, A. Ballato, 4 Frequency control devices, in: R.N. Thurston, A.D. Pierce, E.P. Papadakis (Eds.), Phys. Acoust., Academic Press, 1999: pp. 209–273. doi:10.1016/S0893-388X(99)80026-8.

[39] E. Benes, M. Groschl, W. Burger, M. Schmid, Sensors Based on Piezoelectric Resonators, Sens. Actuators -Phys. 48 (1995) 1–21. doi:10.1016/0924-4247(95)00846-2.

[40] M. Dey, T. Akand, S. Sultana, Power generation for auto street light using PZT, in: 2015 Int. Conf. Adv. Electr. Eng. ICAEE, 2015: pp. 38–41. doi:10.1109/ICAEE.2015.7506791.

[41] Z. Li, G. Zhu, R. Yang, A.C. Wang, Z.L. Wang, Muscle-Driven In Vivo Nanogenerator, Adv. Mater. 22 (2010) 2534–2537. doi:10.1002/adma.200904355.

[42] J. Li, X. Wang, Research Update: Materials design of implantable nanogenerators for biomechanical energy harvesting, APL Mater. 5 (2017). doi:10.1063/1.4978936.

[43] B.B. Lakshmi, P.K. Dorhout, C.R. Martin, Sol−Gel Template Synthesis of Semiconductor Nanostructures, Chem. Mater. 9 (1997) 857–862. doi:10.1021/cm9605577.

[44] Fundamental formulations and recent achievements in piezoelectric, StudFiles. (n.d.). /preview/4444947/ (accessed December 24, 2017).

[45] X.-Q. Fang, J.-X. Liu, V. Gupta, Fundamental formulations and recent achievements in piezoelectric nano-structures: a review, Nanoscale. 5 (2013) 1716–1726. doi:10.1039/C2NR33531J.

[46] K. Whang, C.H. Thomas, K.E. Healy, G. Nuber, A novel method to fabricate bioabsorbable scaffolds, Polymer. 36 (1995) 837–842. doi:10.1016/0032-3861(95)93115-3.

[47] J. Doshi, D.H. Reneker, Electrospinning process and applications of electrospun fibers, J. Electrost. 35 (1995) 151–160. doi:10.1016/0304-3886(95)00041-8.

[48] B. Malič, J. Koruza, J. Hreščak, J. Bernard, K. Wang, J.G. Fisher, A. Benčan, Sintering of Lead-Free Piezoelectric Sodium Potassium Niobate Ceramics, Materials. 8 (2015) 8117–8146. doi:10.3390/ma8125449.

[49] Mohamed N. Rahaman, Ceramic Processing and Sintering (Materials Engineering), n.d. https://www.abebooks.com/9780824709884/Ceramic-Processing-Sintering-Materials-Engineering-0824709888/plp.

[50] J. Cohen, R.A. Siegel, R. Langer, Sintering technique for the preparation of polymer matrices for the controlled release of macromolecules, J. Pharm. Sci. 73 (1984) 1034–1037. doi:10.1002/jps.2600730805.

[51] J.N. Tiwari, R.N. Tiwari, K.S. Kim, Zero-dimensional, one-dimensional, two-dimensional and three-dimensional nanostructured materials for advanced electrochemical energy devices, Prog. Mater. Sci. 57 (2012) 724–803. doi:10.1016/j.pmatsci.2011.08.003.

[52] E.J. Lee, T.Y. Kim, S.-W. Kim, S. Jeong, Y. Choi, S.Y. Lee, High-performance piezoelectric nanogenerators based on chemically-reinforced composites, Energy Environ. Sci. 11 (2018) 1425–1430. doi:10.1039/C8EE00014J.

[53] J.-F. Capsal, E. Dantras, J. Dandurand, C. Lacabanne, Physical structure of P(VDF-TrFE)/barium titanate submicron composites, J. Non-Cryst. Solids. 358 (2012) 794–798. doi:10.1016/j.jnoncrysol.2011.12.028.

[54] J.S. Dodds, F.N. Meyers, K.J. Loh, Piezoelectric Characterization of PVDF-TrFE Thin Films Enhanced With ZnO Nanoparticles, IEEE Sens. J. 12 (2012) 1889–1890. doi:10.1109/JSEN.2011.2182043.

[55] K. Prashanthi, M. Naresh, V. Seena, T. Thundat, V.R. Rao, A Novel Photoplastic Piezoelectric Nanocomposite for MEMS Applications, J. Microelectromechanical Syst. 21 (2012) 259–261. doi:10.1109/JMEMS.2011.2178118.

[56] R. Hadji, V.S. Nguyen, B. Vincent, D. Rouxel, F. Bauer, Preparation and characterization of P(VDF-TrFE)/Al2O3 nanocomposite, IEEE Trans. Ultrason. Ferroelectr. Freq. Control. 59 (2012) 163–167. doi:10.1109/TUFFC.2012.2168.

[57] The memory effect of Dy2.8Sr0.2Fe5O12(DySrIG) nanoparticles - IOPscience, (n.d.). http://iopscience.iop.org/article/10.1088/0964-1726/21/4/045010 (accessed December 24, 2017).

[58] M. Cernea, F. Fochi, G.V. Aldica, B.S. Vasile, R. Trusca, C. Galassi, Spark-plasma-sintering temperature dependence of structural and piezoelectric properties of BNT–BT<Subscript>0.08</Subscript> nanostructured ceramics, J. Mater. Sci. 47 (2012) 3669–3673. doi:10.1007/s10853-011-6215-z.

[59] H. Zhang, J.-F. Li, B.-P. Zhang, Sintering and piezoelectric properties of Co-fired lead zirconate titanate/Ag composites, J. Am. Ceram. Soc. 89 (2006) 1300–1307. doi:10.1111/j.1551-2916.2005.00849.x.

[60] M. Zheng, Y. Hou, M. Zhu, H. Yan, Nanodomains in metal/ferroelectric 0–3 type composites: On the origin of the strong piezoelectric effect, Scr. Mater. 145 (2018) 19–22. doi:10.1016/j.scriptamat.2017.10.007.

[61] C.A. Randall, N. Kim, J.-P. Kucera, W. Cao, T.R. Shrout, Intrinsic and extrinsic size effects in fine-grained morphotropic-phase-boundary lead zirconate titanate ceramics, J. Am. Ceram. Soc. 81 (1998) 677–688.

[62] G. Catalan, J. Seidel, R. Ramesh, J.F. Scott, Domain wall nanoelectronics, Rev. Mod. Phys. 84 (2012) 119–156. doi:10.1103/RevModPhys.84.119.

[63] C. Baek, J.H. Yun, H.S. Wang, J.E. Wang, H. Park, K.-I. Park, D.K. Kim, Enhanced output performance of a lead-free nanocomposite generator using BaTiO3 nanoparticles and nanowires filler, Appl. Surf. Sci. 429 (2018) 164–170. doi:10.1016/j.apsusc.2017.06.109.

[64] S. Roberts, Dielectric and Piezoelectric Properties of Barium Titanate, Phys. Rev. 71 (1947) 890–895. doi:10.1103/PhysRev.71.890.

[65] I. Chinya, A. Pal, S. Sen, Polyglycolated zinc ferrite incorporated poly(vinylidene fluoride)(PVDF) composites with enhanced piezoelectric response, J. Alloys Compd. 722 (2017) 829–838. doi:10.1016/j.jallcom.2017.06.028.

[66] M.P. Patil, N.J. Gaikwad, Characterization of gliclazide-polyethylene glycol solid dispersion and its effect on dissolution, Braz. J. Pharm. Sci. 47 (2011) 161–166. doi:10.1590/S1984-82502011000100020.

[67] L.M. Denis, J. Glaum, M. Hoffman, J.E. Daniels, R.J. Hooper, G. Tutuncu, J.S. Forrester, J.L. Jones, Effect of mechanical depoling on piezoelectric properties of Na0.5Bi0.5TiO3 BaTiO3 in the morphotropic phase boundary region, J. Mater. Sci. 53 (2018) 1672–1679. doi:10.1007/s10853-017-1616-2.

[68] R. Caliò, U.B. Rongala, D. Camboni, M. Milazzo, C. Stefanini, G. de Petris, C.M. Oddo, Piezoelectric Energy Harvesting Solutions, Sensors. 14 (2014) 4755–4790. doi:10.3390/s140304755.

[69] Z.L. Wang, J. Song, Piezoelectric Nanogenerators Based on Zinc Oxide Nanowire Arrays, Science. 312 (2006) 242–246. doi:10.1126/science.1124005.

[70] X. Li, M. Sun, X. Wei, C. Shan, Q. Chen, X. Li, M. Sun, X. Wei, C. Shan, Q. Chen, 1D Piezoelectric Material Based Nanogenerators: Methods, Materials and Property Optimization, Nanomaterials. 8 (2018) 188. doi:10.3390/nano8040188.

[71] R. Araneo, G. Lovat, P. Burghignoli, C. Falconi, Piezo-Semiconductive Quasi-1D Nanodevices with or without Anti-Symmetry, Adv. Mater. 24 (2012) 4719–4724. doi:10.1002/adma.201104588.

[72] A.H. Aly, A. Nagaty, Z. Khalifa, PIEZOELECTRIC MATERIAL AND ONE-DIMENSIONAL PHONONIC CRYSTAL, Surf. Rev. Lett. (2018) 1850144. doi:10.1142/S0218625X18501445.

[73] K. Yu, X. Pan, G. Zhang, X. Liao, X. Zhou, M. Yan, L. Xu, L. Mai, Nanowires in Energy Storage Devices: Structures, Synthesis, and Applications, Adv. Energy Mater. 0 (n.d.) 1802369. doi:10.1002/aenm.201802369.

[74] B. Sen, M. Stroscio, M. Dutta, Piezoelectricity in wurtzite polar semiconductor nanowires: A theoretical study, J. Appl. Phys. 110 (2011) 024506. doi:10.1063/1.3603036.

[75] V. Cauda, S. Stassi, K. Bejtka, G. Canavese, Nanoconfinement: an Effective Way to Enhance PVDF Piezoelectric Properties, ACS Appl. Mater. Interfaces. 5 (2013) 6430–6437. doi:10.1021/am4016878.

[76] B. Liu, B. Lu, X. Chen, X. Wu, S. Shi, L. Xu, Y. Liu, F. Wang, X. Zhao, W. Shi, A high-performance flexible piezoelectric energy harvester based on lead-free (Na 0 . 5 Bi 0 . 5)TiO 3 –BaTiO 3 piezoelectric nanofibers, J. Mater. Chem. A. 5 (2017) 23634–23640. doi:10.1039/C7TA07570G.

[77] Y. Huang, Y. Ding, J. Bian, Y. Su, J. Zhou, Y. Duan, Z. Yin, Hyper-stretchable self-powered sensors based on electrohydrodynamically printed, self-similar piezoelectric nano/microfibers, Nano Energy. 40 (2017) 432–439. doi:10.1016/j.nanoen.2017.07.048.

[78] N. Gogneau, N. Jamond, P. Chrétien, F. Houzé, E. Lefeuvre, M. Tchernycheva, From single III-nitride nanowires to piezoelectric generators: New route for powering nomad electronics, Semicond. Sci. Technol. 31 (2016) 103002. doi:10.1088/0268-1242/31/10/103002.

[79] H.H. Singh, S. Singh, N. Khare, Enhanced β-phase in PVDF polymer nanocomposite and its application for nanogenerator, Polym. Adv. Technol. 29 (2018) 143–150. doi:10.1002/pat.4096.

[80] X. Chen, X. Li, J. Shao, N. An, H. Tian, C. Wang, T. Han, L. Wang, B. Lu, High-Performance Piezoelectric Nanogenerators with Imprinted P(VDF-TrFE)/BaTiO3 Nanocomposite Micropillars for Self-Powered Flexible Sensors, Small. 13 (n.d.) 1604245. doi:10.1002/smll.201604245.

[81] A.S. Dahiya, F. Morini, S. Boubenia, K. Nadaud, D. Alquier, G. Poulin-Vittrant, Organic/Inorganic Hybrid Stretchable Piezoelectric Nanogenerators for Self-Powered Wearable Electronics, Adv. Mater. Technol. 3 (2018) 1700249. doi:10.1002/admt.201700249.

[82] K.J. Alvine, V. Shutthanandan, B.W. Arey, C. Wang, W.D. Bennett, S.G. Pitman, Pb nanowire formation on Al/lead zirconate titanate surfaces in high-pressure hydrogen, J. Appl. Phys. 112 (2012) 013533. doi:10.1063/1.4731721.

[83] X. Feng, B.D. Yang, Y. Liu, Y. Wang, C. Dagdeviren, Z. Liu, A. Carlson, J. Li, Y. Huang, J.A. Rogers, Stretchable Ferroelectric Nanoribbons with Wavy Configurations on Elastomeric Substrates, ACS Nano. 5 (2011) 3326–3332. doi:10.1021/nn200477q.

[84] C. Cui, F. Xue, W.-J. Hu, L.-J. Li, Two-dimensional materials with piezoelectric and ferroelectric functionalities, Npj 2D Mater. Appl. 2 (2018) 18. doi:10.1038/s41699-018-0063-5.

[85] R. Agrawal, H.D. Espinosa, Giant Piezoelectric Size Effects in Zinc Oxide and Gallium Nitride Nanowires. A First Principles Investigation, Nano Lett. 11 (2011) 786–790. doi:10.1021/nl104004d.

[86] R. Hinchet, U. Khan, C. Falconi, S.-W. Kim, Piezoelectric properties in two-dimensional materials: Simulations and experiments, Mater. Today. 21 (2018) 611–630. doi:10.1016/j.mattod.2018.01.031.

[87] A. Almusallam, Z. Luo, A. Komolafe, K. Yang, A. Robinson, R. Torah, S. Beeby, Flexible piezoelectric nano-composite films for kinetic energy harvesting from textiles, Nano Energy. 33 (2017) 146–156. doi:10.1016/j.nanoen.2017.01.037.

[88] S. Park, Y. Kim, H. Jung, J.-Y. Park, N. Lee, Y. Seo, Energy harvesting efficiency of piezoelectric polymer film with graphene and metal electrodes, Sci. Rep. 7 (2017) 17290. doi:10.1038/s41598-017-17791-3.

[89] M.R. Farajpour, A. Rastgoo, A. Farajpour, M. Mohammadi, Vibration of piezoelectric nanofilm-based electromechanical sensors via higher-order non-local strain gradient theory, IET Micro Nano Lett. 11 (2016) 302–307. doi:10.1049/mnl.2016.0081.

[90] H. Parangusan, D. Ponnamma, M.A.A. Al-Maadeed, Stretchable Electrospun PVDF-HFP/Co-ZnO Nanofibers as Piezoelectric Nanogenerators, Sci. Rep. 8 (2018) 754. doi:10.1038/s41598-017-19082-3.

[91] Y. Guo, X.-S. Zhang, Y. Wang, W. Gong, Q. Zhang, H. Wang, J. Brugger, All-fiber hybrid piezoelectric-enhanced triboelectric nanogenerator for wearable gesture monitoring, Nano Energy. 48 (2018) 152–160. doi:10.1016/j.nanoen.2018.03.033.

[92] X. Wang, W.-Z. Song, M.-H. You, J. Zhang, M. Yu, Z. Fan, S. Ramakrishna, Y.-Z. Long, Bionic Single-Electrode Electronic Skin Unit Based on Piezoelectric Nanogenerator, ACS Nano. 12 (2018) 8588–8596. doi:10.1021/acsnano.8b04244.

[93] S.-M. Lee, S.-H. Gong, J.-H. Kang, M. Ebaid, S.-W. Ryu, Y.-H. Cho, Optically pumped GaN vertical cavity surface emitting laser with high index-contrast nanoporous distributed Bragg reflector, Opt. Express. 23 (2015) 11023–11030. doi:10.1364/OE.23.011023.

[94] J.-H. Kang, D.K. Jeong, S.-W. Ryu, Transparent, Flexible Piezoelectric Nanogenerator Based on GaN Membrane Using Electrochemical Lift-Off, ACS Appl. Mater. Interfaces. 9 (2017) 10637–10642. doi:10.1021/acsami.6b15587.

[95] S. Garain, S. Jana, T.K. Sinha, D. Mandal, Design of In Situ Poled Ce3+-Doped Electrospun PVDF/Graphene Composite Nanofibers for Fabrication of Nanopressure Sensor and Ultrasensitive Acoustic Nanogenerator, ACS Appl. Mater. Interfaces. 8 (2016) 4532–4540. doi:10.1021/acsami.5b11356.

[96] J.T. Han, J.I. Jang, H. Kim, J.Y. Hwang, H.K. Yoo, J.S. Woo, S. Choi, H.Y. Kim, H.J. Jeong, S.Y. Jeong, K.-J. Baeg, K. Cho, G.-W. Lee, Extremely efficient liquid exfoliation and dispersion of layered materials by unusual acoustic cavitation, Sci. Rep. 4 (2014) 5133. doi:10.1038/srep05133.

[97] T.K. Sinha, S.K. Ghosh, R. Maiti, S. Jana, B. Adhikari, D. Mandal, S.K. Ray, Graphene-Silver-Induced Self-Polarized PVDF-Based Flexible Plasmonic Nanogenerator Toward the Realization for New Class of Self Powered Optical Sensor, ACS Appl. Mater. Interfaces. 8 (2016) 14986–14993. doi:10.1021/acsami.6b01547.

[98] K. Maity, B. Mahanty, T.K. Sinha, S. Garain, A. Biswas, S.K. Ghosh, S. Manna, S.K. Ray, D. Mandal, Two-Dimensional Piezoelectric MoS2-Modulated Nanogenerator and Nanosensor Made of Poly(vinlydine Fluoride) Nanofiber Webs for Self-Powered Electronics and Robotics, Energy Technol. 5 (2017) 234–243. doi:10.1002/ente.201600419.

[99] S.A. Han, T.-H. Kim, S.K. Kim, K.H. Lee, H.-J. Park, J.-H. Lee, S.-W. Kim, Point-Defect-Passivated MoS2 Nanosheet-Based High Performance Piezoelectric Nanogenerator, Adv. Mater. 30 (2018) 1800342. doi:10.1002/adma.201800342.

[100] G. Melilli, D. Lairez, D. Gorse, E. Garcia-Caurel, A. Peinado, O. Cavani, B. Boizot, M.-C. Clochard, Conservation of the piezoelectric response of PVDF films under irradiation, Radiat. Phys. Chem. 142 (2018) 54–59. doi:10.1016/j.radphyschem.2017.03.035.

[101] M. Minary-Jolandan, R.A. Bernal, I. Kuljanishvili, V. Parpoil, H.D. Espinosa, Individual GaN Nanowires Exhibit Strong Piezoelectricity in 3D, Nano Lett. 12 (2012) 970–976. doi:10.1021/nl204043y.

[102] G. Zhang, P. Zhao, X. Zhang, K. Han, T. Zhao, Y. Zhang, C. Kyu Jeong, S. Jiang, S. Zhang, Q. Wang, Flexible three-dimensional interconnected piezoelectric ceramic foam based composites for highly efficient concurrent mechanical and thermal energy harvesting, Energy Environ. Sci. 11 (2018) 2046–2056. doi:10.1039/C8EE00595H.

[103] C. Kullmann, N.C. Schirmer, M.-T. Lee, S.H. Ko, N. Hotz, C.P. Grigoropoulos, D. Poulikakos, 3D micro-structures by piezoelectric inkjet printing of gold nanofluids, J. Micromechanics Microengineering. 22 (2012) 055022. doi:10.1088/0960-1317/22/5/055022.

[104] Y.K. Fuh, B.S. Wang, Near field sequentially electrospun three-dimensional piezoelectric fibers arrays for self-powered sensors of human gesture recognition, Nano Energy. 30 (2016) 677–683. doi:10.1016/j.nanoen.2016.10.061.

[105] B. Gusarov, E. Gusarova, B. Viala, L. Gimeno, O. Cugat, PVDF piezoelectric voltage coefficient in situ measurements as a function of applied stress, J. Appl. Polym. Sci. 133 (2016) n/a-n/a. doi:10.1002/app.43248.

[106] D.M. Correia, C. Ribeiro, V. Sencadas, L. Vikingsson, M. Oliver Gasch, J.L. Gómez Ribelles, G. Botelho, S. Lanceros-Méndez, Strategies for the development of three dimensional scaffolds from piezoelectric poly(vinylidene fluoride), Mater. Des. 92 (2016) 674–681. doi:10.1016/j.matdes.2015.12.043.

[107] K. Kanda, S. Moriue, T. Fujita, K. Maenaka, Three-dimensional piezoelectric MEMS actuator by using sputtering deposition of Pb(Zr,Ti)O 3 on microstructure sidewalls, Smart Mater. Struct. 26 (2017) 045019. doi:10.1088/1361-665X/aa61eb.

[108] K. Kanda, S. Moriue, T. Fujita, K. Maenaka, Three-dimensional piezoelectric MEMS actuator by using sputtering deposition of Pb(Zr,Ti)O 3 on microstructure sidewalls, Smart Mater. Struct. 26 (2017) 045019. doi:10.1088/1361-665X/aa61eb.

[109] R.C.W. Tsang, K.W. Kwok, H.L.W. Chan, C.L. Choy, Piezoelectric Coefficients of PZT Thin Films, Integr. Ferroelectr. 50 (2002) 143–148. doi:10.1080/10584580215506.

[110] B. Yin, Y. Qiu, H. Zhang, J. Ji, J. Lei, Y. Luo, Y. Zhao, L. Hu, Piezoelectric nanogenerator with 3D-ZnO micro-thornyballs prepared by chemical vapour deposition, J. Mater. Sci. Mater. Electron. 26 (2015) 742–746. doi:10.1007/s10854-014-2458-1.

[111] N. Liu, G. Fang, W. Zeng, H. Long, L. Yuan, X. Zhao, Novel ZnO Nanorod Flexible Strain Sensor and Strain Driving Transistor with an Ultrahigh 107 Scale "On"−"Off" Ratio Fabricated by a Single-Step Hydrothermal Reaction, J. Phys. Chem. C. 115 (2011) 570–575. doi:10.1021/jp108352b.

[112] Y. Huan, X. Zhang, J. Song, Y. Zhao, T. Wei, G. Zhang, X. Wang, High-performance piezoelectric composite nanogenerator based on Ag/(K,Na)NbO3 heterostructure, Nano Energy. 50 (2018) 62–69. doi:10.1016/j.nanoen.2018.05.012.

[113] T. Shiosaki, A. Kawabata, Future trends in piezoelectric materials and applications, Ferroelectrics. 95 (1989) 9–14. doi:10.1080/00150198908245171.

[114] Siang Jee, Lim M.H., Salman Leong M., Review of vibration-based energy harvesting technology: Mechanism and architectural approach, Int. J. Energy Res. 42 (2018) 1866–1893. doi:10.1002/er.3986.

[115] Y.R. Wang, J.M. Zheng, G.Y. Ren, P.H. Zhang, C. Xu, A flexible piezoelectric force sensor based on PVDF fabrics, Smart Mater. Struct. 20 (2011) 045009. doi:10.1088/0964-1726/20/4/045009.

[116] M.-P. Lu, J. Song, M.-Y. Lu, M.-T. Chen, Y. Gao, L.-J. Chen, Z.L. Wang, Piezoelectric Nanogenerator Using p-Type ZnO Nanowire Arrays, Nano Lett. 9 (2009) 1223–1227. doi:10.1021/nl900115y.

[117] B. Yang, K.S. Yun, Efficient energy harvesting from human motion using wearable piezoelectric shell structures, in: 2011 16th Int. Solid-State Sens. Actuators Microsyst. Conf., 2011: pp. 2646–2649. doi:10.1109/TRANSDUCERS.2011.5969874.

[118] Energy harvesting during human walking to power a wireless sensor node - ScienceDirect, (n.d.). https://www.sciencedirect.com/science/article/pii/S0924424716306768 (accessed June 13, 2018).

[119] C. Wei, X. Jing, A comprehensive review on vibration energy harvesting: Modelling and realization, Renew. Sustain. Energy Rev. 74 (2017) 1–18. doi:10.1016/j.rser.2017.01.073.

[120] Y. Nishi, K. Fukuda, W. Shinohara, Experimental energy harvesting from fluid flow by using two vibrating masses, J. Sound Vib. 394 (2017) 321–332. doi:10.1016/j.jsv.2017.01.037.

[121] U. Khan, R. Hinchet, H. Ryu, S.-W. Kim, Research Update: Nanogenerators for self-powered autonomous wireless sensors, APL Mater. 5 (2017) 073803. doi:10.1063/1.4979954.

[122] S.-H. Shin, Y.-H. Kim, M.H. Lee, J.-Y. Jung, J.H. Seol, J. Nah, Lithium-Doped Zinc Oxide Nanowires–Polymer Composite for High Performance Flexible Piezoelectric Nanogenerator, ACS Nano. 8 (2014) 10844–10850. doi:10.1021/nn5046568.

[123] E. Nilsson, A. Lund, C. Jonasson, C. Johansson, B. Hagström, Poling and characterization of piezoelectric polymer fibers for use in textile sensors, Sens. Actuators Phys. 201 (2013) 477–486. doi:10.1016/j.sna.2013.08.011.

[124] C. Curie, J. P., Development by pressure of polar electricity in crysatls with angled face, Comput. Rend. Acad. Sci. Paris. 91 (1880) 294–297.

[125] X. Zhang, Y. Ma, C. Zhao, W. Yang, High dielectric constant and low dielectric loss hybrid nanocomposites fabricated with ferroelectric polymer matrix and BaTiO3 nanofibers modified with perfluoroalkylsilane, Appl. Surf. Sci. 305 (2014) 531–538. doi:10.1016/j.apsusc.2014.03.131.

[126] E. Lee, J.-Y. Hong, G. Ungar, J. Jang, Crystallization of poly(ethylene oxide) embedded with surface-modified SiO2 nanoparticles, Polym. Int. 62 (n.d.) 1112–1122. doi:10.1002/pi.4402.

[127] Z.-M. Dang, H.-Y. Wang, H.-P. Xu, Influence of silane coupling agent on morphology and dielectric property in BaTiO3/polyvinylidene fluoride composites, Appl. Phys. Lett. 89 (2006) 112902. doi:10.1063/1.2338529.

[128] S. Dalle Vacche, F. Oliveira, Y. Leterrier, V. Michaud, D. Damjanovic, J.-A. Månson, Effect of silane coupling agent on the morphology, structure, and properties of poly(vinylidene fluoride-trifluoroethylene)/BaTiO3 composites, J. Mater. Sci. 49 (2014) 4552–4564. doi:10.1007/s10853-014-8155-x.

[129] J.T. Wescott, P. Kung, A. Maiti, Conductivity of carbon nanotube polymer composites, Appl. Phys. Lett. 90 (2007) 033116. doi:10.1063/1.2432237.

[130] R. Ram, M. Rahaman, D. Khastgir, Electrical properties of polyvinylidene fluoride (PVDF)/multi-walled carbon nanotube (MWCNT) semi-transparent composites: Modelling of DC conductivity, Compos. Part Appl. Sci. Manuf. 69 (2015) 30–39. doi:10.1016/j.compositesa.2014.11.003.

[131] S.K. Ghosh, T.K. Sinha, B. Mahanty, D. Mandal, Self-poled Efficient Flexible "Ferroelectretic" Nanogenerator: A New Class of Piezoelectric Energy Harvester, Energy Technol. 3 (2015) 1190–1197. doi:10.1002/ente.201500167.

[132] K.H. Shim, S.K. Lee, B.S. Kang, S.M. Hwang, Investigation on blanking of thin sheet metal using the ductile fracture criterion and its experimental verification, J. Mater. Process. Technol. 155–156 (2004) 1935–1942. doi:10.1016/j.jmatprotec.2004.04.284.

[133] S. Sorrell, Reducing energy demand: A review of issues, challenges and approaches, Renew. Sustain. Energy Rev. 47 (2015) 74–82. doi:10.1016/j.rser.2015.03.002.

[134] N. Abas, A. Kalair, N. Khan, Review of fossil fuels and future energy technologies, Futures. 69 (2015) 31–49. doi:10.1016/j.futures.2015.03.003.

[135] S. Rathore, S. Sharma, B.P. Swain, R.K. Ghadai, A Critical Review on Triboelectric Nanogenerator, IOP Conf. Ser. Mater. Sci. Eng. 377 (2018) 012186. doi:10.1088/1757-899X/377/1/012186.

[136] Conductive glass free carbon nanotube micro yarn based perovskite solar cells - ScienceDirect, (n.d.). https://www.sciencedirect.com/science/article/pii/S0169433219302636 (accessed February 5, 2019).

[137] Z.L. Wang, J. Song, Piezoelectric Nanogenerators Based on Zinc Oxide Nanowire Arrays, Science. 312 (2006) 242–246. doi:10.1126/science.1124005.

[138] F.-R. Fan, Z.-Q. Tian, Z. Lin Wang, Flexible triboelectric generator, Nano Energy. 1 (2012) 328–334. doi:10.1016/j.nanoen.2012.01.004.

[139] B. Dudem, L.K. Bharat, H. Patnam, A.R. Mule, J.S. Yu, Enhancing the output performance of hybrid nanogenerators based on Al-doped BaTiO3 composite films: a self-powered utility system for portable electronics, J. Mater. Chem. A. 6 (2018) 16101–16110. doi:10.1039/C8TA04612C.

[140] G. Hassan, F. Khan, A. Hassan, S. Ali, J. Bae, C.H. Lee, A flat-panel-shaped hybrid piezo/triboelectric nanogenerator for ambient energy harvesting, Nanotechnology. 28 (2017) 175402. doi:10.1088/1361-6528/aa65c3.

[141] W.-S. Jung, M.-G. Kang, H.G. Moon, S.-H. Baek, S.-J. Yoon, Z.-L. Wang, S.-W. Kim, C.-Y. Kang, High Output Piezo/Triboelectric Hybrid Generator, Sci. Rep. 5 (2015) 9309. doi:10.1038/srep09309.

[142] S. Qin, Q. Zhang, X. Yang, M. Liu, Q. Sun, Z.L. Wang, Hybrid Piezo/Triboelectric-Driven Self-Charging Electrochromic Supercapacitor Power Package, Adv. Energy Mater. 8 (2018) 1800069. doi:10.1002/aenm.201800069.

[143] G. Suo, Y. Yu, Z. Zhang, S. Wang, P. Zhao, J. Li, X. Wang, Piezoelectric and Triboelectric Dual Effects in Mechanical-Energy Harvesting Using BaTiO3/Polydimethylsiloxane Composite Film, ACS Appl. Mater. Interfaces. 8 (2016) 34335–34341. doi:10.1021/acsami.6b11108.

[144]C. Zhao, Q. Zhang, W. Zhang, X. Du, Y. Zhang, S. Gong, K. Ren, Q. Sun, Z.L. Wang, Hybrid piezo/triboelectric nanogenerator for highly efficient and stable rotation energy harvesting, Nano Energy. 57 (2019) 440–449. doi:10.1016/j.nanoen.2018.12.062.

[145]P. Sahatiya, S. Kannan, S. Badhulika, Few layer MoS2 and in situ poled PVDF nanofibers on low cost paper substrate as high performance piezo-triboelectric hybrid nanogenerator: Energy harvesting from handwriting and human touch, Appl. Mater. Today. 13 (2018) 91–99. doi:10.1016/j.apmt.2018.08.009.

[146]H.H. Singh, N. Khare, Flexible ZnO-PVDF/PTFE based piezo-tribo hybrid nanogenerator, Nano Energy. 51 (2018) 216–222. doi:10.1016/j.nanoen.2018.06.055.

[147]L. Cheng, Q. Xu, Y. Zheng, X. Jia, Y. Qin, A self-improving triboelectric nanogenerator with improved charge density and increased charge accumulation speed, Nat. Commun. 9 (2018) 3773. doi:10.1038/s41467-018-06045-z.

[148]B. Bera, M.D. Sarkar, Piezoelectricity in PVDF and PVDF Based Piezoelectric Nanogenerator: A Concept, IOSR J. Appl. Phys. 09 (2017) 95–99. doi:10.9790/4861-0903019599.

[149]S.K. Karan, D. Mandal, B.B. Khatua, Self-powered flexible Fe-doped RGO/PVDF nanocomposite: an excellent material for a piezoelectric energy harvester, Nanoscale. 7 (2015) 10655–10666. doi:10.1039/C5NR02067K.

[150]Z. Han, A. Fina, Thermal conductivity of carbon nanotubes and their polymer nanocomposites: A review, Prog. Polym. Sci. 36 (2011) 914–944. doi:10.1016/j.progpolymsci.2010.11.004.

[151]A. Eatemadi, H. Daraee, H. Karimkhanloo, M. Kouhi, N. Zarghami, A. Akbarzadeh, M. Abasi, Y. Hanifehpour, S.W. Joo, Carbon nanotubes: properties, synthesis, purification, and medical applications, Nanoscale Res. Lett. 9 (2014) 393. doi:10.1186/1556-276X-9-393.

[152]M. Ma, Z. Kang, Q. Liao, Q. Zhang, F. Gao, X. Zhao, Z. Zhang, Y. Zhang, Development, applications, and future directions of triboelectric nanogenerators, Nano Res. 11 (2018) 2951–2969. doi:10.1007/s12274-018-1997-9.

[153]Y. Wang, Y. Yang, Z.L. Wang, Triboelectric nanogenerators as flexible power sources, Npj Flex. Electron. 1 (2017) 10. doi:10.1038/s41528-017-0007-8.

[154]L. Dhakar, F.E.H. Tay, C. Lee, Investigation of contact electrification based broadband energy harvesting mechanism using elastic PDMS microstructures, J. Micromechanics Microengineering. 24 (2014) 104002. doi:10.1088/0960-1317/24/10/104002.

[155]B. Raisi Dehkourdi, S. Fatahian, K. Shahanipoor, Synthesis, Characterization and renal toxicity of ZnO and polyethylene glycol Coated ZnO nanoparticles, Nanomedicine J. 4 (2017) 55–60. doi:10.22038/nmj.2017.8054.

[156]Surface Adsorption of Polyethylene Glycol and Polyvinyl Alcohol with Variable Molecular Weights on Zinc Oxide Nanoparticles, Iran. J. Chem. Eng. 8 (2011) 20–30.

[157]K. Pradeev Raj, K. Sadaiyandi, A. Kennedy, R. Thamizselvi, Structural, optical, photoluminescence and photocatalytic assessment of Sr-doped ZnO nanoparticles, (2016) 24–36.

[158]B. Pal, D. Sarkar, P.K. Giri, Structural, optical, and magnetic properties of Ni doped ZnO nanoparticles: Correlation of magnetic moment with defect density, Appl. Surf. Sci. 356 (2015) 804–811. doi:10.1016/j.apsusc.2015.08.163.

[159]D.H. Zhang, Z.Y. Xue, Q.P. Wang, The mechanisms of blue emission from ZnO films deposited on glass substrate by r.f. magnetron sputtering, J. Phys. Appl. Phys. 35 (2002) 2837–2840. doi:10.1088/0022-3727/35/21/321.

[160]B. Panigrahy, M. Aslam, D.S. Misra, M. Ghosh, D. Bahadur, Defect-Related Emissions and Magnetization Properties of ZnO Nanorods, Adv. Funct. Mater. 20 (2010) 1161–1165. doi:10.1002/adfm.200902018.

[161]K. Vanheusden, C.H. Seager, W.L. Warren, D.R. Tallant, J.A. Voigt, Correlation between photoluminescence and oxygen vacancies in ZnO phosphors, Appl. Phys. Lett. 68 (1996) 403–405. doi:10.1063/1.116699.

[162]N. Shakti, C. Devi, A.K. Patra, P.S. Gupta, S. Kumar, Lithium doping and photoluminescence properties of ZnO nanorods, AIP Adv. 8 (2018) 015306. doi:10.1063/1.5008863.

[163]M. Wang, E. Jung Kim, S. Hong Hahn, Photoluminescence study of pure and Li-doped ZnO thin films grown by sol–gel technique, J. Lumin. 131 (2011) 1428–1433. doi:10.1016/j.jlumin.2011.03.036.

[164]S.H. Lee, J.S. Lee, W.B. Ko, J.I. Sohn, S.N. Cha, J.M. Kim, Y.J. Park, J.P. Hong, Photoluminescence Analysis of Energy Level on Li-Doped ZnO Nanowires Grown by a Hydrothermal Method, Appl. Phys. Express. 5 (2012) 095002. doi:10.1143/APEX.5.095002.

[165]K. MEZIANE, A. ELHICHOU, A. ELHAMIDI, A. ALMAGGOUSSI, M. CHHIBA, Synthesis of lithium doped zinc oxide by sol gel, J. Phys. Conf. Ser. 758 (2016) 012019. doi:10.1088/1742-6596/758/1/012019.

[166]F.S. Husairi, A. Azlinda, M. Rusop, S. Abdullah, Photoluminescence properties of Zinc Oxide nanostructures on different substrates obtained by an immersion method, Microelectron. Eng. 108 (2013) 145–149. doi:10.1016/j.mee.2013.01.064.

[167]V. Ischenko, S. Polarz, D. Grote, V. Stavarache, K. Fink, M. Driess, Zinc Oxide Nanoparticles with Defects, Adv. Funct. Mater. 15 (2005) 1945–1954. doi:10.1002/adfm.200500087.

[168]X. Wang, B. Yang, J. Liu, Y. Zhu, C. Yang, Q. He, A flexible triboelectric-piezoelectric hybrid nanogenerator based on P(VDF-TrFE) nanofibers and PDMS/MWCNT for wearable devices, Sci. Rep. 6 (2016) 36409. doi:10.1038/srep36409.

[169]J.H. Lee, K.S. Hwang, T.S. Kim, The Microscopic Origin of Residual Stress for Flat Self-Actuating Piezoelectric Cantilevers, Nanoscale Res. Lett. 6 (2010) 55. doi:10.1007/s11671-010-9810-z.

[170]J.D. Schäfer, H. Näfe, F. Aldinger, Macro- and microstress analysis in sol-gel derived Pb(ZrxTi1−x)O3 thin films, J. Appl. Phys. 85 (1999) 8023–8031. doi:10.1063/1.370638.

BIOGRAPHICAL SKETCH

Aminur Rashid Chowdhury received his B.Sc. in Chemical Engineering and Polymer Science from Shahjalal University of Science and Technology, Bangladesh in 2013 and joined Photonics and Energy Research Laboratory (Dr. Uddin's research group) at the University of Texas Rio Grande Valley in 2017 as a graduate student. Previously he worked for Oil & Gas industry for 3.5 years. His research interests in hybridization of nanogenerators using nanostructured functional interfaces, renewable energy and electromechanical sensors, nanoengineered device. Aminur R. Chowdhury is recently awarded: Prestigious Dean's Graduate Fellowship (2017-2019), HSS Competition Award (First Prize-Co mentor) 2018, First Position Graduate Showcase 2019. He is joining the University of Texas at Austin as PhD student in the department of Materials Science and Engineering. He received his Masters of Science degree in Chemistry in August of 2019. He can be reached at aminur.cep@gmail.com.